STRUCTURES, DYNAMICS AND INTERACTIONS OF EPHA5, EPHA7 AND NOGO-66 INVOLVED IN CNS REGENERATION INHIBITION

HUAN XUELU

B. ENG., Zhejiang University

A THESIS SUBMITTED FOR THE DEGREE OF DOCTOR OF PHILOSOPHY

NUS GRADUATE SCHOOL FOR INTEGRATIVE SCIENCES AND ENGINEERING

NATIONAL UNIVERSITY OF SINGAPORE

2012

Declaration

I hereby declare that the thesis is my original work and it has been written by me in its entirety. I have duly acknowledged all the sources of information which have been used in the thesis.

This thesis has also not been submitted for any degree in any university previously.

Huan Xuelu

Acknowledgements

I would like to express my deepest gratitude to my supervisor, A/P Song Jianxing, for his constant encouragement and guidance throughout my candidature. During these years, I have learnt a lot from his incredible passion for science and integral view on research. I am grateful to him not only for his scientific guidance but also emotional support. Without his consistent support and illuminating instructions, it is impossible for me to finish my PhD study.

In addition I would like to express my sincere thanks to my colleagues, Dr. Qin Haina, Dr. Shi Jiahai, Dr. Liu Jingxian, Mr. Zhu Wanlong, and other lab members for their friendship and valuable advices. In particular I am grateful to Dr. Fan Jingsong for NMR experiment training and collecting NMR spectra on the 800 MHz and 500MHz spectrometer.

I am grateful to NUS Graduate School For Integrative Sciences and Engineering, National University of Singapore for providing me research scholarship, which enabled me to complete my PhD degree.

And lastly, my heartfelt thanks to my beloved family, especially to my mother, whose support and encouragement has always been much treasured all through these years.

Table Of Contents

Abstract

CNS (Central Nerves System) injuries, caused by many reasons, usually lead to the permanent paralysis of patients because the transected axons in CNS could not regenerate beyond the lesion site. 16 erythropoietin-producing hepatocellular (Eph) kinases constitute the largest family of the receptor tyrosine kinases, which are activated by 9 membrane-associated ephrin ligands. Interactions between Eph kinases and ephrins have been extensively investigated for their developmental roles in axon guidance, topographic mapping, hindbrain segmentation etc. For example, EphA5 is characterized as an axon guidance molecule during neural development and also engaged in inhibition of the neurite outgrowth of the hippocampal, striatal, retinal and cortical neurons. Another Eph receptor, EphA7, is involved in gastric colon, prostate cancers, non-small cell lung cancer and acts as a tumor suppressor in follicular lymphoma. To understand the structural basis underlying their very diverse functions, we first solved the crystal structures of EphA5 and EphA7 ligand binding domains, followed by mapping their dynamic properties on different time scales, as well as interactions with peptides and small ligands by NMR spectroscopy.

Mammalian adult CNS failed in axon regeneration, while fish CNS is capable of axon regeneration. Nogo-66 is an important region of Nogo proteins with multiple functions, especially in inhibiting of human CNS axonal regeneration.

Fish Nogo-66 was thought to be different, so that it does not impair axon regeneration. Thus, the structure of its buffer-soluble form, Nogo-54 in Medaka fish was solved by NMR spectroscopy and subsequently compared with the NMR structure of the human Nogo-54.

These findings may help in design and optimization of peptides and small molecules with high affinity and specificity for enhancing CNS regeneration and treating cancers.

List Of Figures

List Of Tables

Abbreviations

(RP-)HPLC	(Reversed-Phase) High Performance Liquid
(θ)MRW	Mean Molar Ellipticity per Residue in CD
1J/ 2J / 3J	Scalar Coupling Through One Bond/ Two bonds/
AU	Asymmetric Unit
CD	Circular Dichroism
CNS	Central Nervous System
DNA	Deoxyribonucleic Acid
DTT	Dithiothreitol
dαN/ dβN / dNN	NOE Connectivity Between CαH/ CβH/ NH with NH
E.coli	Escherichia coli
Eph receptors	Erythropoietin-Producing Human
EphA5 LBD	EphA5 Ligand Binding Domain
ER	Endoplasmic Reticulum
FID	Free Induction Decay
GST	Gluthathione S-transferase
Haddock	High Ambiguity Driven protein-protein Docking
HSQC	Heteronuclear Single Quantum Coherence
IPTG	Isopropyl β-D-thiogalactopyranoside
ITC	Isothermal Titration Calorimetry

LB	Luria-Bertani
NMDA receptor	N-methyl D-aspartate receptor
NMR	Nuclear Magnetic Resonance
NOE	Nuclear Overhauster Effect
NOESY	Nuclear Overhauser Enhancement Spectroscopy
OD	Optical Density
PBS	Phosphate-buffered Saline
PCR	Polymerase Chain Reaction
RMSD	Root Mean-square Deviation
SDS-PAGE	Sodium Dodecyl Sulphate Polyacrylamide Gel
TOCSY	Total Correlation Spectroscopy
UV	Ultraviolet

CHAPTER I. Introduction

CHAPTER I. Introduction

1.1 Biological Background

1.1.1 Central Nervous System

Human nervous system consists of two parts, central nervous system (CNS) and peripheral nervous system (PNS). The central nervous system contains majority of the nervous system including brain, spinal cord and retina. It has a fundamental and important role in control of behaviors of human body. So once the central nervous system is damaged, it can be a fatal illness.

The common causes of central nervous system diseases are: trauma, infections, degeneration, structural defects, tumors, autoimmune disorders, stroke etc. Any one of them can result in a wide spectrum of disabilities of human beings. Worldwide people suffered from central nervous system illness: the consequences of trauma including memory loss, speech problems; the CNS diseases including Alzheimer’s, Parkinson's and many other diseases. For example, over 35 million people in the world have Alzheimer’s disease, which is a neurodegenerative disease typically found in people over the age of 65 years (Alzheimer's-Association, 2011). The cause of Alzheimer’s is still unknown and there is no cure for this disease. Therefor, it is quite critical and urgent to investigate CNS diseases and develop the medical therapies for them.

1.1.2 Axonal Regeneration and Inhibitory molecules

Due to the failure of central neurons to regenerate dendritic connections and correct axonal, CNS injury does not only cause a break in communication between healthy neurons, it also lead to neuronal degeneration and cell death (Horner and Gage, 2000). It was shown decades ago, unlike fish, amphibian and mammalian peripheral nervous system, adult central mammalian nervous system is unable to regenerate functional axons after injury (Ramon y Cajal, 1928). While after implanted to peripheral nervous system tissues, neurons of central nervous system would grow, suggesting that it might be the environment, not the neuron, that is prevent the regeneration within central nervous system (David and Aguayo, 1981; Tello, 1911). The mechanism for inability of neuron regeneration of injured CNS has been extensively investigated over the past several decades, while it is still unclear.

Although not all of the mechanisms for the failure of CNS neurons regeneration have been clarified, one hypothesis that CNS has inhibitory molecules that can block axonal regeneration has been approved. Caroni, Schwab and Savio (1988) first found that CNS contains actual growth inhibitors (Caroni et al., 1988; Caroni and Schwab, 1988). Since 1988, several other factors have been identified to be capable of inhibiting the regeneration. The identified inhibitory molecules include the chondroitin sulfate proteoglycans (CSPG) Neurocan, Brevican, Phosphacan, Tenascin, and NG2, as either membrane-bound or secreted molecules; Ephrins expressed on astrocyte/fibroblast invading the scar; and the

myelin-associated inhibitors Nogo, MAG, and Omagp (Sandvig et al., 2004).

My thesis mainly emphasizes EphA5/EphA7, receptors of ephrins, which involved in neuron regeneration and many other functions; and Nogo-66, an important domain of Nogo derived from Medaka fish.

1.1.3 Eph Family

One of the largest receptor tyrosine kinases families identified to date is the erythropoietin-producing hepatocellular carcinoma (Eph) family, which is divided into two subclasses, A and B, based on their binding preferences and sequence conservation (Eph-Nomenclature-Committee, 1997). There are 16 structurally similar family members, 10 EphA receptors (EphA1- EphA10) and 6 EphB (EphB1- EphB6) receptors. In general, EphA receptors bind to glycosyl phosphatidyl inositol (GPI) – anchored ephrinA ligands (ephrinA1- ephrinA6), whereas EphB receptors interact with transmembrane ephrinB ligands (ephrinB1-ephrinB3); interactions between Eph receptors and ephrins within each A or B subclass are quite promiscuous with various binding affinities. Interactions between different subclasses are relatively rare, except that EphA4 can bind to all three ephrinB ligands and EphB2 can bind to ephrinA5 ligand (Gale et al., 1996; Pasquale, 2008; Qin et al., 2008).

Eph receptors have a modular structure that consists of a conserved N-terminal ephrin binding domain adjacent to a cysteine-rich domain and two fibronectin juxtamembrane domains, followed by a conserved tyrosine kinase

domain, a C-terminal sterile a-domain, and a PDZ binding motif (Figure 1.1.1). The N-terminal 180 amino acid globular domain is sufficient for high-affinity ligand binding. The adjacent cysteine-rich domain might be involved in receptor-receptor oligomerization often observed on ligand binding according to previous study (Pasquale, 2005; Qin et al., 2008).

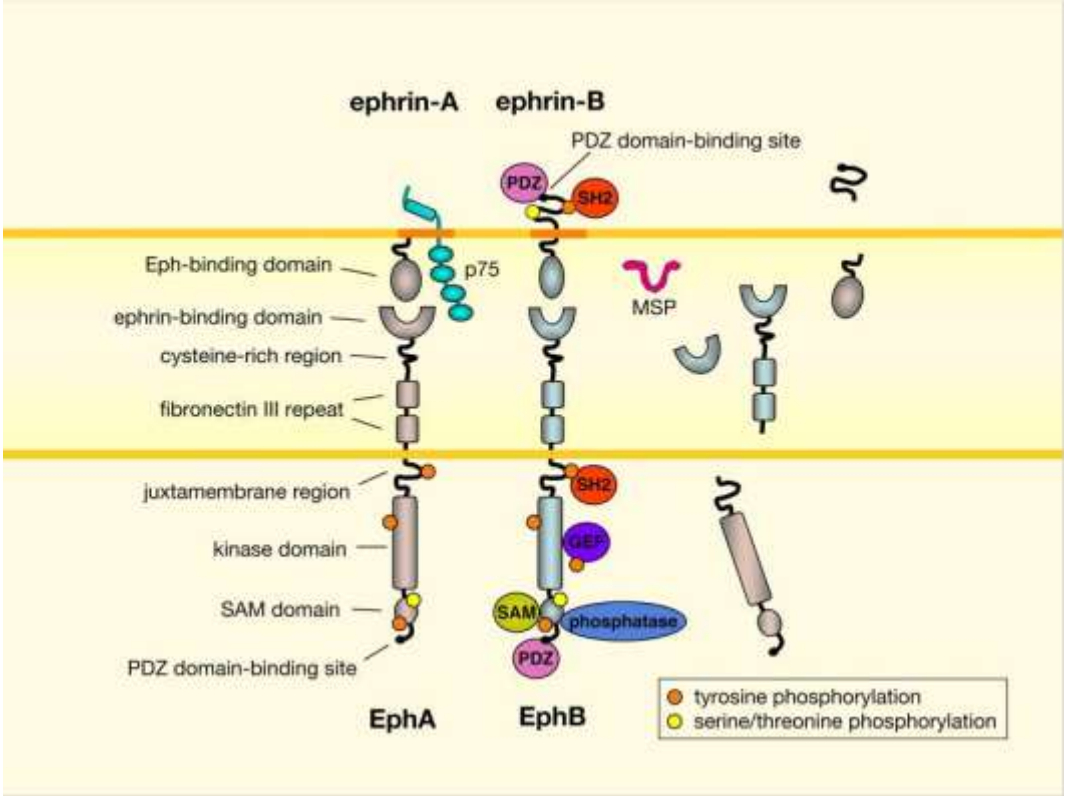

Figure 1.1.1: Eph receptor and ephrin domain structure and signaling interactions (Pasquale, 2010).

The direct protein-protein interactions between ligands carrying signals, and cell-surface receptors recognizing and transforming the information into the receiving cells are the key methods of the communication between cells (Himanen et al., 2001). Communications of biochemical signals between cells are crucial for

the development and existence of multicellular organisms. The Eph/ephrin family is one of the largest groups of receptors and ligands that are able to emanate bidirectional signals: forward signals propagate in the receptor-expressing cells depended on the tyrosine kinase domain activity upon ephrin binding, and reverse signals to the ligand-expressing cells (Flanagan and Vanderhaeghen, 1998; Himanen and Nikolov, 2003; Himanen et al., 2007; Holland et al., 1996; Kullander and Klein, 2002; Pasquale, 2005). The members of Eph/ephrin family play important and different roles in both developing and adult tissues. For example, previous studies showed that the Eph-ephrinB interactions involved in mediating neuronal regeneration, learning and memory formation, pain processing, and differential expression levels of ephrinB are also correlated with tumor genesis (Battaglia et al., 2003; Ran and Song, 2005). Eph receptors have been most extensively studied for their developmental roles in biological processes such as hindbrain segmentation, tissue patterning, vascular system development, axonal guidance, and neuronal development (Brantley-Sieders and Chen, 2004; Palmer and Klein, 2003; Pasquale, 2005, 2008; Wilkinson, 2001). They also play roles in immunity, bone remodeling, blood clotting and stem cells (Edwards and Mundy, 2008; Matsuo, 2010; Prevost et al., 2002; Prevost et al., 2004; Yu et al., 2004).

1.1.4 Structures of Eph Receptors and Eph/ephrin Complexes

The structural study of the Eph receptors and complexes with their ligands

will help us understand the recognition and interaction between Eph receptors and their ligands to further explain the important and different functional roles they played in various biological processes. The ligand-binding domains of EphA2, EphA4, EphB2 and EphB4 in unbound state and in complex with ephrins or peptides have been solved by X-ray crystallography (Chrencik et al., 2006a; Chrencik et al., 2006b; Chrencik et al., 2007; Himanen et al., 2004; Himanen et al., 2009; Himanen et al., 1998; Himanen et al., 2001; Qin et al., 2008). These previous studies showed that despite of different subclasses of Eph receptors they belong to, all the Eph receptor ligand-binding domains adopt a conserved jellyroll β-sandwich architecture that are composed of 11 antiparallel β-strands connected by loops of various lengths. The ectodomain of the ephrin ligands also showed a conserved structure, which is consist of an eight-stranded β-barrel with a Greek key topology, linked by several very flexible and highly conserved functional loops, such as the G-H and C-D loops (Himanen et al., 2004; Himanen et al., 2009; Himanen et al., 2001; Toth et al., 2001).

From the crystal structures of Eph receptor ligand-binding domains and ephrin ligands complex, it is showed that through the penetration of an extended G–H loop of the ephrin ligand into a hydrophobic channel on the surface of the receptor, Eph receptors are capable of binding to ephrin with high affinity. The convex sheet of four β-strands surrounded by the D-E, G-H and J-K loops forms the high-affinity binding channel (Himanen et al., 2009). There are three other interfaces also contribute to Eph-ephrin binding, including: (1) additional residues

on both the receptor and ephrin surfaces; (2) a low affinity interface also involving the Eph receptor ligand-binding domain, which was identified in the EphB2-ephrinB2 complex and appears to mediate the association of two receptor-ephrin dimers (tetramerization) (Himanen et al., 2001); (3) an interface involving the cysteine-rich region adjacent to the ligand-binding domain, which was identified by mutagenesis in the EphA3-ephrinA5 complex but has not been structurally characterized and which might be implicated in high order clustering (Smith et al., 2004).

Two binding interfaces have been found from the structure of EphB2-ephrinB4 complex: the first one is the high affinity ligand-binding channel of EphB2 receptor which is formed by the flexible J-K, G-H, and D-E loops, located at the upper convex surface of EphB2, accommodated the solvent-exposed ephrin G-H loop upon Eph-ephrin binding; another low affinity binding interface, which interacts with the C-D loop of ephrinB4 has also been identified at the concave surface of the receptor H-I loop to mediate two receptor-ephrin dimers tetramerization (Chrencik et al., 2006b).

The structure of EphA2/ephrinA1 heterodimer is architecturally similar to EphB2-ephrinB4 complex structure. The ligand/receptor interface centers around the G–H loop of ephrinA1, which is inserted in the traditional ephrin-binding channel on the surface of EphA2. Eph receptor strands D, E, G, J and M, define the border of this channel. A second contact area, which is adjacent to the channel/G–H-loop interactions but structurally separated, was found to encompass

the ephrinA1 docking site along the upper surface of the receptor. Here, the ephrin β-sandwich consisted of strands C, G and F interacts with EphA2 strands D, E and the B-C loop region through a network of hydrogen bonds and salt bridges (Himanen et al., 2009).

Although Eph receptors interact promiscuously with ephrin ligands of the same subclasses, interactions of Eph receptors with ephrin ligands of the different subclasses are quite rare. EphA4 receptor is one exception that can interact with all three ephrinB ligands. The overall architecture of the EphA4-ephrinB2 complex is very similar to other Eph-ephrin complexes. The high affinity interface of the complex can be divided into two relatively independent regions. One mostly involves hydrophobic interactions between the EphA4 ligand-binding channel and the ephrinB2 G-H loop. The other, which was observed in EphB-ephrinB complexes (Chrencik et al., 2006a; Himanen et al., 2001) but was greatly reduced in the EphA2-ephrinA1 complex and absent in the EphB2-ephrinA5 complex (Himanen et al., 2004; Himanen et al., 2009), involves polar interactions between surface residues Gln^{12} and Glu^{14} in EphA4 and Gln^{109} and Lys^{112} in ephrinB2.

Comparison of these released structures of unbound Eph receptors or in complexes with their ephrin ligands yields insight into the molecular basis for observed Eph receptor/ephrin subclass specificity. The differences among the structures of the A- and B-class molecules result in different architectural arrangements of receptor-ligand complexes, which probably maintained Eph receptor subclass specificity (Himanen et al., 2009). Upon complex formation

with ephrinB2, several notable structural variations are observed in EphA4. The B-class Eph-ephrin complexes have also been reported for significant structural rearrangements when binding to their ephrin ligands. In contrast, only minor structural changes have been observed upon formation of EphA-ephrinA complex. With intimate interactions between the Eph receptor B-C region and the juxtaposing C, F and G ephrin strands, complexes of EphB-ephrinB adopt a more ‘compact’ conformation, whereas with a smaller number of interactions in the same region, the A-class complex is more ‘open’ with a more intimate interaction network between ephrin G-H loop and D-E, J-K and G-H loops of Eph receptor (Himanen et al., 2009).

Previous study suggest that the A-class Eph receptor/ephrin interactions better described by a ‘lock-and-key’-type binding mechanism based on the small conformational rearrangements upon ephrin ligand binding, in contrast to the ‘induced fit’ mechanism defining the B-class molecules (Himanen et al., 2009). While a recent protein dynamics study of EphA4 receptor ligand binding domain done by crystallography, NMR and molecular dynamic (MD) simulation showed that, based on the previous EphA4 ligand binding domain structures as a unbound state or binding with different ligands solved by X-ray crystallography and NMR, two groups of EphA4 receptor ligand binding domains presenting open and closed state already exist before binding to different ligands in crystal or solution. A third theory, ‘conformational selection and population shift’, was suggested to explain the promiscuity and specificity of the EphA4 ligand-binding domain to bind with

multiple A- and B-class ephrin ligands and small molecules (Nussinov and Ma, 2012; Qin et al., 2012).

1.1.5 Inhibitor design for Eph receptors and ephrin ligands

As members of the largest RTK family, together with their ephrin ligands, Eph receptors form a cell communication system with important and wide spread roles in normal physiology and disease pathogenesis. Imbalance of Eph/ephrin function may therefore contribute to a variety of diseases, such as diabetes, tumor, spinal cord injury, abnormal blood clotting and bone remodeling diseases. For example, EphB4 is widely expressed in cancer cells and its increased abundance has been correlated with cancer progression (Kumar et al., 2007; Kumar et al., 2009; Noren and Pasquale, 2007). The critical roles of Eph receptors in various physiological and pathological processes and their correlation to cancers and diseases have validated the Eph receptor as the promising targets for the development of anti-tumor and neuronal regeneration drugs (Fabes et al., 2007; Fabes et al., 2006; Fry and Vassilev, 2005; Goldshmit et al., 2004; Klein, 2004; Tang et al., 2007; Yamaguchi and Pasquale, 2004). Most of the Eph receptor/ephrin interactions involve the extended G–H ephrin loop interacting with the Eph receptor surface channel according to the previous structural information of Eph receptors and ephrin ligands. It has been reported that some peptides and small chemical compounds could bind to the Eph receptor channel as antagonists and block Eph receptor signaling by preventing ephrin binding to Eph

receptor (Chrencik et al., 2006b; Chrencik et al., 2007; Koolpe et al., 2005; Koolpe et al., 2002; Murai et al., 2003; Qin et al., 2008). Those peptides that target the high affinity ligand-binding site are sufficient to inhibit Eph receptor-ephrin binding although there are several binding interfaces existing on Eph receptors. Moreover, unlike the ephrin ligands which bind to Eph receptors in a highly promiscuous manner, a number of the peptides identified by phage display selectively bind to only one or a few of the Eph receptors (Chrencik et al., 2007; Koolpe et al., 2005; Murai et al., 2003). Two small molecules (2,5-dimethylpyrrolyl benzoic acid derivative and its isomeric compound), identified by a high throughput screening, are able to antagonize ephrin-induced effects in EphA4-expressing cells. By interacting with residues in the D–E and J–K loops, the antagonizing benzoic acid derivatives occupy a cavity in the tradition ephrin-binding channel of EphA receptor (Noberini et al., 2008; Qin et al., 2008).

Beside the antagonistic peptides and small molecules targeted to the traditional ephrin ligand binding domain of Eph receptors, the antibodies and soluble forms of Eph receptors and ephrins extracellular domains that modulate Eph-ephrin interactions have also been identified (Ireton and Chen, 2005; Noren and Pasquale, 2007; Pasquale, 2005; Wimmer-Kleikamp and Lackmann, 2005). Several small inhibitors of the Eph receptor kinase domain have also been reported. These inhibitors occupy the ATP-binding pocket of the receptors and are usually broad specificity inhibitors that target different families of tyrosine kinases

(Caligiuri et al., 2006; Karaman et al., 2008).

1.1.6 Functions of EphA5 and EphA7 receptors

As a member of the Eph receptor tyrosine kinase family, EphA5 receptor is wildly expressed in most tissues, and higher expression mainly occurs in the hippocampus, striatum, hypothalamus, and amygdale in the adult brain (Gerlai et al., 1999). One of the most important functions of the EphA5 receptor is to work as an axon guidance molecule during neural development. By acting as a repellent cue during the migratory process, EphA5 receptor and its ligands prevent axons from entering inappropriate territories, and restrict the cells to specific pathways. During neural development, Eph receptors and their ligands are expressed in the projecting and target sites, respectively (Castellani et al., 1998; Wilkinson, 2001).

Depending on the cell type, the binding of EphA5 receptors with ligands expressing neurons results in different consequences at the cellular level. It has been demonstrated that this interaction causes inhibition of the neurite outgrowth of the hippocampal, striatal, retinal, and cortical neurons (Brownlee et al., 2000). At the circuit level, over expression of a truncated form of EphA5 receptor cause a miswiring of the hippocamposeptal pathway and corpus callosum connections in vivo (Yue et al., 2002). Taken together, EphA5 receptor and its ligands serve as repulsive axon guidance cues in the developing brain. Binding of EphA5 and the ligands inhibits the neurite outgrowth and triggers growth cone collapse in vitro. Furthermore, abnormal expression of these molecules results in the disruption of

axonal path finding and mid-line crossing in vivo (Hu et al., 2003).

EphA7 receptor also plays different functional roles in variety of signaling pathways. EphA7 is frequently silenced in gastric colon, prostate cancers (Dawson et al., 2007; Pasquale, 2010); somatic mutations affecting EphA7 have been reported in non-small cell lung cancer (Ding et al., 2008). Co-expression of an endogenously expressed truncated form of EphA7 suppresses tyrosine phosphorylation of the full-length EphA7 receptor and shifts the cellular response from repulsion to adhesion *in vitro* (Holmberg et al., 2000). A recent study showed that knockdown of EphA7 drives lymphoma development in a murine follicular lymphoma (FL) model. A soluble splice variant of EphA7 ($EphA7^{TR}$) can interfere with full-length EphA2 and blocks oncogenic signals in lymphoma cells (Oricchio et al., 2011). This study proved that EphA7 receptor could act as a tumor suppressor in follicular lymphoma with immediate therapeutic potential.

1.1.7 Nogo as an Inhibitor of Axon Regeneration in CNS

Among the myelin-associated inhibitors for CNS axon regeneration, Nogo, MAG, and Omagp, Nogo is the most widely studied myelin-associated inhibitor (Prinjha et al., 2000). Nogo (RTN4) belongs to the reticulon family of membrane proteins, which is a eukaryotic gene family with ubiquitous expression and distinctive topological features (Oertle et al., 2003). Three different isoforms of Nogo, Nogo-A, -B and –C, are generated by alternative promoter and/or splicing (Figure 1.1.2). These three isoforms express ubiquitously, with some tissue

specificity. Among the three isoforms, Nogo-A is the longest one with an N-terminus around 1016 residues; Nogo-B has a N-terminus that is identical to the first 200 residues of Nogo-A and Nogo-C has a very short N-terminus. All the three Nogo isoforms share a conserved C-terminal domain consisting of 188 residues called the reticulon-homology domain (RHD), which is highly conserved within RTN protein members (Oertle et al., 2003).

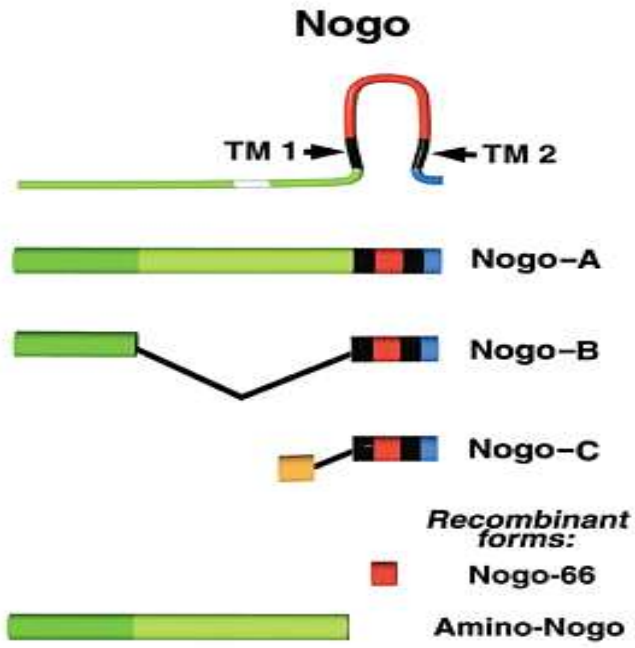

Figure 1.1.2: The domain organization and dissection of the human Nogo proteins (Brittis and Flanagan, 2001).

As a well-studied protein, two inhibitory domains of Nogo-A responsible for the neurite growth inhibiting have been identified. The first one is a unique N-terminal region, which do not exist in Nogo-B and –C (Oertle et al., 2003). The second one is an extracellular 66 amino acid loop (Nogo-66) shared by all the three Nogo isoforms (Prinjha et al., 2000). Nogo-66 contains the three helices and

can bind to the Nogo-66 receptor family (NgR) consisting in three glycophosphatidylinositol (GPI)-anchored receptors (NgR1, NgR2 and NgR3) (Fournier et al., 2001; Li et al., 2006; Li et al., 2004).

Previous studies for Nogos showed that they are involved in a variety of functional processes including apoptosis, CNS neurite regeneration, neuron pathologies, vascular remodeling and so on. For example, the protein level of Nogo-A is correlated with the most common neurodegenerative disease, Alzheimer's disease. Nogo-B was identified as an apoptosis-inducing gene (Li et al., 2001) and a regulator of vascular remodeling (Miao et al., 2006). Nogo-C expressed in HEK293 could induce cell apoptosis by inducing caspase-3 and p53 activation through the JNK-c-Jun dependent pathway (Chen et al., 2006).

Shared by the three isoforms, Nogo-66 is an important region with multiple functions, especially in inhibiting of human CNS axonal regeneration. In contrary to human CNS, CNS in fish is able to regenerate axons. Previous study showed that the Nogo-A-specific domain lost in fish, but also Nogo-66 was modified so that Nogo does not impair axon regeneration (Abdesselem et al., 2009; Diekmann et al., 2005; Schweigreiter, 2008). Experiments also show that Nogo-66 in Zebrafish is growth permissive for both Zebrafish and mouse neurons, while the Nogo-66 homolog in rat inhibits growth in both species, even the two homologs have 70% sequence similarity (Abdesselem et al., 2009). Previously, our lab rationally designed and solved the NMR structure of a soluble form of Nogo-66 in human, Nogo-54 (Li et al., 2008). Nogo-54 is buffer soluble, well structured and

able to mimic Nogo-66 in inhibiting neurite outgrowth. In my thesis, the structure of Nogo-54 derived from Medaka fish was studied and determined by CD and NMR experiments and compared with the human Nogo-54 to get some clues related to the functional differences.

1.2 Protein Structure Determination

Protein is an essential functional component of life, which presents in all living organisms. Protein is made of amino acids arranged in a linear chain and the tertiary structure of a protein is very important in understanding its function, dynamics and enzymatic mechanism at the atomic level. Common experimental methods to study the protein tertiary structures include X-ray crystallography, Nuclear Magnetic Resonance (NMR) spectroscopy, and cyro-electron microscopy. Both X-ray crystallography and NMR spectroscopy can yield information at atomic resolution.

1.2.1 Nuclear Magnetic Resonance (NMR) spectroscopy

1.2.1.1 NMR Phenomenon

Nuclear magnetic resonance (NMR) is a property that magnetic nuclei have when the nuclei of certain atoms are placed in a static magnetic field and exposed to a second oscillating magnetic field, which cause the nuclei to absorb energy and then radiate it back out. The nuclear spin property of the nuclei decides whether the nuclei can experience the NMR phenomenon. Nuclear spin (I) is the angular momentum quantum number, a fundamental property of a nucleus. Based on the spin number (I) of a nucleus, the nuclei can be divided into three groups. The first group, when $I = 0$, ^{12}C and ^{16}O for example, has even mass numbers and even atomic numbers. This group has no magnetic moment and thus is NMR inactive.

The second group, when $I = 1/2$ (like ^{1}H, ^{15}N and ^{13}C), are NMR active, which can give simple and interpretable signals and are widely used in NMR. The third group, when $I > 1/2$ (like ^{2}H, ^{14}N), is NMR active while the NMR signals of these nuclei are broaden and very difficult to be detected. In the external magnetic field, the nucleus, which has spin number of 1/2, can orient parallel or antiparallel to it. There are slightly different energies between the two possible orientations, which spins can jump from one to the other and absorb or emit the energy difference in the form of electromagnetic radiation. The different numbers of parallel and antiparallel spins contributes to the NMR signal. NMR signal sensitivity is proportional to γ^3, in which γ is gyromagnetic ratio (or magnetogyric ratio), another intrinsic property of a nucleus. Among the three widely utilized nuclei, ^{1}H, ^{15}N and ^{13}C, ^{1}H has the largest gyromagnetic ratio.

1.2.1.2 Chemical shift

Chemical shift, which is caused by electric de-shielding effect, is one of the most basic parameters of NMR spectroscope. The nuclei have different resonance frequencies and appear in the spectrum at different positions within different chemical environment. This is due to a small magnetic field created by electrons circulating around the nucleus, which can shield the nucleus from the external field. Therefore, each nucleus with its unique chemical environment in an NMR spectrum gives rise to a unique resonance. Chemical shift is denoted as δ and described by following equation, where V represents the precession frequency and

the unit of δ is parts per million (ppm). The reference is normally D_2O in protein NMR spectroscopy.

$$\delta=(V-V_{REF})/V_{REF}*10^6$$

Chemical shifts of the amino acids are used to identify individual residues of a protein in NMR spectrum (Wuthrich, 1986). By comparing the observed chemical shifts with random coil values of the amino acids, the secondary structure of the protein can be predicted (Figure 1.2.1) (Wishart et al., 1991).

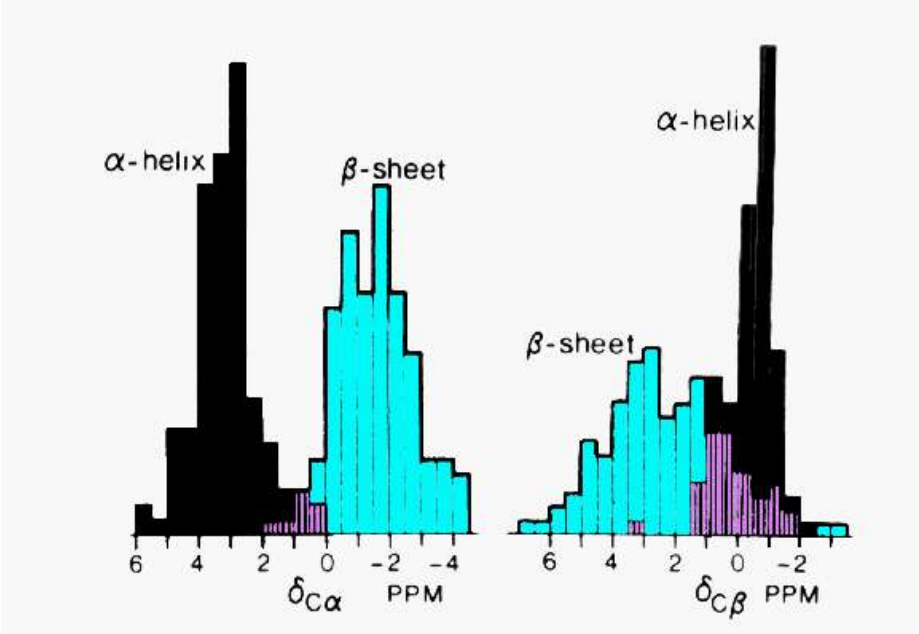

Figure 1.2.1: Chemical shift deviations of Cα and Cβ from random coil values and the correlation with secondary structures (Spera and Bax, 1991).

1.2.1.3 J coupling

J coupling is also known as spin-spin coupling or scalar coupling, which can be observed when the nuclei have different environments or different chemical shifts and the distances between them are less than or equal to three bond lengths (Simon and Sattler, 2004). There are two types of J couplings: the coupled nuclei

with the same magnetogyric ratio γ and different chemical shifts have homonuclear coupling, such as proton-proton coupling. The J coupling for coupled nuclei with different magnetogyric ratios, such as coupling between nuclei ^{1}H-^{15}N, ^{1}H-^{13}C, or ^{15}N-^{13}C are heteronuclear coupling. The Karplus equation can be used to estimate the correlation between J coupling and dihedral angels:

$$J(\theta)=A\cos^2\theta+B\cos\theta+C$$

Where J is the ^{3}J coupling constant and θ is the dihedral angle. Deviation of $^{3}J_{NH\alpha}$ values from random coil values can also provide valuable secondary structural information of protein similar to chemical shift deviation (Figure 1.2.2). β structures have larger coupling constant values (8 to 10 Hz) than α-helical structures (3 to 5 Hz) in folded proteins, while in unfolded proteins the coupling constants are average (6 to 7.5 Hz) (Dyson and Wright, 2004; Pardi et al., 1984).

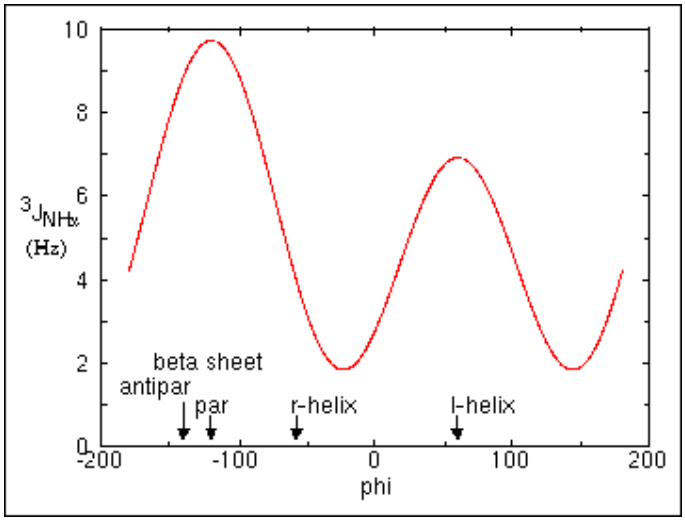

Figure 1.2.2: Correlation between J coupling and protein secondary structure (Pardi et al., 1984).

1.2.1.4 Nuclear Overhauser Effect (NOE)

Nuclear Overhauser Effect (NOE) is defined as a dipolar cross-relaxation phenomenon between spins through space magnetization transfer. NOE is proportional to the inverse sixth power of the distance (NOE ~ $1/r^6$) between protons at short mixing time as a function of interproton distances. NOE can normally be detected if the distances of the nuclei are less than 5 Å, otherwise it is too small to be observed.

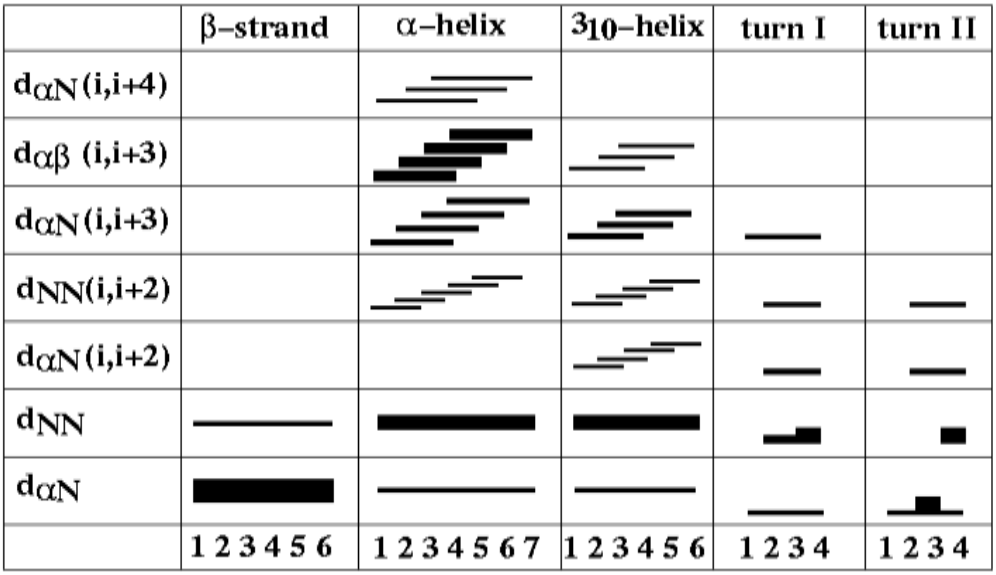

Figure 1.2.3: NOE patterns associated with secondary structure (Wuthrich, 1986).

Due to the correlation with distances between nuclei, NOE can provide much information for the 3D structure determination of protein. Intra-residue and sequential NOEs are not only used for establishing connections among amino acids, but also used to reveal protein secondary structure through the observed NOE patterns (Figure 1.2.3). Moreover, protons which far away on protein sequence but close to each other when proteins are well-folded in space can be

correlated by long-range NOE signals, providing the information for the protein tertiary structure calculation and determination (Wuthrich, 1986).

1.2.1.5 Relaxation

When apply a 90° plus to the equilibrium longitudinal magnetization, the z-magnetization disappears and the transverse magnetization is created. The system is in a non-equilibrium state. The xy magnetization may eventually return to the thermal equilibrium state along the z-axis. The duration of this process is called relaxation and T1 and T2 are the two parameters used to describe it. T1 is called the longitudinal (or spin-lattice) relaxation after which the z magnetization reappears. Transverse relaxation time T2 is also called spin-spin relaxation time, which is the decay constant for the magnetization perpendicular to the ambient magnetic field. The backbone $\{^{1}H\}$-^{15}N heteronuclear NOE (hetNOE) provides information about the magnetization transferred from ^{1}H to a heteronucleus. The flexible residues of protein those undergo motion faster than the overall tumbling of the molecules (i.e. in the picosecond to nanosecond time scale) would have decreased NOE intensities relative to the average intensity observed for most of the residues. Thus, it is very convenient to find the flexible residues of the protein. For instance, both N- and C-terminal ends of the protein probably have decreased value of hetNOE.

1.2.1.6 NMR Structure Determination

The determination of a protein structure by NMR can be carried out in five major steps (Figure 1.2.4).

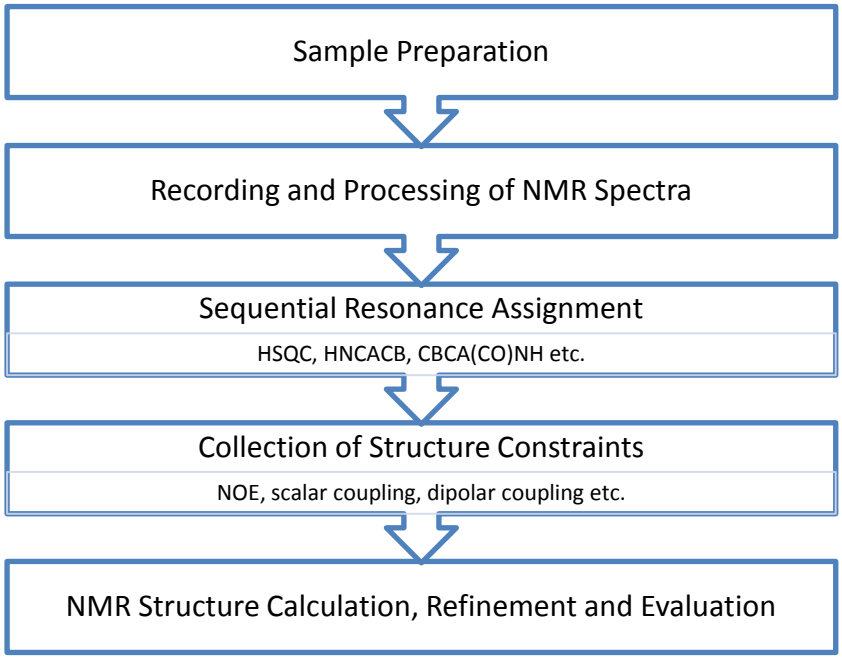

Figure 1.2.4: Strategy of structure determination by NMR.

1.2.1.6.1 NMR Sample Preparation

For NMR structure study, the protein sample is usually prepared at a concentration of 500 μM to 1 mM, depends on the protein solubility and stability. Based on the protein size and the NMR experiments need to be done, the protein is usually labeled with ^{15}N or ^{15}N and ^{13}C. The experiment parameter like sample pH, ionic strength and temperature should be adjusted to optimize the protein behavior in solution. Usually the protein solution is around 0.5 ml with 6% to 10% D_2O inside.

1.2.1.6.2 Recording and Processing of NMR Spectra

A set of multidimensional NMR experiments was recorded using the prepared protein sample. The spectra raw data were processed using Fourier transformation to obtain frequency domain data for assignments.

1.2.1.6.3 Sequential Resonance Assignment

Assignment is to associate the resonance in an NMR spectrum with a particular nucleus of a certain residue of the examined protein. The protein backbone atoms (NH, C, CO, CA and CB) can be assigned using several 2D and 3D NMR spectra, HSQC, HNCACB, and CBCA(CO)NH for example. Based on the assigned backbone atoms of the protein, the side chain atoms of particular residues can also be assigned using certain NMR spectra (NOESY etc.).

1.2.1.6.4 Collection of Structure Constraints

NMR spectra can give useful geometric conformational information for protein structure determination. By adding the structure constraints like NOE-derived distance restrains, scalar coupling constants, residual dipolar coupling, torsion angles and hydrogen bonds, the protein structure quality can be increased.

1.2.1.6.5 NMR Structure Calculation, Refinement and Evaluation

The software can calculate the protein structure according to the empirical data and the know amino acid sequence of the protein and satisfy the majority of the experimental derived constraints. Then the calculated structures would be optimized following the energy minimization rules. Finally, PROCHECK is used to evaluate the calculated NMR structure (Laskowski et al., 1993). To get the good quality structures, the constrains violations, root mean square deviation (RMSD) of the structure ensemble and the Ramachandran plot of the calculated structures should be at reasonable value/region.

1.2.1.7 Unique Features of NMR

Bloch and Purcell first detected the NMR phenomenon independently in 1946, and NMR spectroscopy was first used to determine the structure of small molecules in organic chemistry. Only after Wuthrich developed the 2D experiment in the early 1980s (Wuthrich, 1986), NMR was applied for protein structure determination.

Nowadays, for determining the three dimensional structures of biological macromolecules, NMR has become a powerful technique the same as X-ray crystallography. Compared with X-ray crystallography, NMR is able to solve protein structures in solution. Based on different aims, the condition of protein solution such as salt concentration and pH can be adjusted and protein conformational changes can be traced. NMR is more suitable for proteins with low

stability or solubility, especially for proteins that are unable to be crystalized compared with X-ray crystallography. Furthermore, NMR is also used to study protein dynamics, protein folding and intermolecular protein interactions.

1.2.2 X-ray Crystallography

1.2.2.1 Introduction

X-ray crystallography is the major technology to determine the protein tertiary structure. By using a beam of X-rays to strike a crystal and diffract into many specific directions, the arrangement of atoms within the crystal can be told. From the angles and intensities of these diffracted beams, the three-dimensional picture of electron densities within the crystal can be produced. Using these data, the tertiary structure of the protein can be calculated by software.

Max Perutz and Sir John Cowdery Kendrew solved the first crystal structures of sperm whale myoglobin protein (Kendrew et al., 1958). So far, among 78477 biological macromolecule structures in the Protein Data Bank (PDB) (access on January 2012), over 87% of the structures (68639 protein structures) were solved by X-ray crystallography (Table 1.2.1, Figure 1.2.5) (Berman et al., 2000) (http://www.pdb.org). X-ray crystallography has a big advantage on solving structures of arbitrarily large molecules, whereas solution-state NMR is restricted to relatively small ones (less than 70 kDa).

Table 1.2.1: PDB Current Holdings Breakdown (Berman et al., 2000) (http://www.pdb.org)

Experimental Method	Proteins	Nucleic Acids	Protein/NA Complexes	Other	Total
X-ray	64155	1335	3147	2	68639
NMR	8071	967	185	7	9230
Electron Microscopy	277	22	101	0	400
Hybrid	42	3	2	1	48
Other	138	4	5	13	160
Total	72683	2331	3440	23	78477

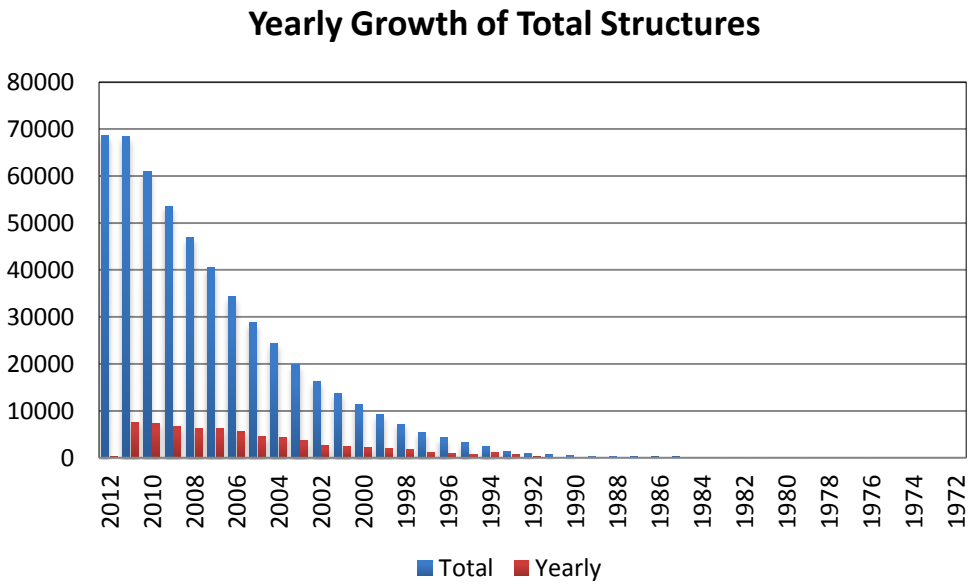

Figure 1.2.5: Yearly Growth of Total Structures on PDB (Berman et al., 2000) (http://www.pdb.org).

1.2.2.2 Crystallization

Crystallization is the first step to use X-ray crystallography for protein structure determination. Crystallization of proteins includes three stages: nucleation, growth and cessation of growth. The most common methods to get the

protein crystals are: the hanging drop vapor-diffusion, the sitting drop vapor-diffusion, and the dialysis and batch methods. These methods can screen numerous protein crystallization conditions. There are many factors that may affect protein crystallization, such as protein concentration, precipitant, salt, additives and pH. Therefore, to get the protein crystallized well, it is very important to optimize the crystallization conditions. After getting the protein crystal, some post-crystallization methods, such as dehydration and soaking may help to improve the crystal quality.

1.2.2.3 X-ray Crystallography

To solve a protein structure by X-ray crystallography, a protein crystal should be well ordered. It should be a symmetrical macromolecular package of protein molecules and solvent molecules. The crystal symmetry, the unit cell parameters, the crystal orientation and the resolution limits information are important parameters for the protein crystals.

Direct methods, multiple isomorphous replacement (MIR), multi-wavelength anomalous dispersion (MAD), single-wavelength anomalous dispersion (SAD) and molecular replacement (MR) are the methods used to solve the phase problem in macromolecular structure determination. Molecular replacement is the simplest and very useful method to solve the phase problem when the protein molecule has high sequence and structural similarity to an already solved protein structure: A patterson map would be computed from the already solved homologous protein

structure, which is considered as a fingerprint. This patterson map is then modified in the new crystal unit-cell according to means of rotation functions. By the support of a convincing correlation factor and a residual factor, a best fit can be achieved finally. All these methods only yield phase estimates for a limited set of reflections. Furthermore, to improve the accuracy of the phase and to get an interpretable electron density map, with the help of Fourier transformation, refinement of both reciprocal and real space is carried out.

The initial model generated with the MR method is usually not optimal. Refinement is needed to improve the model. Refinement of a model is the optimization of a function of a set of observations so that the correlation between the atomic model and the diffraction data is maximized. During the refinement, R-factor and R_{free}-factor are monitored, which reflect the data quality. R-factor (also refers to ‘reliability’) is the agreement index between the refined structural models and experimentally observed X-ray diffraction data. R_{free}-factor is the factor calculated from a subset (~10%) of reflections that were not included in the structure refinement.

1.3 Research Aims

Eph receptors and Nogos play very important roles in the growth of neuron and many signal pathways as mentioned above. To illustrate the mechanism and interaction details of how they function in real life, three dimensional protein structures and dynamics of them invested by X-ray crystallography and NMR are very essential. Furthermore, some peptides and small compounds have been studied as inhibitors, which can inhibit interactions of Eph receptors and their ephrin ligands. These studies provide the possibility to treat Eph receptors and Nogos as therapeutic targets for central nerve system diseases, especially for anti-tumor and neuronal regeneration drug development, concerning the functional importance.

Research aims of this study focus on three proteins.

(1) For EphA5 and EphA7 receptor ligand-binding domains:

Crystallize the EphA5/7 ligand-binding domains and resolve the 3D structures by X-ray crystallography. NMR spectroscopy was used to study their dynamic properties as unbound state. For EphA5, dynamic properties of its bound state with peptide/compound were studied. The binding abilities of EphA5 ligand-binding domain with peptides or small compounds have been investigated by different methods. Their binding interfaces have been mapped out and compared by computer docking.

(2) For Nogo-54:

The 3D structure of Nogo-54 in Medaka fish has been investigated by NMR

spectroscopy. Human central nervous system does not have the ability to regenerate new axons compare to fish. Thus the 3D structure of fish Nogo-54 was subsequently compared with the NMR structure of the human Nogo-54.

CHAPTER II. Material and Method

Chapter II. Material and Method

2.1 Cloning.

The DNA fragment of the human EphA5 ligand-binding domain (residues 59–235) was amplified from a HeLa cell cDNA library using two primers containing BamHI and XhoI (New England Biolab) restriction sites, 5'- GGA TCC AAC GAA GTG AAT TTA TTG GAT TCA CGC -3' (forward) and 5'- CTC GAG TCA AGA AGG CGC TTC TTT ATA GTA TAC -3' (reverse). The PCR fragments were cloned into a BamHI and XhoI cut pET32a vector (Novagen), and then was transformed into *E. coli* DH5α cells (Novagen) for colony screening. Plasmids were amplified in *E. coli* DH5α cells and purified by QIAprep Spin Miniprep Kit (Qiagen). The free Cysteine 233 in this construct was mutated to Alanine by use of the site-directed mutagenesis kit (Stratagene) to avoid the formation of non-native disulfide bridges. All the performances were followed the protocols provided by the manufacturers. The procedures were monitored by Agarose DNA electrophoresis (Bio-Rad). Before expression of the recombinant proteins, the DNA sequences were confirmed by automated DNA sequencing.

The DNA fragment of the human EphA7 ligand-binding domain with Sushi domain (EphA7L, residues 31–283) was also amplified from a HeLa cell cDNA library using two primers containing BamHI and XhoI (New England Biolab) restriction sites, 5'- CG GGA TCC AAG GAA GTA CTA CTG CTG -3' (forward) and 5'- GGG CTC GAG TCA GAA CCC ACG GCC CGC GGG TTC ACA AGT GTC -3' (reverse). The PCR fragments were cloned into a BamHI and XhoI cut

pET32a vector (Novagen), and then was transformed into *E. coli* DH5α cells (Novagen) for colony screening. Plasmids were amplified in *E. coli* DH5α cells and purified by QIAprep Spin Miniprep Kit (Qiagen). The free Cysteine 279 in this construct was mutated to Alanine to avoid the formation of non-native disulfide bridges. All the performances were followed the protocols provided by the manufacturers. The procedures were monitored by Agarose DNA electrophoresis (Bio-Rad). The DNA sequences were confirmed by automated DNA sequencing.

PCR-based strategy was utilized to synthesize the genes encoding WDC peptide (peptide sequence: WDCNGPYCHWLG) and WTF peptide (peptide sequence: WTFPVLWDDKHP) (Wei and Song, 2005). Briefly, the gene encoding WDC was obtained by PCR with two long oligonucleotides: Forward Primer (5'- GGA TCC TGG GAT TGC AAC GGC CCG TAT TGC CAT TG- 3') and Reverse Primer (5'- CTC GAG TCA GCC CAG CCA ATG GCA ATA CGG GCC -3') with a 17-mer overlap designed with *E. coli* preferred codons containing BamHI and XhoI restriction sites. The gene encoding WTF peptide was obtained by PCR with two long oligonucleotides: Forward Primer (5'- TGG ACC TTT CCG GTG CTG TGG GAT GAT -3') and Reverse Primer (5'- CGG ATG TTT ATC ATC CCA CAG CAC CGG -3') with a overlap designed with *E. coli* preferred codons containing BamHI and XhoI restriction sites. The PCR fragment was cloned into a BamHI and XhoI cut pGEX-4T-1 vector (Amersham Biosciences), and the vector was transformed into *E. coli* DH5α cells (Novagen).

2.2 Preparation of Competent *E. coli* Cells.

Competent cell (DH5α, BL21 or Rosetta-gami) grew on LB (Bio Basic Inc.) plate without ampicillin at 37°C overnight. Single bacterial colony was picked into 2 ml LB media with necessary antibiotics, grow overnight at 37°C while shaking at 200 rpm. Overnight culture was diluted into 100 ml fresh LB broth at a ratio of 1:100. Cells were grown at 37°C (200 rpm) till OD_{600} reached 0.4~0.5. The bacterial cells were transferred to sterile, disposable, ice-cold 50 ml polypropylene tubes and stored on ice for 10 minutes to reach 0°C. The cells were spun down at 3000*g for 10 minutes at 4°C. The cell pellet was then gently resuspended by swirling or gentle vortexing in 30 ml of ice-cold, sterile, fresh $MgCl_2$-$CaCl_2$ solution (80 mM $MgCl_2$, 20 mM $CaCl_2$). The cells were then recovered by centrifuged at 3000*g for 10 minutes at 4°C. After discarding the supernatant, cell pellet was resuspended by swirling or gentle vortexing in 2 ml of ice-cold 0.1 M $CaCl_2$ with 15% glycerol (BDH Laboratory Supplies) for each 50 ml of original culture. Cell resuspension was distributed in aliquots into 1.5 ml sterile eppendorf tubes. Competent cells were quick frozen by liquid nitrogen and then stored at -80°C for long time storage.

2.3 Transformation of *E. coli* Cells

1 or 2 μl plasmid DNA (about 100 ng/μl) was added into 100 μl of *E. coli*

competent cells and mixed well by gently tapping. The cells were incubated on ice for around 30 minutes, followed by a heat shock for 50 seconds and a subsequent incubation on ice for 2 minutes. 500µl of LB medium was added into the tube and incubated at 37°C for 60 minutes before plating cells onto LB Agar plates containing ampicillin.

2.4 Protein Expression and Purification

2.4.1 Expression and Purification of the EphA LBD

The recombinant his-tag proteins of EphA receptor ligand-binding domains (EphA5/EphA6/EphA7) and EphA7 ligand-binding domain with sushi domain (EphA7L) were over expressed in *E. coli* Rosetta-gami (DE3) cells (Novagen) allowing more efficient formation of disulfide bonds and expression of eukaryotic proteins, which contain codons rarely used by *E. coli*. The cells were cultured in Luria-Bertani (LB) medium at 37°C while shaking at 200 rpm until the absorbance at 600 nm reached around 0.6. Then Isopropyl 1-thio-D-galactopyranoside (IPTG) was added into the cell culture to a final concentration of 0.1 mM (for EphA5 and EphA7L) or 0.4mM (for EphA6 and EphA7) to induce protein expression at 18°C (for EphA5 and EphA7L) or 20°C (for EphA6 and EphA7) for overnight culture. The harvested cells were sonicated in the PBS lysis buffer containing 20 mM sodium phosphate (pH 7.5) and 150 mM sodium chloride to release soluble his-tagged EphA proteins. Then the

recombinant proteins were subsequently purified by affinity chromatography using nickel-nitrilotriacetic acid-agarose (Qiagen) under native condition. EphA proteins were cleaved using in-gel cleavage at room temperature by incubating the fusion protein attached to nickel-nitrilotriacetic acid-agarose with thrombin overnight. The released EphA proteins were then purified on an AKTA FPLC machine (Amersham Biosciences) using a gel filtration column (HiLoad 16/60 Superdex 75) equilibrated in 20 mM sodium phosphate containing 150 mM sodium chloride, pH7.5.

For the crystallization of EphA5/EphA6/EphA7, the harvested cells were sonicated in 25 mM Tris-HCl (pH 7.8), containing 150 mM NaCl and 5 mM $CaCl_2$. EphA proteins were then purified by in-gel cleavage and gel filtration in the same Tris buffer using nickel beads and gel filtration column Superdex 75. To increase the purity of the samples, the eluted fractions from gel filtration step were then buffer exchanged to 25 mM Tris-HCl (pH 7.8) containing 150 mM NaCl, and then purified by ion-exchange chromatography using anion-exchange column (Mono Q 10/100) with a gradient of NaCl from 0 to 1 M in 25 mM Tris-HCl (pH 7.8). The eluted fractions which contained the EphA ligand-binding domains were collected and again dialyzed to 25 mM Tris-HCl buffer (pH 7.8), containing 150 mM NaCl and 5 mM $CaCl_2$ and stored at 4°C. The purity of the proteins was verified by the SDS-PAGE, and the identity of the samples was verified by MALDI-TOF mass spectrometry.

2.4.2 Expression and Purification of WDC and WTF Peptides

The recombinant GST-tag WDC peptide was overexpressed in *E. coli* Rosetta-gami (DE3) cells and the GST-tag WTF peptide was overexpressed in BL21 cells. The cells were cultured in Luria-Bertani medium at 37°C until the absorbance at 600 nm reached ~0.6. Isopropyl 1-thio-D-galactopyranoside was then added to a final concentration of 0.5 mM to induce peptides expression at 20°C overnight. The harvested cells were sonicated in lysis buffer containing 20 mM sodium phosphate (pH 7.5) and 150 mM sodium chloride to release soluble GST-tagged peptides, which were subsequently purified with glutathione-Sepharose (Amersham Biosciences). The peptides were released from the GST fusion proteins by in-gel thrombin cleavage at room temperature for 4 hours, followed by HPLC purifications on a RP-18 column (Vydac). The formation of disulfide bridge of WDC was determined by both HPLC and MALDI-TOF mass spectrometry. The identity of the WTF sample was also verified by MALDI-TOF mass spectrometry.

2.4.3 Expression and Purification of Nogo-54

The recombinant his-tag Nogo-54 protein was expressed in the bacterial strain BL21. The cells were cultured at 37°C to an OD_{600} of around 0.6. IPTG was then added at a final concentration of 0.3 mM to induce the recombinant protein expression at 20°C overnight. Then the Nogo-54 protein was purified by

Ni^{2+}-affinity chromatography under native conditions and subsequently purified by HPLC on a reverse-phase C8 column (Vydac).

2.5 Preparation of Isotope Labeled Proteins

The generation of the isotope-labeled protein for heteronuclear NMR experiments followed the similar expression and purification procedures except that the *E. coli* cells were grown in M9 medium (Na_2HPO_4•$12H_2O$: 17.1 g/L (J. T. Baker); KH_2PO_4: 3 g/L (J. T. Baker); NaCl: 0.5 g/L; $(NH_4)2SO_4$: 1 g/L (Cambridge Isotope Laboratories Inc.); Glucose: 4 g/L (Sigma); $MgSO_4$: 1 mM (Merck); Thiamine: 2 mg/L (Sigma); ampicillin: 75 mg/L) with the addition of $(^{15}NH_4)_2SO_4$ for ^{15}N labeling and $(^{15}NH_4)_2SO_4$/[^{13}C]glucose for ^{15}N-/^{13}C double labeling.

2.6 Protein Analysis by SDS-PAGE

Hoefer Mighty small II electrophoresis unit (Amersham Pharmacia Biotech) was used to perform SDS-polyacrylamide gel electrophoresis. 5 μl of low range prestained SDS-PAGE standard (Bio-Rad) was used. After electrophoresis, SDS-PAGE was placed in staining solution (0.025% Coomassie brilliant blue R250; 40% methanol, 7% acetic acid) for about 10 minutes with gentle shaking. The gel was then destained using destaining solution.

2.7 Determination of Protein Concentration by Spectroscopy

The concentration of a protein solution is determined by measuring the absorbance of 280 nm (A) and using the Beer-Lambert Law: $A = \varepsilon * l * C$, where ε is the molar absorption coefficient ($M^{-1}cm^{-1}$), l is the path length (cm), and C is the protein concentration (M). The absorption A of a protein at 280 nm depends on the content of Tryptophan, Tyrosine, and Cysteine (disulfide bonds), extinction efficient ε can be determined by following equation:

$$\varepsilon(280)(M^{-1}cm^{-1}) = (\#Try)(5500) + (\#Tyr)(1490) + (\#Cys)(125)$$

#Try, *#Tyr* and *#Cys* are the numbers of each corresponding residue in a protein (Pace et al., 1995).

8M Urea was added into the protein solutions to denature them, and then the solutions were measured by UV/visible spectrophotometer using 0.1 mm quartz cuvette at 280 nm.

2.8 Circular Dichroism (CD) Measurement

A Jasco J-810 spectropolarimeter equipped with a thermal controller was used to perform the Circular Dichroism (CD) experiments of peptides and proteins. The far UV and near UV CD spectra of samples were recorded at 25°C in 10 mM phosphate buffer (pH 6.3) at a protein concentration of 10-50 μM using a 1 mm path length capped quartz cuvette (Liu et al., 2006) with a 0.1 nm spectral resolution. Data from three independent scans were added and averaged.

2.9 Protein Crystallization

For the X-ray crystallography experiments, to avoid the phosphate crystals, the buffer system changed from the phosphate buffer system to the Tris-HCl buffer system. The EphA receptor (EphA5/EphA6/EphA7) ligand binding domains were prepared in a buffer containing 25 mM Tris-HCl (pH 7.8), 150 mM NaCl and 5 mM $CaCl_2$ at a concentration of 10 mg/ml. Crystal screen was set up by preparing 1 μl of the protein solution mixed with 1μl of the reservoir solution as hanging drops at room temperature in a well containing different reservoir solution. Rock-like crystals of EphA5 ligand binding domain formed in the well containing 0.1 M Tris-HCl (pH 8.5) and 2.0 M ammonium sulfate. After optimization, high quality crystals grew after 5 days under the condition of 0.1 M Tris-HCl (pH 8.5) and 2.0 M ammonium sulfate.

2.10 Data Collection and Structure Determination

X-ray diffraction images for a single crystal were collected using an in-house Bruker X8 PROTEUM x-ray generator with a CCD detector. The crystal was protected by cryoprotectant (0.1 M Tris-HCl, 2.0 M ammonium sulfate, 25% glycol, pH 8.5). The data were indexed and scaled in the space group $C222_1$, with one molecule per asymmetric unit, using the program HKL2000 (Otwinowski and Minor, 1997).

The crystal structure of EphA5 ligand binding domain was determined by the Molecular Replacement method using EphA4 ligand binding domain (Protein Data Bank code 3CKH) as a search module using Phaser and MolRep in the Suite CCP4. The crystal structure was subsequently completed by manual fitting with the program COOT (Emsley and Cowtan, 2004) and several rounds of structure refinements were done using CNS (Brunger et al., 1998). Water molecules were added into the model using CNS water-pick model. The final structure was analyzed by PROCHECK (Laskowski et al., 1993), and details of the data collection and refinement statistics are shown in chapter 3. All figures were prepared using the PyMOL molecular graphics system (W. L. DeLano, DeLano Scientific LLC, San Carlos, CA).

2.11 Isothermal Titration Calorimetry (ITC)

All of the Isothermal Titration Calorimetry (ITC) experiments were performed using a Microcal VP ITC machine. Titration experiments were conducted in 10 mM phosphate buffer (pH 6.3) at 25°C. The samples were first degassed for 15 min and then centrifugation for 15 min to remove bubbles before experiments. The protein sample was placed in a 1.4 ml reaction cell while the peptides/ligands were loaded into a 300 μl injection syringe. Control experiments with the same parameter setting were also done to subtract the contribution of buffer or sample dilution. After subtracting the results of control experiments, ITC data were fitted by using the built-in software ORIGIN to yield the

thermodynamic binding parameters.

2.12 HSQC Characterization of the Binding of EphA Receptors with Peptides and Ligands

To characterize the binding interactions of WDC/WTF peptides and the ligands with EphA receptor ligand-binding domains, two-dimensional ^{1}H-^{15}N HSQC spectra of the ^{15}N labeled EphA proteins were acquired at a protein concentration of ~100 μM in the absence or presence of WDC/WTF peptides or the compounds at different molar ratios. The shifted HSQC peaks were assigned by superimposing the HSQC spectra.

2.13 NMR Backbone Assignment

0.5 mM of ^{15}N-^{13}C double-labeled EphA5 ligand-binding domain with or without WDC was prepared in 10 mM phosphate buffer (pH 6.3) containing 0.02% (w/v) sodium azide and an addition of 10% D_2O for NMR spin-lock. Two pairs of triple-resonance NMR spectra, HNCACB and CBCA(CO)NH were collected for the preliminary backbone sequential assignment at 25°C on an 800-MHz Bruker Avance spectrometer equipped with a shielded cryoprobe.

0.5 mM double-labeled EphA7 ligand-binding domain was prepared in 10 mM phosphate buffer (pH 6.3) containing 0.02% (w/v) sodium azide and an addition of 10% D_2O for NMR spin-lock. A pair of triple-resonance NMR spectra,

HNCACB and (H)CC(CO)NH were collected for the preliminary backbone sequential assignment at 25°C on an 800-MHz Bruker Avance spectrometer equipped with a shielded cryoprobe.

NMR data were processed with NMRPipe and analyzed with NMRView.

2.14 NMR Structure Determination

A 0.8 mM solution of ^{15}N-labeled nogo-54 protein sample was prepared in 10mM phosphate buffer (pH 5.2) containing 0.02% (w/v) sodium azide with the addition of 10% D_2O for the ^{15}N-edited HSQC-TOCSY and HSQC-NOESY experiments. The NMR spectra were collected at 25°C on an 800-MHz Bruker Avance spectrometer equipped with a shielded cryoprobe. All NMR data were processed with NMRPipe and analyzed with NMRView.

For structural calculation, NOE were collected from NOESY spectra. A set of manually-assigned unambiguous NOE restrains together with dihedral angel restraints, which were predicted by TALOS program based on chemical shift values (Hα), were used to calculate initial structures of Nogo-54 by CYANA program (Guntert, 2004). More NOE cross-peaks in the NOESY spectra were added in the structure calculation with the availability of the initial structures. After many rounds of refinement, 10 lowest-energy structures were selected by CYANA program, and then were analyzed by the graphic software MolMol (Koradi et al., 1996).

2.15 NMR Relaxation Experiment

^{15}N-labeled EphA5 protein samples with or without WDC/WTF peptides, ligands were prepared at a concentration of 0.8 mM in 10mM phosphate buffer (pH 6.3) containing 0.02% (w/v) sodium azide with the addition of 10% D_2O for NMR spin-lock. ^{15}N T1 and T2 relaxation times and {^{1}H}-^{15}N steadystate NOEs were determined at 25°C on an 800-MHz Bruker Avance spectrometer equipped with a shielded cryoprobe (Clore et al., 1990; Farrow et al., 1994; Kay et al., 1989). ^{15}N T1 values were measured from HSQC spectra recorded with relaxation delays of 10, 250, 650, 900, 1000, 1100 and 1300 msec. ^{15}N T2 values were determined with relaxation delays of 1, 22, 35, 48, 60, 70 and 76 msec. {^{1}H}-^{15}N steadystate NOEs spectra were obtained when with and without ^{1}H presaturation of duration 3 sec plus a relaxation delay of 5 sec at 800 MHz.

2.16 Molecular Docking

The modules of the EphA receptor ligand-binding domains in complex with the antagonistic molecules were constructed by use of the HADDOCK software (de Vries et al., 2007; Dominguez et al., 2003) in combination with CNS (Brunger et al., 1998). They use the chemical shift perturbation data to derive the docking, while at the same time, allowing various degrees of flexibility. Three steps of the docking procedure were followed: first, randomization and rigid body energy

minimization; second, semi-flexible simulated annealing; and third, flexible explicit solvent refinement.

To conduct the docking, by using of the CNS protocol, hydrogen atoms were added to the structures. The online PRODRG server (Schuttelkopf and van Aalten, 2004) was used to generate and energy-minimize the geometric coordinates and parameters for the small molecules.

Before the docking procedure, all the residues of EphA receptor ligand-binding domains with a chemical shift perturbation greater than the threshold value were set to be “active” residues, whereas according to HADDOCK definition, the neighbors of active residues were defined as “passive” residues. The residues located on the loop were set to be “fully flexible” residues during calculation. As a result, 1000 structures were generated for rigid body docking, and the best 100 ones out of all 1000 structures were chosen for semi-flexible simulated annealing and water refinement. Detailed analysis and display of three structures with the lowest energies are in next chapter.

CHAPTER III. Results and Discussion

CHAPTER III. Results and Discussion

3.1 EphA5 Ligand-Binding Domain

3.1.1 Expression and Purification of EphA5 LBD

The recombinant his-tag protein of EphA5 ligand-binding domain was over expressed in *E. coli* Rosetta-gami (DE3) cells (Novagen) to get the correct formation of disulfide bonds. The harvested cells were sonicated in the PBS lysis buffer to release soluble His-tag EphA5 proteins. Then the recombinant proteins were subsequently purified under native condition and cleaved by in-gel cleavage at room temperature with thrombin overnight. The released EphA5 protein was purified on an AKTA FPLC machine using a gel filtration column. As assessed by FPLC size-exclusion chromatography, the EphA5 LBD is a monomer in solution (data not shown).

For the crystallization of EphA5 LBD, the harvested cells were sonicated in Tris buffer. After purified by gel filtration column, to increase the purity of the EphA5, the eluted fractions from gel filtration step were then purified by ion-exchange chromatography. The whole expression and purification process of EphA5 ligand-binding domain and the purity of the purified protein were assessed by SDS-PAGE using 15% gel. His-tag has a molecular weight of ~2 kDa, EphA5 LBD without His-tag is around 20 kDa, the identity of EphA5 was verified by MALDI-TOF mass spectrometry (data not shown).

3.1.2 Structural Characterization of EphA5 LBD by CD

The structural properties of EphA5 ligand-binding domain were fist investigated by far-UV CD spectroscopy. As shown in Figure 3.1.1A, the spectrum of EphA5 protein in 10mM phosphate buffer (pH 6.3) had a maximal negative peak at around 212 nm, which implied that EphA5 ligand-binding domain has a typical β-conformation. The near-UV CD spectra of EphA5 in the absence and presence of 8 M urea were also done to see the overall tertiary packing of EphA5 LBD (Figure 3.1.1B). The near-UV spectra showed that without the 8 M urea, EphA5 adopted tight tertiary packing. While with 8M urea which is used to denature the protein sample, the property was lost under denatured condition. All the data were from three independent scans and were added and averaged.

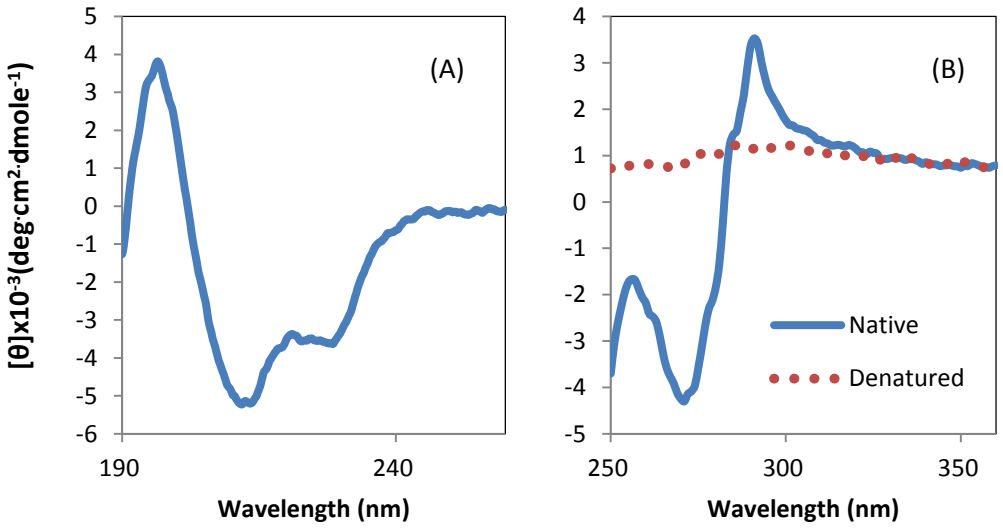

Figure 3.1.1: Preliminary structural characterization of EphA5 by CD. (A) Far-UV CD spectrum of 10 µM EphA5 in the 10 mM phosphate buffer (pH 6.3). (B) Near-UV CD spectra of EphA5 in 10 mM phosphate buffer (pH 6.3) without (blue) and with 8 M urea (red).

3.1.3 Preliminary NMR Structural Characterization of EphA5 LBD

NMR HSQC experiment was used to further assess the structural properties of the EphA5 ligand-binding domain, which is a sensitive probe to both secondary structure and tertiary packing. As shown in Figure 3.1.2, ^{1}H-^{15}N NMR HSQC spectra of EphA5 ligand binding domain showed a well-dispersed HSQC spectrum in both dimensions (~4 ppm over ^{1}H and ~26 ppm over ^{15}N dimensions), indicating that EphA5 protein had a well-packed tertiary structure as confirm by the CD spectra. Therefore, NMR experiments would be suitable for studying the structure of EphA5, binding affinity and dynamic characterizations of EphA5 binding with peptides/ligands.

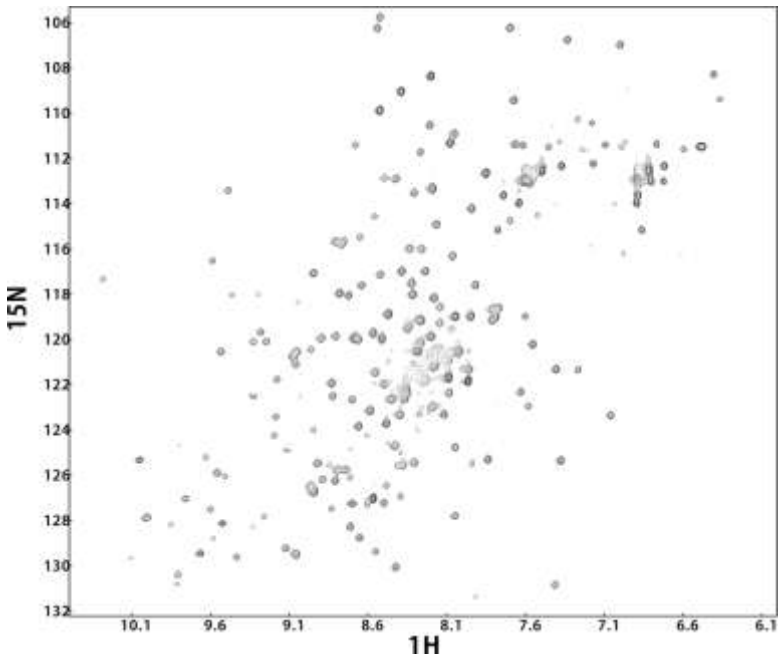

Figure 3.1.2: ^{1}H-^{15}N HSQC spectrum of the EphA5 ligand-binding domain collected in a phosphate buffer at pH 6.3.

3.1.4 Crystal Structure of EphA5 LBD

The EphA5 ligand binding domain was prepared in a buffer containing 25 mM Tris-HCl (pH 7.8), 150 mM NaCl and 5 mM $CaCl_2$ at a concentration of 10 mg/ml. Crystal screen was set up by preparing 1 µl of the protein solution mixed with 1µl of the reservoir solution as hanging drops at room temperature in a well containing the reservoir solution. Rock-like crystals formed in the well containing 0.1 M Tris-HCl (pH 8.5) and 2.0 M ammonium sulfate after 5 days.

3.1.4.1 Structure of EphA5 Ligand Binding Domain Determined from Crystal

X-ray diffraction images for a single crystal were collected using an in-house Bruker X8 PROTEUM x-ray generator with a CCD detector. The crystal was protected by cryoprotectant (0.1 M Tris-HCl, 2.0 M ammonium sulfate, 25% glycol, pH 8.5). The data were indexed and scaled in the space group $C222_1$ (a=54.80, b=83.34, c=81.30), with one molecule per asymmetric unit, using the program HKL2000. The Matthews coefficient was 2.29 with 46.20% solvent constant.

The crystal structure of EphA5 ligand binding domain was determined by the Molecular Replacement method using EphA4 ligand binding domain (Protein Data Bank code 3CKH) as a search module using Phaser and MolRep in the Suite CCP4. The crystal structure was subsequently completed by manual fitting with the program COOT and further refined with program suite Crystallography & NMR System (CNS) (Brunger et al., 1998) at 2.99 Å resolution with a final

R-factor of 0.2504 (R_{free}=0.2940). Only one EphA5 molecule contained in one asymmetric unit, and there are no tight contacts with other EphA5 molecules in the neighboring units. The final structure was analyzed by PROCHECK, and details of the data collection and refinement statistics are shown in Table 3.1.1. All figures were prepared using the PyMOL molecular graphics system (W. L. DeLano, DeLano Scientific LLC, San Carlos, CA).

From the 3D structure, all the residues of EphA5 ligand binding domain are visible except for the last three residues (Figure 3.1.3). The EphA5 ligand-binding domain adopts the conserved jellyroll folding architecture previous revealed for other Eph receptors. The jellyroll consists of 11 anti-parallel beta-sheets arranged as a compact beta-sandwich, which connected by loops of different length and two disulfide bonds. The concave sheet is composed of strands C, F, L, H and I and the convex sheet of strand D, E, A, M, G, K and J.

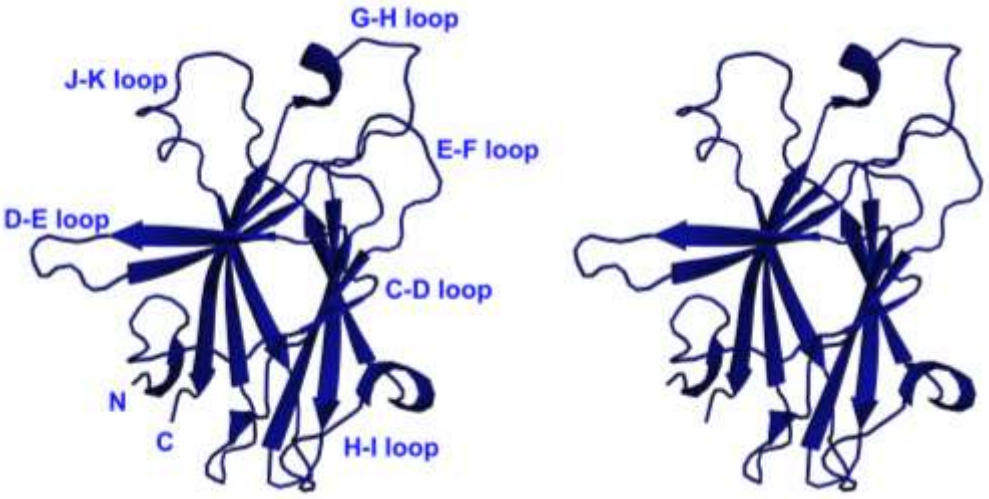

Figure 3.1.3: Crystal Structure of the EphA5 Ligand Binding Domain.

Table 3.1.1: Crystallographic data and refinement statistics for the EphA5 ligand-binding domain structure.

Data collection	
Wavelength (Å)	1.5418
Resolution range (Å)	50.0 to 2.9
Space group	C222(1)
Cell parameters	
a, b, c (Å)	54.80, 83.34, 81.30,
α, β, γ (°)	90, 90, 90
Observed Reflections	8975
Unique Reflections	3682
Redundancy	4.0
Completeness (%)	97.67%
Overall (*I/σI)*	19.12
Rsym	0.288
Refinement	
Resolution range (Å)	24.78 to 2.99
R_{work}*	0.2504
No. of reflections	3429
R_{free}**	0.2940
No. of reflections	253
RMSD bond lengths (Å)	0.019
RMSD bond angles (°)	2.117
Ramachandran Plot	
Most favored region (%)	74.8
Additional allowed regions (%)	24.5
Generously allowed regions (%)	0
Disallowed regions (%)	0.6
B-factors	
Protein	3.751
Water	3.925

*$R_{work}= \Sigma |F_{obs} - F_{calc}|/ \Sigma F_{obs}$ where F_{calc} and F_{obs} are the calculated and observed structure factor amplitudes, respectively.
**R_{free}=as for R_{work}, but for 10.3% of the total reflections chosen at random and omitted from refinement.

3.1.4.2 Comparison of EphA5 LBD Structure with Previous Eph LBD Structures

As seen in Figure 3.1.4, EphA5 LBD has two conserved disulfide bridges, one within the G-H loop (Cys^{137}-Cys^{147}) and the other between the E-F and L-M loops (Cys^{102}-Cys^{220}). This pattern of disulfide bonds is identical to that observed previously in other EphA and EphB receptor ligand binding domains (Chrencik et al., 2006a; Chrencik et al., 2006b; Chrencik et al., 2007; Himanen et al., 2004; Himanen et al., 2009; Himanen et al., 1998; Himanen et al., 2001; Qin et al., 2008).

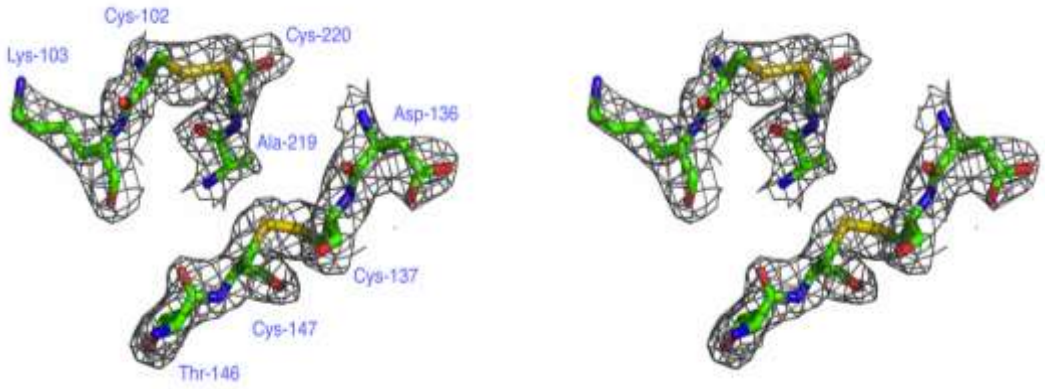

Figure 3.1.4: Stereo view of the two disulfide bridges in the EphA5 ligand binding domain built into the simulated-annealing $2F_o$-F_c electron density map contoured at 1.6σ.

The D-E and J-K loops, which cap the high affinity ephrin-binding pocket, are well defined in the crystal structure, while the quality of electronic densities is not high due to the low resolution (Figure 3.1.5). This is unique because in most previously determined unbound Eph receptor LBD structures, the D-E and J-K loops were either entirely or partially invisible due to their high intrinsic dynamics.

The only exception is the EphA2 LBD structure (Figure 2A), which was determined at a higher resolution (2.0 Å).

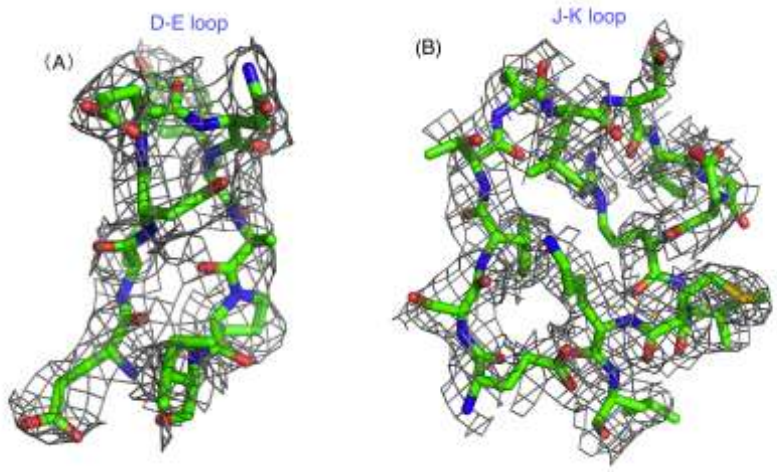

Figure 3.1.5: Electron density map of the D-E and J-K loops in the EphA5 ligand binding domain built into the simulated-annealing $2F_o$-F_c electron density map contoured at 1.6σ.

EphA5 was compared with other previously determined Eph receptor ligand binding domain structures both in the unbound state and in the bound state of their ephrin ligands (Figure 3.1.6). The structure of EphA5 ligand binding domain bears a highly similar jellyroll folding architecture composed of eleven antiparallel beta-stands to the previously determined ligand binding domains of the EphA2, EphA4, EphB2 and EphB4 receptor. The backbone r.m.s.d. of the EphA5 ligand-binding domain over 11 beta-strands are quite small compared with the previous solved Eph receptor structures. On the other hand, over the loop region, very large variations could be observed not only between EphA5 and the EphB receptors but also between Eph receptors from the same A- or B-subclasses, in particular over the D-E and J-K loops, which are critical for ligand binding. A

recent protein dynamics study of EphA4 receptor ligand binding domain done by crystallography, NMR and molecular dynamic (MD) simulation showed that, based on the previous EphA4 ligand binding domain structures as a free state or binding with different ligands solved by X-ray crystallography and NMR, two groups of EphA4 receptor ligand binding domain presenting open and closed state already exist before binding to the different ligands in crystal or solution. Compared with the EphA4 LBD in the open form that has a 3_{10}-helix in the J-K loop, the EphA4 LBD in the closed form adopted an additional short beta-sheet. Interestingly, the J-K loop in the unbound EphA5 LBD appears more similar to the J-K loops in the ephrin-bound structures of other Eph receptors (Figure 3.1.6B) than in the unbound structures (Figure 3.1.6A). The J-K loops in the unbound Eph receptor LBD structures previously reported contain a short antiparallel beta-sheet, as exemplified in the EphB2 and EphA4 structures (Figure 3.1.6A). In contrast, the J-K loop adopts a helical-like conformation in the unbound EphA5 LBD crystal structure, similar to that observed only in ephrin-bound Eph receptor LBDs (Figure 3.1.6B). This observation suggests that EphA5 molecule may go through the small conformational rearrangements upon ephrin ligand binding, which is similar to the previous studied A-class Eph receptor/ephrin interaction described by a ‘lock-and-key’-type binding mechanism, in contrast to the ‘induced fit’ mechanism defining the B-class molecules (Himanen et al., 2009).

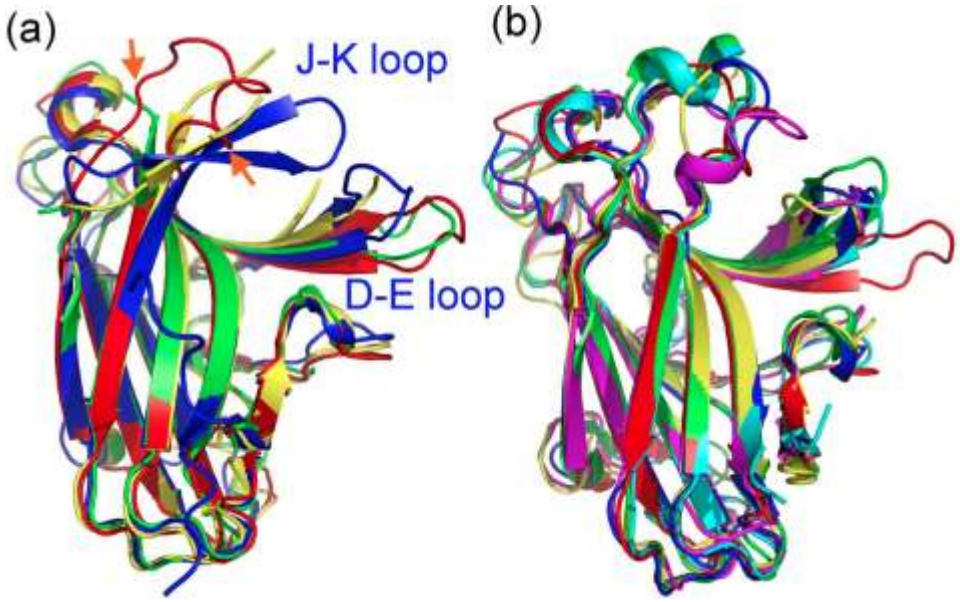

Figure 3.1.6: Structure comparison. (a) Superimposition of the LBD structure of EphA5 (red) with those of EphA2 (green, 3C8X), EphA4 (yellow, 3CKH) and EphB2 (blue, 3ETP) in the unbound state. It is interesting to note that a short β-sheet is formed by EphA2, EphA4 and EphB2 residues corresponding to EphA5 residues Ala179-Ser182 and Gly189-M193 (brown arrows). (b) Superimposition of the LBD structure of EphA5 (red) with those of EphA2 in complex with ephrin-A2 (green, 3CZU), EphA4 in complex with ephrin-A2 (cyan, 3WO3), EphA4 in complex with ephrin-B2 (blue, 3GXU), EphB2 in complex with ephrin-B2 (pink, 1KGY) and EphB4 in complex with ephrin-B2 (yellow, 2HLE).

3.2 EphA5 LBD with Antagonistic Peptides

EphA5 receptor and its ligands serve as repulsive axon guidance cues in the developing brain. Their interaction triggers growth cone collapse and inhibits the neurite outgrowth in vitro. A number of peptides identified by phage display show their selectivity, high binding affinity with EphA5 receptor (Chrencik et al., 2006b; Chrencik et al., 2007; Koolpe et al., 2005; Koolpe et al., 2002; Murai et al., 2003; Qin et al., 2008). Those peptides that target the high affinity ligand-binding site are sufficient to inhibit Eph receptor-ephrin binding although there are several binding interfaces existing on Eph receptors. Moreover, unlike the ephrin ligands which bind to Eph receptors in a highly promiscuous manner, a number of the peptides identified by phage display selectively bind to only one or a few of the Eph receptors (Chrencik et al., 2007; Koolpe et al., 2005; Murai et al., 2003). To assess whether the purified EphA5 LBD retains the ligand binding properties expected for the EphA5 receptor, we measured its binding to the WDC (WDCNGPYCHWLG) and WTF (WTFPVLWDDKHP) peptides. These peptides were previously identified in a phage-display screen based on its binding to the entire extracellular domain of rat EphA5 (Murai et al., 2003).

3.2.1 Characterization of Binding Interactions between EphA5 LBD and WDC/WTF Peptides by NMR and ITC

As shown in Figure 3.2.1, the NMR titration and ITC experiments were performed to analyze the binding affinity between EphA5 ligand binding domain and WDC/WTF peptides.

From Figure 3.2.1 B, C and Table 3.2.1 of ITC experiments; the K_d for the binding of EphA5 with WDC was 6.22 μM, demonstrating that the WDC peptide binds to the LBD of human EphA5, and not other domains in the extracellular region. Consistent with this, in ELISA assays the WDC peptide antagonizes EphA5-ephrin-A5 interaction with an IC50 value of around 50 μM (data not shown). The synthetic WDC peptide inhibits ephrin binding to EphA5 and not other Eph receptors, with the possible exception of a slight inhibition of EphA6, consistent with the high selectivity of the phage-displayed peptide (Murai et al., 2003). These results suggest that the WDC peptide binds to the high affinity ephrin-binding pocket of EphA5, where it competes with ephrins for binding. Moreover, the high selectivity of WDC implies that the high affinity ephrin binding pocket of EphA5 has some unique structural or/and dynamic properties that are not shared by other Eph receptors.

For binding between EphA5 ligand binding domain and WDC peptide, the NMR spectra showed that the HSQC peak set from the free ^{15}N-labeled EphA5 all shifted to become identical compared to the set from the complex of EphA5 and WDC when the molar ratio of EphA5 to WDC reached 1:3 (Figure 3.2.1A). This

is consistent with its low micromolar affinity as the KYL peptide is also capable of inducing extensive shifting of the HSQC peaks of the EphA4 LBD, with a K_d of 0.8 μM (Lamberto et al., 2012).

For binding between EphA5 ligand binding domain and WTF peptide, dislike the binding between EphA5 ligand binding domain and WDC peptide, NMR spectra showed that many HSQC peaks from the free ^{15}N-labeled EphA5 disappeared in the presence of WTF peptide, when the molar ratio of EphA5 to WTF reached 1:1 (Figure not shown). More peaks have disappeared when the molar ratio of EphA5 to WTF reached 1:3 (Figure 3.2.2A). When the molar ratio of EphA5 to WTF reached 1:4, the HSQC peaks showed no significant differences, indicating that the binding of EphA5 and WTF had become saturated. From Figure 3.2.2 B, C and Table 3.2.1 of ITC experiments, the K_d for the binding of EphA5 with WTF was 8.69 μM, which indicated the binding between EphA5 and WTF is a litter weaker than the binding between EphA5 and WDC.

We also probed the uniqueness of the EphA5 ligand-binding pocket by using C1, an antagonistic small molecule that shows selectivity for the EphA2 and EphA4 receptors and has been shown to cause shifts in the HSQC peaks of the EphA4 LBD (Noberini et al., 2011; Qin et al., 2008). Consistent with the reported selectivity of C1 for EphA2 and EphA4 (Noberini et al., 2008), addition of C1 at ratios of even up to 1:20 (EphA5: C1) resulted in no detectable shifts of the HSQC peaks (data not shown). This clearly demonstrates that the EphA5 LBD does not significantly bind to C1, suggesting that the unique structural features of the J-K

loop in the EphA5 LBD crystal structure may play a key role in defining its ligand binding specificity.

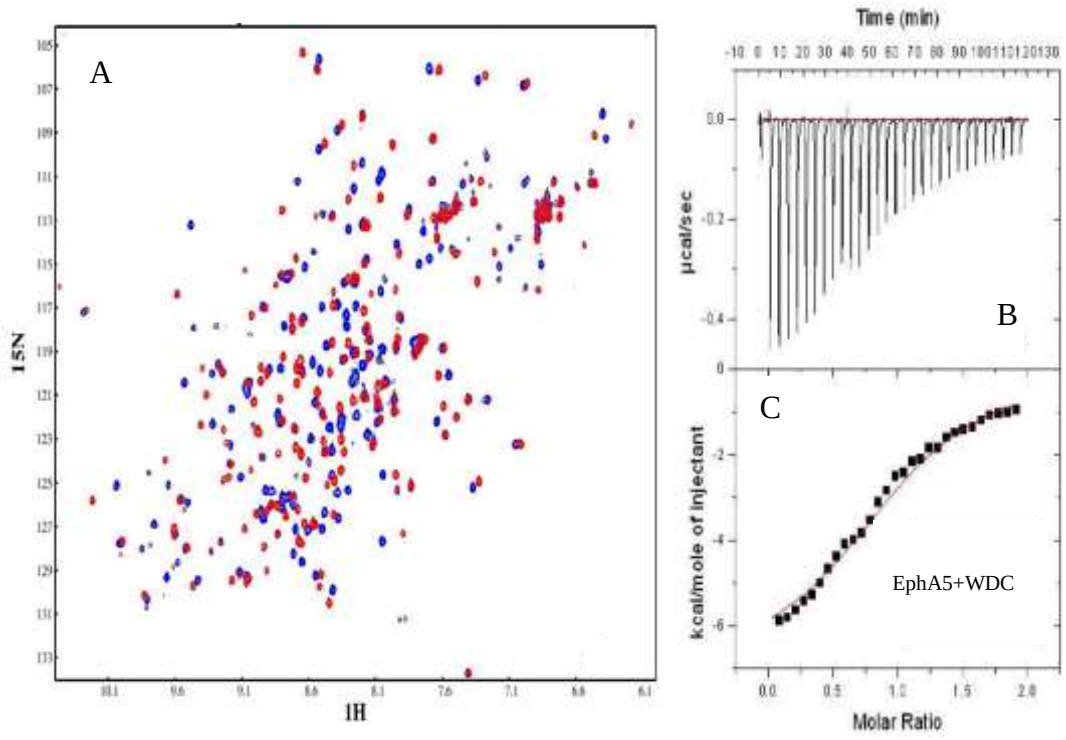

Figure 3.2.1: NMR and ITC characterization of the binding between EphA5 and WDC. (A) Superimposition of the HSQC spectra of the ^{15}N-labeled EphA5 in the absence (blue) and presence (red) of WDC at a molar ratio of 1:3. (B) ITC titration profiles of the binding reaction between EphA5 and WDC. (C) Integrated values for reaction heat with subtraction of the corresponding blank results normalized by the amount of ligand injected versus WDC/EphA5 molar ratio. The detailed conditions and setting of the ITC experiments are presented in Materials and Methods as well as Table 3.2.1.

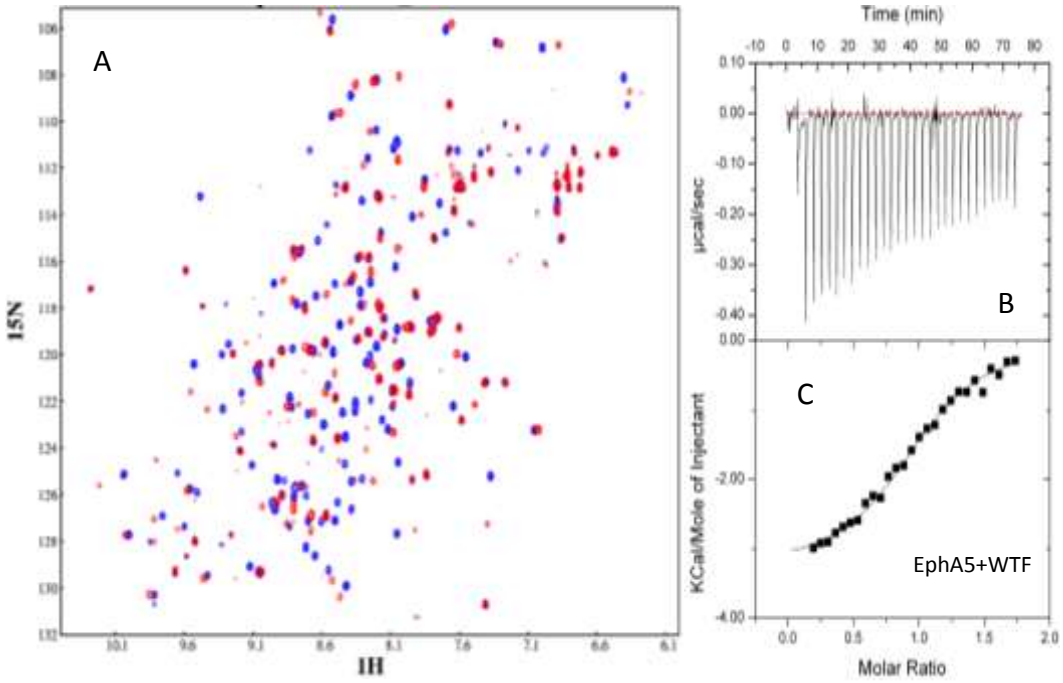

Figure 3.2.2: NMR and ITC characterization of the binding between EphA5 and WTF. (A) Superimposition of the HSQC spectra of the ^{15}N-labeled EphA5 in the absence (blue) and presence (red) of WTF at a molar ratio of 1:3. (B) ITC titration profiles of the binding reaction between EphA5 and WTF. (C) Integrated values for reaction heat with subtraction of the corresponding blank results normalized by the amount of ligand injected versus WTF/EphA5 molar ratio. The detailed conditions and setting of the ITC experiments are presented in Materials and Methods as well as Table 3.2.1.

Table 3.2.1: Thermodynamic parameters of the binding interactions between EphA5 receptor with WDC/WTF peptides.

Syringe	Cell	Temp (^{0}C)	Injection Volume (μL)	Ka (M^{-1})	Kd (μM)	Δ*S* (cal/mol*K)	Δ*H* (cal/mol)
WDC (500 μM)	EphA5 (28 μM)	25	5	1.608×10^5 $\pm1.412\times10^4$	6.22	-42.63	-7118 ±138.6
WTF (1.135mM)	EphA5 (100 μM)	25	5	1.15×10^5 $\pm6.13\times10^4$	8.69	12.1	-3295 ±292.0

3.2.2 Mapping of Binding Interfaces between EphA5 and WDC/WTF

WDC/WTF peptides could bind with EphA5 receptor with high affinity. The interface between EphA5 ligand binding domain and WDC/WTF peptides was an interesting target to be studied by NMR spectroscopy. A series of three-dimensional heteronuclear NMR experiments were done for mapping the binding interface between EphA5 and WDC/WTF peptides.

3.2.2.1 Backbone Sequential Assignments of EphA5 LBD in the Presence and Absence of WDC Peptide

Two pair of triple-resonance NMR spectra, HNCACB and CBCA(CO)NH were collected from a $^{15}N/^{13}C$ double-labeled EphA5 protein sample without/with the addition of WDC peptide (the molar ratio of WDC to EphA5 is 1:3) to obtain the preliminary backbone sequential assignment for EphA5, respectively. Figure

3.2.3 and Figure 3.2.4 showed the HSQC spectra of assigned EphA5 backbone peaks in the absence and presence of WDC peptide, respectively.

Previous study of NMR show that the chemical shift deviation of Cα, Cβ, Hα, and C=O from random coil value reflects the secondary structure of protein (Wishart and Sykes, 1994). After finishing all the chemical shift assignment, secondary structures of free EphA5 ligand binding domain and EphA5 protein binding with WDC peptide were calculated by both Cα and Cβ chemical shifts to evaluate the conformational changes of EphA5 ligand binding domain induced by binding with WDC peptide. Figure 3.2.5 and Figure 3.2.6 show that the secondary structures calculated by Cα and Cβ were consistent with the EphA5 crystal structure obtained by X-ray crystallography. Meanwhile, compare the secondary structures calculated for free EphA5 and EphA5 binding with WDC (Figure 3.2.5 and Figure 3.2.6), the binding of WDC to EphA5 did not induce significant conformational changes to the secondary structure of EphA5 ligand binding domain.

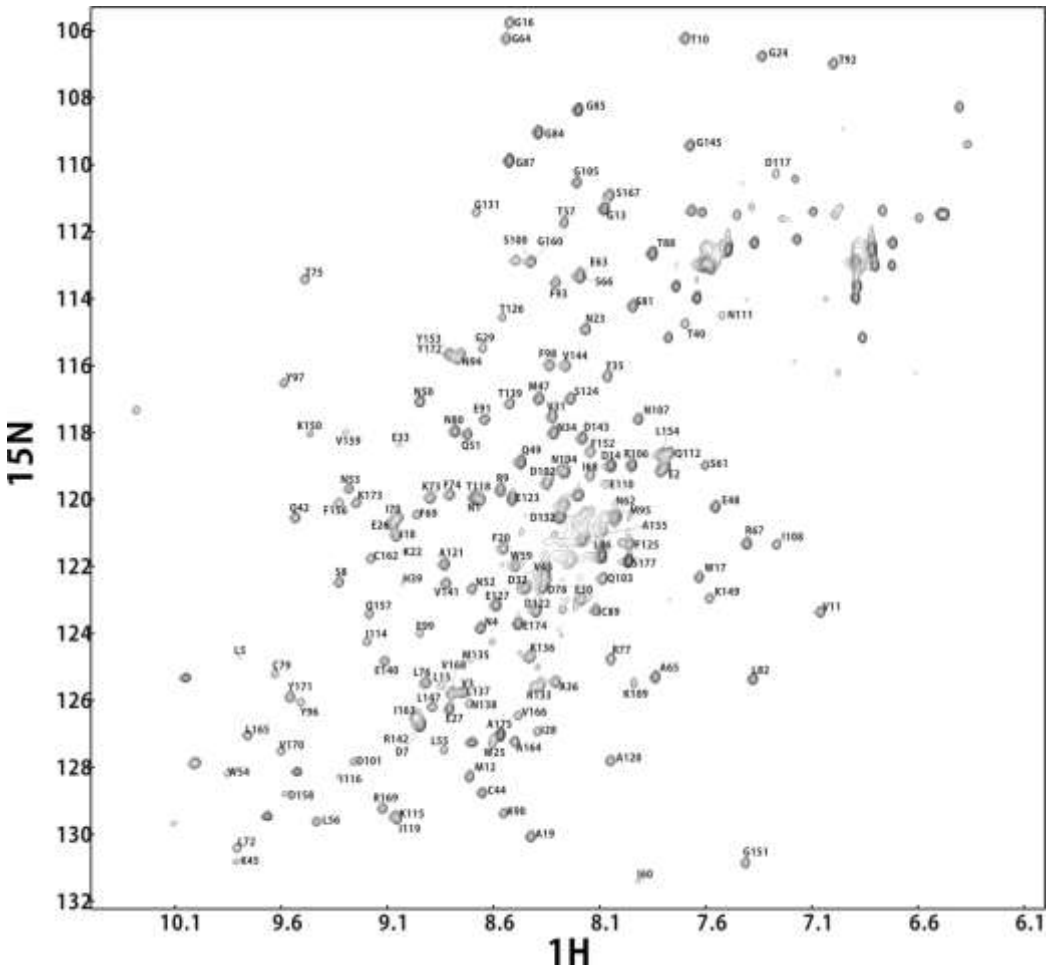

Figure 3.2.3: Assigned ^{1}H-^{15}N HSQC spectrum of the EphA5 ligand-binding domain in the absence of WDC peptide.

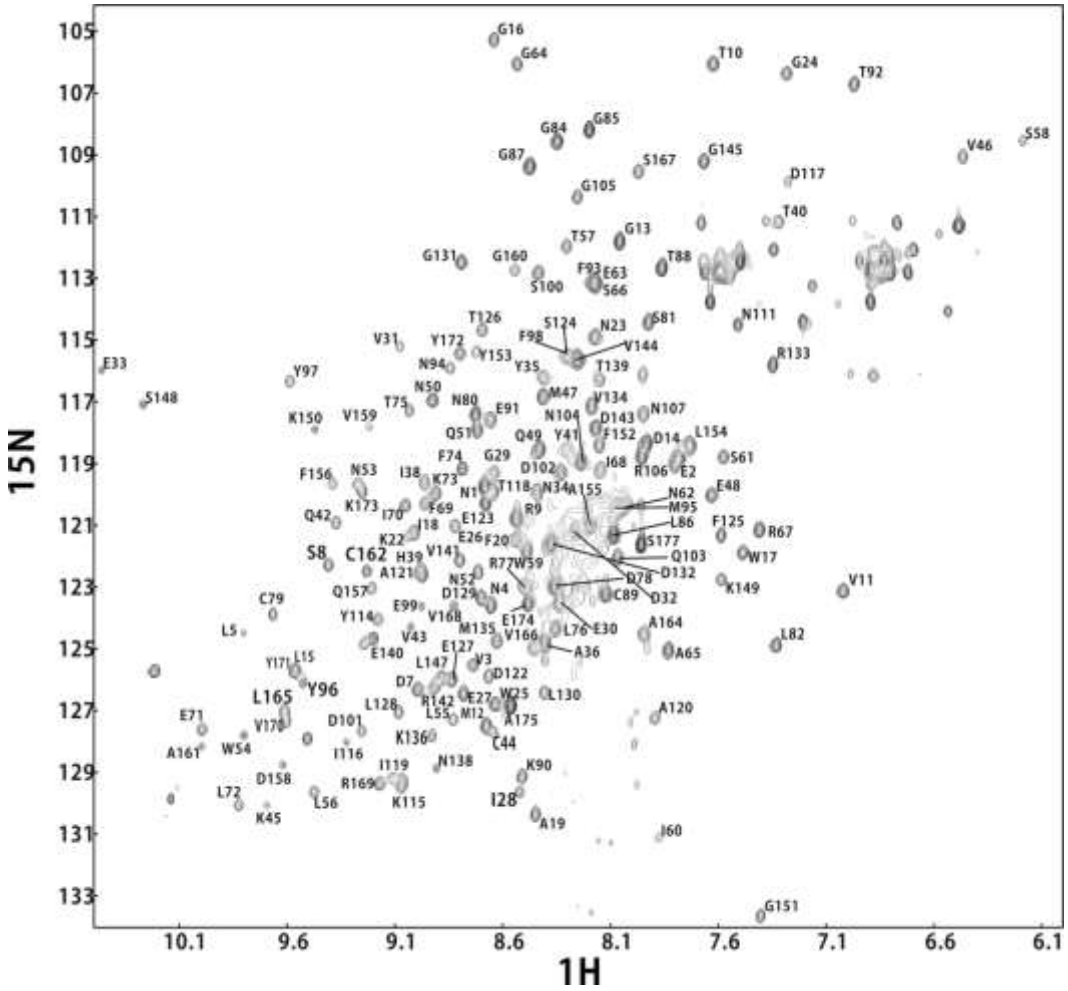

Figure 3.2.4: Assigned ^{1}H-^{15}N HSQC spectrum of the EphA5 ligand-binding domain in the presence of 3-fold WDC peptide.

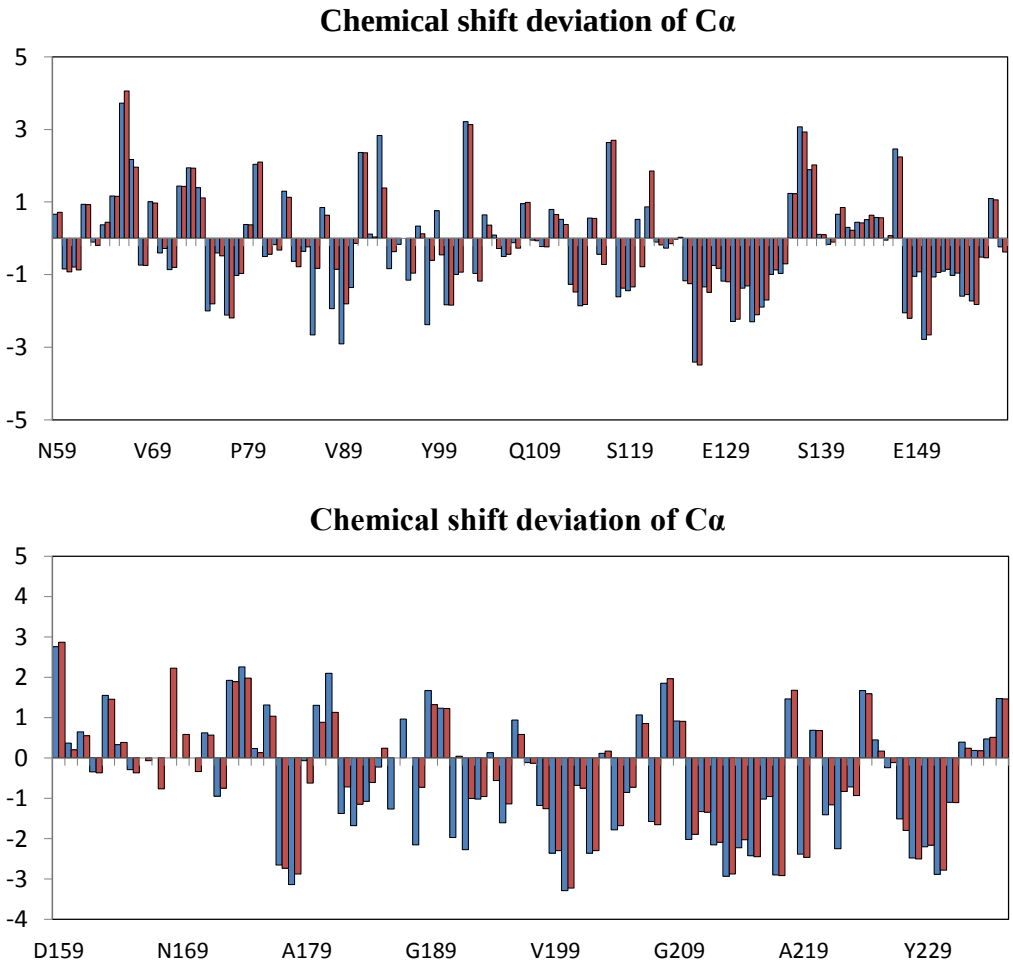

Figure 3.2.5: EphA5 LBD chemical shift deviation of Cα from random coil value provides insights in its secondary structure. Cα conformational shifts deviation of EphA5 LBD from random coil value ($C\alpha_0$) in the presence (blue) and absence (red) of WDC.

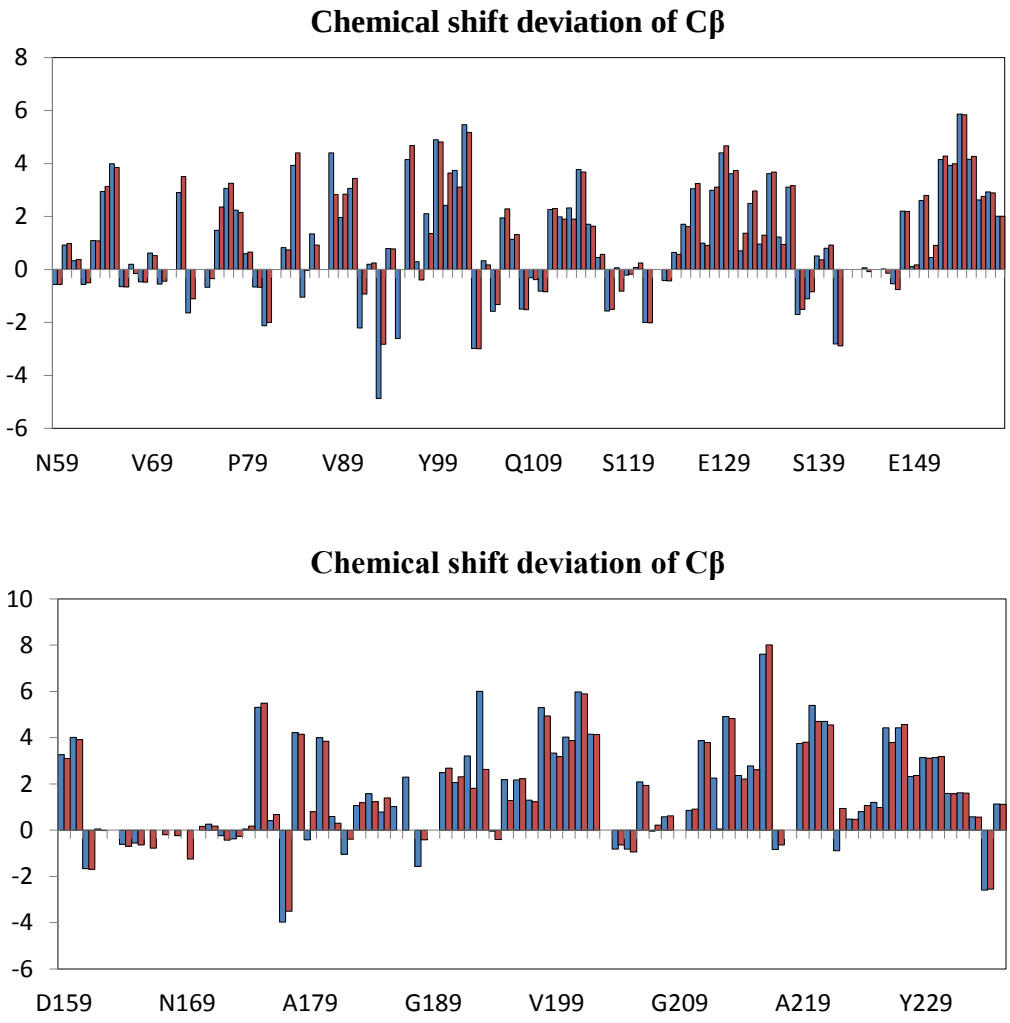

Figure 3.2.6: EphA5 LBD chemical shift deviation of Cβ from random coil value provides insights in its secondary structure. Cβ conformational shifts deviation of EphA5 LBD from random coil value ($C\beta_0$) in the presence (blue) and absence (red) of WDC.

3.2.2.2 Mapping of Binding Interface between EphA5 and WDC by Chemical Shift Perturbation Analysis

Because the chemical shift value of an NMR active atom is sensitive to its chemical environment, chemical shift perturbation analysis upon titration of ligands represents a powerful method for identifying residues that directly contact the ligands or that are indirectly affected by the binding event (Qin et al., 2008).

As shown in Figure 3.2.1A, most of the HSQC peaks of the free ^{15}N-labeled EphA5 shifted to become identical with the HSQC peaks of the complex of EphA5 and WDC spectrum when the molar ratio of EphA5 to WDC reached 1:3. When the molar ratio of EphA5 to WDC reached 1:4, the HSQC peaks showed no significant shift, indicating that the binding of EphA5 and WDC had become saturated. Therefore, the chemical shift differences (CSD) between the free EphA5 state and the complex state (the molar ratio of EphA5 to WDC was 1:3) could be calculated according to the formula $((\Delta^{1}H)^{2} + (\Delta^{15}N)^{2}/5)^{1/2}$, and the results were plotted against EphA5 sequence as shown in Figure 3.2.7.

From the results, thirteen residues of EphA5 that gave shifted resonance peaks were found with significant CSD (peaks of EphA5 with CSD value larger than 1.0 ppm). Residues of I28, G29 and V31 were located on the D β-strand, E33 was located on the D-E loop, T40 and V43 were located on the E β-strand, T75 on the G β-strand, D122, E127, R133 and K136 were on the J-K loop, N138 on the K β-strand and A164 was located on the M β-strand (Figure 3.2.8).

Previous research showed that D-E and J-K loops are the key component of the high affinity ephrin binding pocket of the Eph receptors (Himanen et al., 2009; Qin et al., 2008). In this chemical shift perturbation analysis, most of the residues with significant chemical shift differences (CSD) values were located inside the traditional binding pocket surrounded by D-E and J-K loops or on the D-E and J-K loops. Therefore, the NMR titration results suggested that WDC peptide probably bind to the highly conserved high affinity ephrin-binding pocket of EphA5 ligand binding domain with high binding affinity.

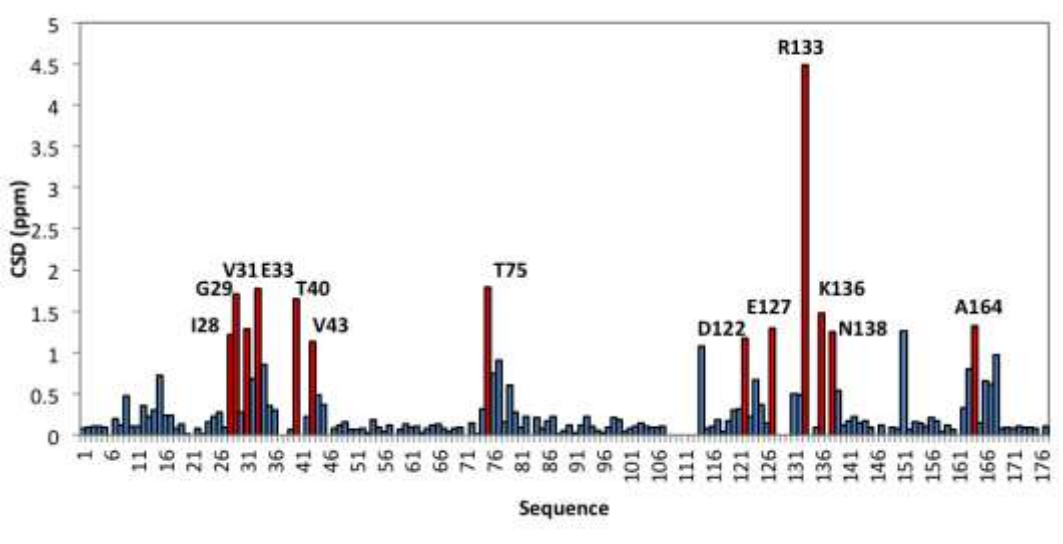

Figure 3.2.7: Residue-specific chemical shift differences (CSD) of the EphA5 ligand-binding domain in the presence of 3-fold WDC. Red bars indicate residues of EphA5 ligand-binding domain with CSD larger than 1.0 ppm.

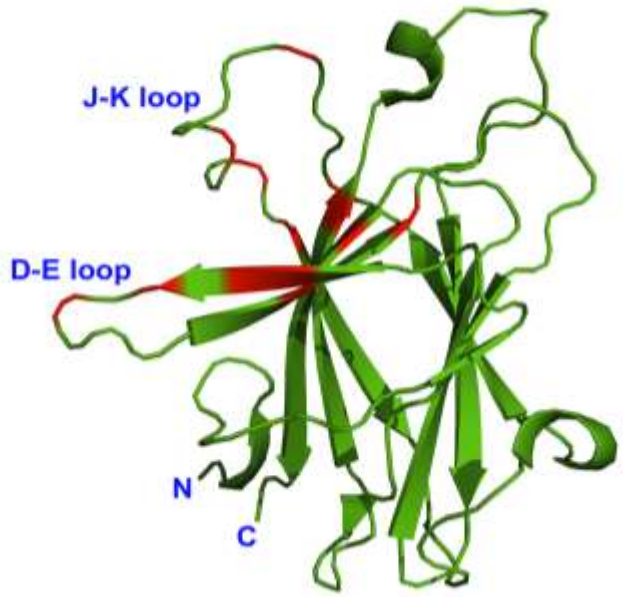

Figure 3.2.8: EphA5 ligand binding domain crystal structure with red color indicating residues of EphA5 with CSD larger than 1.0 ppm after binding with WDC peptide.

3.2.2.3 Mapping of Binding Interface between EphA5 and WTF Peptide

Figure 3.2.2A shows that dislike the binding between EphA5 ligand binding domain and WDC peptide, many HSQC peaks from the free ^{15}N-labeled EphA5 disappeared in the presence of WTF peptide, when the molar ratio of EphA5 to WTF is 1:3. Therefore, disappeared and shifted peaks were identified on the crystal structure of EphA5 ligand binding domain according to the NMR titration results, to show the active residues involved in the binding interaction of EphA5 and WTF peptide (data not shown). From the results, the HSQC peaks of 32 out of 177 residues of EphA5 ligand binding domain disappeared and two shifted when compare the spectra of free EphA5 and the molar ratio of EphA5 to WTF equal to 1:1; and the HSQC peaks of 26 residues of EphA5 ligand binding domain disappeared when compare the spectra of the molar ratio of EphA5 to WTF equal

to 1:1 and the molar ratio of EphA5 to WTF equal to 1:3. Most identified residues were located on the ephrin-binding channel, D-E loop, J-K loop, and G-H loop, indicating that WTF peptide binding with EphA5 ligand binding domain at the highly conserved ephrin-binding site. Interestingly, there are some identified residues located at the opposite site of ephrin-binding channel, suggesting that these residues may indirectly affected by the binding event due to the conformational changes when EphA5 LBD binds to WTF peptide.

3.2.3 Molecular Docking for EphA5 LBD and WDC/WTF Peptides

The structure of EphA5 ligand binding domain and the two antagonistic peptides could not be calculated with NMR distance constraints due to the absence of intermolecular NOEs between them. As an alternative, the modules of the EphA receptor ligand-binding domains in complex with the antagonistic molecules were constructed by use of the HADDOCK software (de Vries et al., 2007; Dominguez et al., 2003) in combination with CNS (Brunger et al., 1998). HADDOCK is a well-established docking procedure that makes use of the chemical shift perturbation data to drive the docking of protein-protein and protein-small molecule complexes, while at the same time, allowing various degrees of flexibility.

The x-ray structure of EphA5 ligand binding domain was used to build up the docking model. From the structures obtained from the computational docking,

complex structures with the lowest energies were selected for further display and analysis.

3.2.3.1 Molecular Docking for EphA5 LBD in complex with WDC Peptide

Attempts to co-crystalize EphA5 with WDC were not successful, so the modules of the EphA receptor ligand-binding domains in complex with GS-WDC were constructed by use of the HADDOCK software based on previous NMR titration results and CSD analysis. The solution accessible residues of the EphA5 ephrin-binding domain with larger chemical shift perturbation values were set as active residues according to the Haddock definition. As shown in Figure 3.2.9, GS-WDC peptide binds to EphA5 within its traditional ephrin ligand-binding channel. The side chain amide protons of GS-WDC residues G1 bind to two side chain oxygen atoms of E30 and Q42 on EphA5 LBD. The side chain amide proton of EphA5 residue Q42 can also interact with the backbone oxygen of S2 on GS-WDC peptide. EphA5 residue G29 backbone oxygen formed one hydrogen bond with side chain amide proton of N6 on GS-WDC peptide, consistent with the large chemical shift perturbation value showed previously. Furthermore, side chain amide protons of H11 on GS-WDC formed two hydrogen bonds with E127 and D129 on EphA5 separately. The last residue of GS-WDC, G14 also interacted with side chain amide proton of EphA5 residue R77. Hydrophobic WDC residues W3, W12 and L13 also contact with the hydrophobic patches of the ephrin-binding pocket of EphA5 (Figure 3.2.9B).

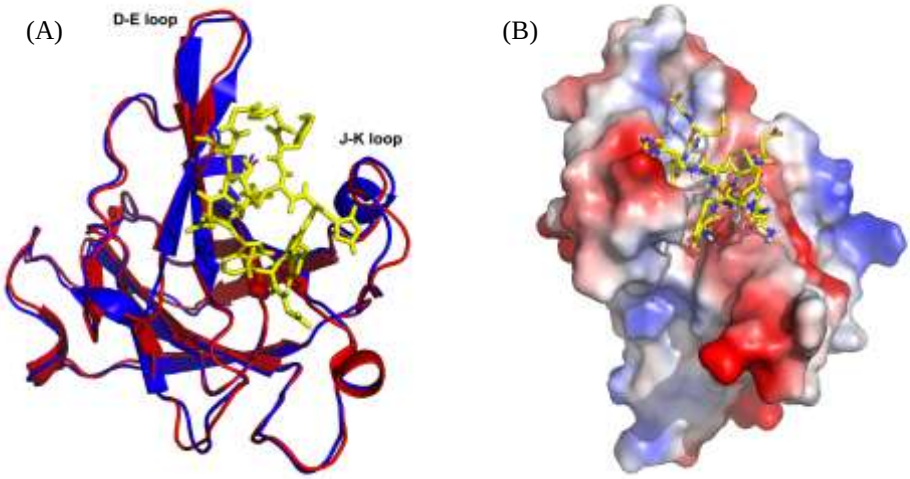

Figure 3.2.9: Models of EphA5 ligand binding domain in complex with WDC peptide. (A) Stereo view of the superimposition of the unbound EphA5 structure (red) with the selected docking model in complex with WDC peptide (blue). (B) Surface representation of the EphA5 ephrin-binding domain showing electrostatic potentials (blue: positive, red: negative, gray: neutral) and stick representation of the GS-WDC peptide (yellow).

3.2.3.2 Molecular Docking for EphA5 LBD in complex with WTF Peptide

Attempts to co-crystalize EphA5 with WTF were not successful, so the modules of the EphA receptor ligand-binding domains in complex with WTF were constructed by use of the HADDOCK software based on previous NMR titration results. As shown in Figure 3.2.10, WTF peptide also binds to EphA5 ligand binding domain within the traditional ephrin-binding pocket. Based on the docking result, hydrogen bonds forming between backbone oxygen atoms of WTF residue L6 and D9 with EphA5 residue G131 backbone amide proton on the J-K loop and S167 side chain proton separately. Side chain oxygen atoms of WDC residue D8 and D9 also interact with EphA5 residue R8 and K73 amide proton on

the side chain. The side chain amide protons of WTF residue K10 form two hydrogen bonds with two EphA5 residues on the D-E loop, D32 and E33. The side chain amide protons of WTF residue H11 also form two hydrogen bonds with the EphA5 residues D7 and E71. Hydrophobic WTF residues W1, F3, P4 and W7 establish extensive contacts with the hydrophobic patches of the ephrin-binding pocket of EphA5 (Figure 3.2.10B). For example, W1 is involved in hydrophobic contacts with EphA5 residues M47, L82, P83 and L86.

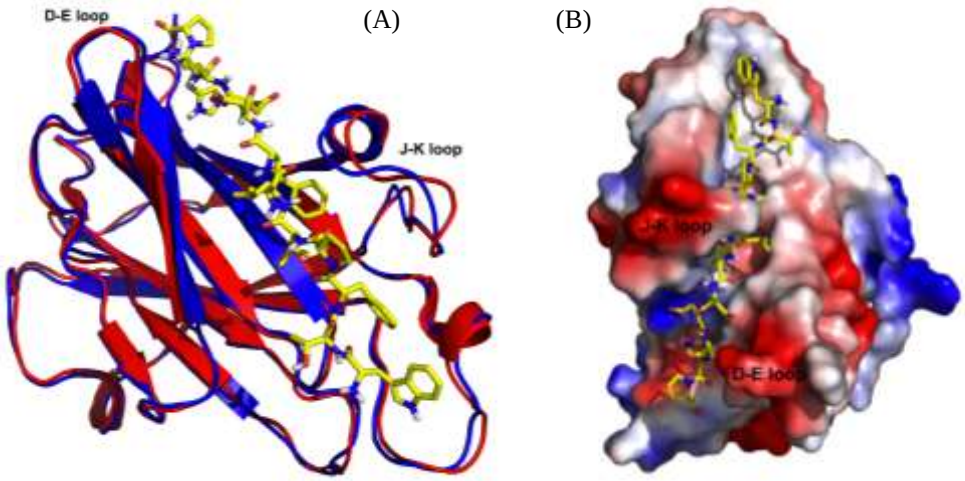

Figure 3.2.10: Docking models of EphA5 ligand binding domain in complex with WTF peptide. (A) Stereo view of the superimposition of the unbound EphA5 structure (red) with the selected docking model in complex with WTF peptide (blue). (B) Surface representation of the EphA5 ephrin-binding domain showing electrostatic potentials (blue: positive, red: negative, gray: neutral) and stick representation of the WTF peptide (yellow).

3.3 Interactions of EphA5 LBD with small molecules

As mentioned before, EphA5 receptor and its ligands play different roles in various physiological and pathological processes. Until now, not only the antagonistic peptides, but also some small molecules have been identified by high throughput screening to antagonize ephrin-induced effects by targeting Eph-ephrin binding pocket (Noberini et al., 2008). Besides these antagonistic small molecules, Doxazosin Mesylate (in short as Dox), a quinazoline compound that can selectively and competitively blocks postsynaptic alpha-1-adrenergic receptors and used for treatment of arterial hypertension and congestive heart failure, could bind to and active EphA2 and EphA4 as an agonist.

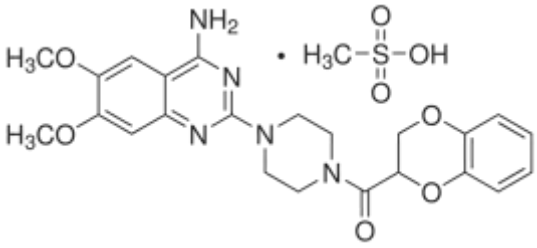

Figure 3.3.1: The chemical structures of Doxazosin Mesylate.

3.3.1 Characterization of Binding Interactions between EphA5 LBD and Doxazosin Mesylate by NMR and ITC

The NMR titration and ITC experiments were performed to assess whether Doxazosin Mesylate molecule directly interacts with the EphA5 ligand-binding domain. For visible precipitations would form with adding the Doxazosin

Mesylate solutions into the EphA5 ligand binding domain samples, we succeeded in obtaining these parameters of ITC experiments by using a low EphA5 ligand binding domain concentration (30 μM). The NMR and ITC experiments data are presented in Figure 3.3.2 and Table 3.3.1, that clearly confirming that Doxazosin Mesylate do interact with the ligand binding domain of EphA5.

For binding between EphA5 ligand binding domain and Doxazosin Mesylate, the NMR spectra showed that some of the HSQC peaks of the complex of EphA5 ligand binding domain and Doxazosin Mesylate shifted obviously compared to the free ^{15}N-labeled EphA5 when the molar ratio of EphA5 to Doxazosin Mesylate reached 1:14 (Figure 3.3.2A). From Figure 3.3.2B, C and Table 3.3.1 of ITC experiments, the K_d value for the binding of EphA5 with Doxazosin Mesylate was 6.64 μM, which was quite similar to the binding affinity between EphA5 and WDC/WTF peptides.

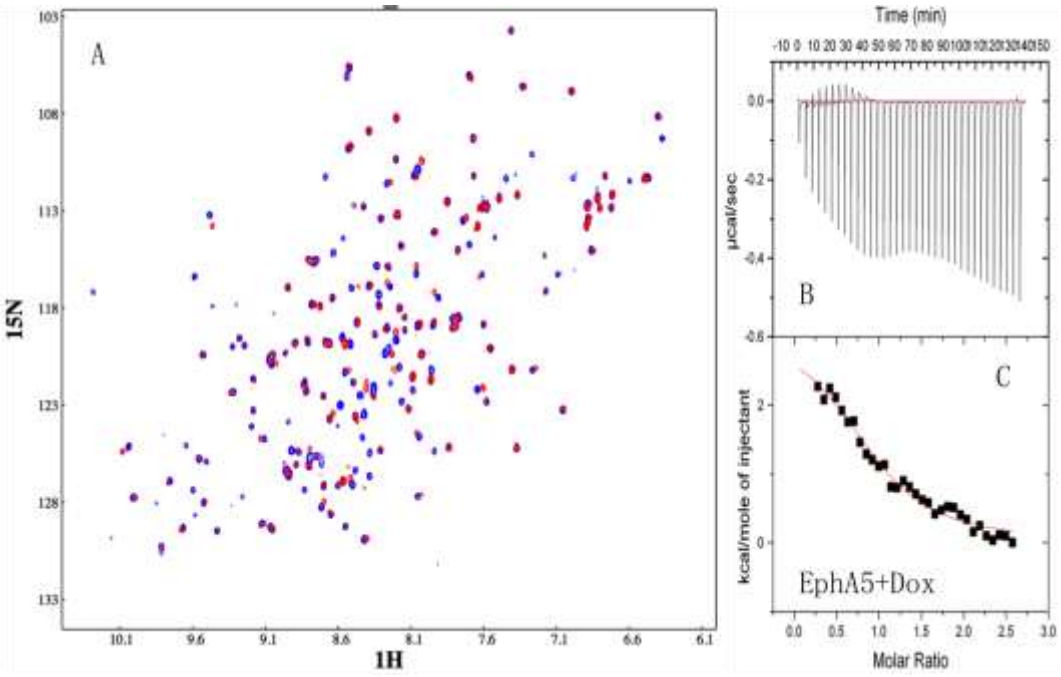

Figure 3.3.2: NMR and ITC characterization of the binding between EphA5 and Doxazosin Mesylate. (A) Superimposition of the HSQC spectra of the ^{15}N-labeled EphA5 in the absence (blue) and presence (red) of Doxazosin Mesylate at a molar ratio of 1:14. (B) ITC titration profiles of the binding reaction between EphA5 LBD and Doxazosin Mesylate. (C) Integrated values for reaction heat with subtraction of the corresponding blank results normalized by the amount of ligand injected versus Doxazosin Mesylate/EphA5 molar ratio. The detailed conditions and setting of the ITC experiments are presented in Materials and Methods as well as Table 3.3.1.

Table 3.3.1: Thermodynamic parameters of the binding interactions between EphA5 receptor with Doxazosin Mesylate.

Syringe	Cell	Temp (^{0}C)	Injection Volume (µL)	Ka (M^{-1})	Kd (µM)	Δ*S* (cal/mol*K)	Δ*H* (cal/mol)
Dox (600µM)	EphA5 (30µM)	25	5	1.506×10^5 $\pm2.832\times10^4$	6.64	34.27	3156 ±254.8

3.3.2 Mapping of Binding Interface between EphA5 LBD and Doxazosin Mesylate by Chemical Shift Perturbation Analysis

From the NMR titration experiments, a gradual shift of the EphA5 HSQC peaks were observed, correlating with the increase concentration of Doxazosin Mesylate molecules, which suggested that the free and bond EphA5 molecules undergo a fast exchange on the chemical shift timescale. To further identify the exact binding interface of EphA5 ligand binding domain and Doxazosin Mesylate complex, chemical shift perturbation analysis was done upon titration of the small compounds.

As shown in Figure 3.3.2A, some of the HSQC peaks of the complex of EphA5 ligand binding domain and Doxazosin Mesylate shifted obviously compared to the free ^{15}N-labeled EphA5 when the molar ratio of EphA5 to Doxazosin Mesylate reached 1:14. While when the molar ratio of EphA5 to Doxazosin Mesylate was higher than 1:5, the shift of many HSQC peaks was largely saturated and visible precipitation could be found inside the complex solution. Therefore, the chemical shift differences (CSD) between the free EphA5 state and the complex state (the molar ratio of EphA5 to Doxazosin Mesylate was 1:5) was calculated according to the formula $((\Delta^{1}H)^{2} + (\Delta^{15}N)^{2}/5)^{1/2}$, and the results were plotted against EphA5 sequence as shown in Figure 3.3.3.

From the results, fifteen residues of EphA5 that gave shifted resonance peaks with significant CSD (peaks of EphA5 with CSD value larger than 0.1 ppm, more than 3.0 standard deviations from the mean CSD) and two residues of EphA5 that

with peaks disappeared were identified according to the sequence. Residues of M12 was located on the A-C loop, I28, G29 and E30 were located on the D β-strand, D32, E33 and Y35 were located on the D-E loop, H39 and T40 were located on the E β-strand, T75 on the G β-strand, E127 was on the J-K loop, N138 on the K β-strand and I163, A164, V166, S167 and V168 were located on the M β-strand. All the identified residues of EphA5 ligand binding domain were labeled on the crystal structure of EphA5 as shown in Figure 3.3.4.

Previous research showed that D-E and J-K loops are the key component of the high affinity ephrin binding pocket of the Eph receptors (Himanen et al., 2009; Qin et al., 2008). Very similar to the interaction between EphA5 and WDC peptides, in this chemical shift perturbation analysis, most of the residues with significant chemical shift differences (CSD) values were located inside the traditional binding pocket surrounded by D-E and J-K loops or on the D-E and J-K loops at the presence of 5-fold Doxazosin Mesylate. Therefore, the NMR titration results suggested that Doxazosin Mesylate probably also bind to the highly conserved high affinity ephrin-binding pocket of EphA5 ligand binding domain.

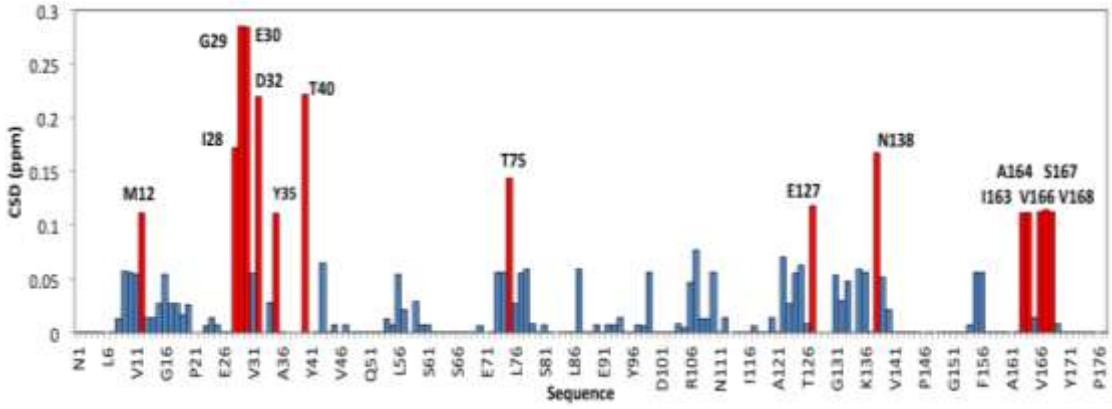

Figure 3.3.3: Residue-specific chemical shift differences (CSD) of the EphA5 ligand-binding domain in the presence of 5-fold Doxazosin Mesylate. Red bars indicate residues of EphA5 ligand-binding domain with CSD larger than 0.1 ppm (more than 3.0 standard deviations from the mean CSD).

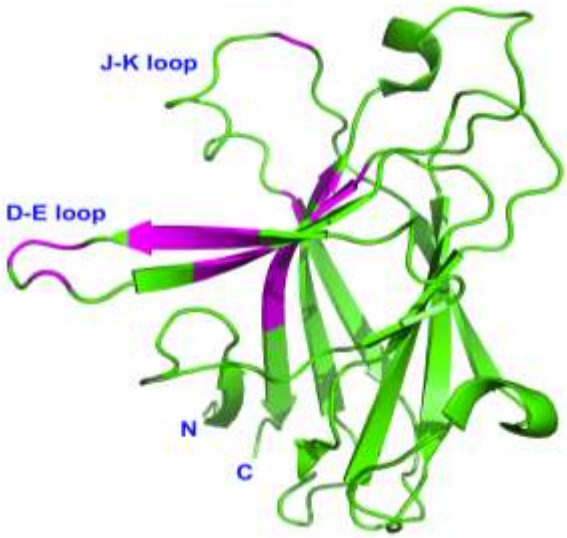

Figure 3.3.4: EphA5 ligand binding domain crystal structure with red color indicating residues of EphA5 with CSD larger than 0.1 ppm after binding with Doxazosin Mesylate.

3.3.3 Molecular Docking for EphA5 LBD and Doxazosin Mesylate

The structure of EphA5 ligand binding domain and Doxazosin Mesylate could not be calculated with NMR distance constraints due to the absence of intermolecular NOEs between them. The crystal structure of EphA5 and Doxazosin Mesylate was also difficult to get due to the gradually precipitation correlating to Doxazosin Mesylate addition. As a result, the modules of the EphA receptor ligand-binding domain in complex with the small molecules were constructed by use of the HADDOCK software (de Vries et al., 2007; Dominguez et al., 2003) in combination with CNS (Brunger et al., 1998). The x-ray structure of EphA5 ligand binding domain was used to build up the docking model. From the structures obtained from the computational docking, three complex structures with the lowest energies were selected for further display and analysis.

As shown in Figure 3.3.5, docking models EphA5 LBD with Doxazosin Mesylate showed that Doxazosin Mesylate could bind to EphA5 in its conserved ephrin-binding pocket. Consistent to the large chemical shift perturbations of residues I28, G29, E30 and D32 of EphA5 showed as Figure 3.3.3, Doxazosin Mesylate mainly bind to the D-E loop and D, E beta-strand of EphA5 ligand binding domain.

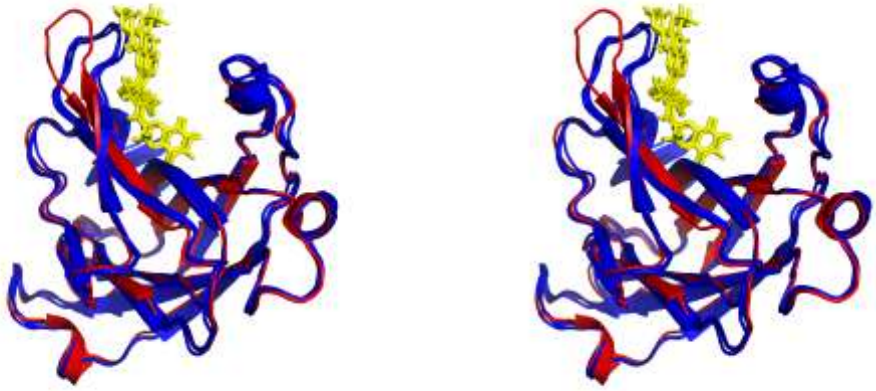

Figure 3.3.5: Docking models of EphA5 ligand binding domain in complex with Doxazosin Mesylate. Stereo view of the superimposition of the unbound EphA5 structure (red) with the selected docking model in complex with Doxazosin Mesylate (blue).

3.4 NMR Dynamics Study of EphA5 LBD

Nowadays, for determining the three dimensional structures of biological macromolecules, NMR has become a powerful technique the same as X-ray crystallography. Compared with X-ray crystallography, NMR is able to solve protein structures in solution. Based on different aims, the condition of protein solution such as salt concentration and pH can be adjusted and protein conformational changes can be traced. Furthermore, NMR is also used to study protein dynamics, protein folding and intermolecular protein interactions. In the previous sections, the crystal structure of EphA5 ligand binding domain was reported, and interactions between EphA5 ligand binding domain with different binding partner were discussed. As a complementary aspect for understanding the EphA5 ligand-binding domain, the dynamics of EphA5 in free state and in complex with other binding partners were also studied.

3.4.1 Structure Properties of EphA5 LBD Studied by NMR

As shown in Figure 3.1.3, ^{1}H-^{15}N NMR HSQC spectra of EphA5 ligand binding domain showed a well-dispersed HSQC spectrum in both dimensions (~4 ppm over ^{1}H and ~26 ppm over ^{15}N dimensions), indicating that NMR experiments would be suitable for further study of EphA5. However, the peak intensities of HSQC spectrum are not uniform, suggesting that some regions might undergo conformational exchanges on μs-ms time scale.

A pair of triple-resonance NMR spectra, HNCACB and CBCA(CO)NH were collected from a $^{15}N/^{13}C$ double-labeled EphA5 protein sample to obtain the preliminary backbone sequential assignment for EphA5. As a result, almost all 177 residues were assigned except Leu6, Pro21, Pro37, Ile38, Tyr41, Val46, Ser58, Glu71, Pro83, Tyr113, Leu128, Asp129, Leu130, Val134, Pro146, Ser148, Ala161 and Pro176, whose HSQC peaks could not be observed under the experimental conditions (Figure 3.2.3).

Previous study of NMR show that the chemical shift deviation of Cα, Cβ, Hα, and C=O from random coil value reflects the secondary structure of protein (Wishart and Sykes, 1994). After finishing all the chemical shift assignment, secondary structure of free EphA5 ligand-binding domain was calculated by both Cα and Cβ chemical shifts. Figure 3.2.5 and Figure 3.2.6 show that the secondary structures calculated by Cα and Cβ were consistent with the EphA5 crystal structure obtained by X-ray crystallography. The deviation of Cα is negative in most regions and the deviation of Cβ is positive in most regions, indicating that these regions are β-strands. To enhance the chemical shift differences, ΔCα-ΔCβ (differences of Cα-$Cα_0$ and Cβ-$Cβ_0$) was plotted to show the secondary structure characterization of EphA5 ligand binding domain. As shown in Figure 3.4.1, the positive Cα conformational shifts for the J-K loop residues Asp180-Glu181 and Gly189-Asp190 indicate that these two regions adopt a helical/loop-like conformation in solution, rather than an extended β-stranded conformation. This is

consistent with the information obtained from the crystal structure of the EphA5 LBD.

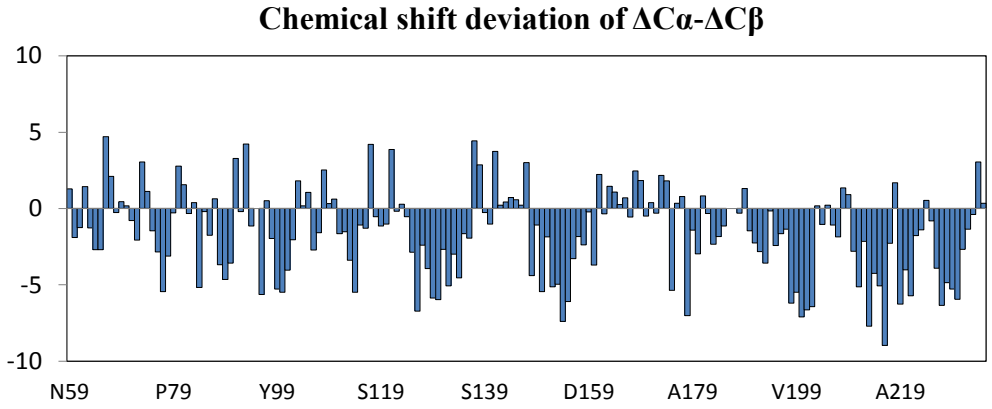

Figure 3.4.1: EphA5 LBD chemical shift deviation of ΔCα-ΔCβ.

3.4.2 NMR Dynamics Study of Free EphA5 LBD

3.4.2.1 Dynamics Study of Free EphA5 and Analysis of Relaxation Data

^{15}N NMR relaxation data, including longitudinal relaxation time T1, transverse relaxation time T2, and {^{1}H}-^{15}N steady-state NOE (hNOE) could sensitively indicate the dynamics of protein local environment on the pico- to nano-second timescale as well as dynamic aggregation. The relaxation data of free EphA5 ligand binding domain was shown in Figure 3.4.2. {^{1}H}-^{15}N steady-state NOE (hNOE) offers a reliable measure of the backbone flexibility (Clore et al., 1990; Farrow et al., 1994; Palmer et al., 1991; Ran et al., 2008). Due to the overlap and /or weak intensity of many resonance peaks resulting from the relative large size and presence of many exposed loop residues, only 128 out of 172 non-proline peaks are suitable for quantitative analysis. As shown in Figure 3.4.2C, most residues forming secondary structures have hNOE values higher than 0.75,

indicating these residues have significantly limited backbone conformational movement. Besides the N- and C-terminal residues, six additional regions also have low hNOE values. These include the A-C (Met70-Asp72), D-E (Glu88-Asn92), E-F (Met105-Asn108), G-H (Ser139-Cys147), I-J (Gly163-I166) and J-K (Asp180-Lys194) loops (Figures 5c,d). These results indicate that the loop regions are also intrinsically dynamic on the ps-ns time scale. In other words, many conformations co-exist over these loops, which are exchangeable on the ps-ns time scale.

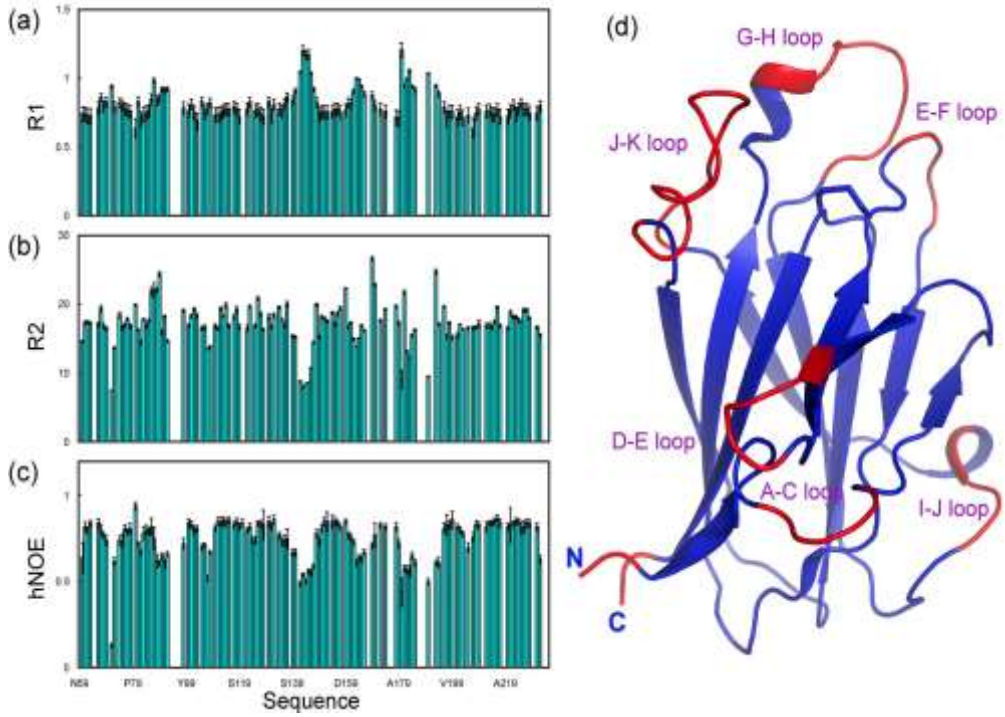

Figure 3.4.2: the ^{15}N NMR backbone relaxation data of the EphA5 ligand-binding domain in the 10 mM phosphate buffer (pH 6.3). (A) R1, inverse of ^{15}N T1 (longitudinal) relaxation times. (B) R2, inverse of ^{15}N T2 (transverse) relaxation times. (C) {^{1}H}-^{15}N steady-state NOE intensities (hNOE). (D) EphA5 LBD structure with the residues having hNOE values < the average (0.65) colored in red.

3.4.2.2 Model-free Analysis of Free EphA5 Relaxation Data

In order to obtain a general description of diverse internal dynamics in the protein, an approach based on the "Model-free" formalism was used to analyze the NMR relaxation data of free EphA5 ligand binding domain (Fairbrother et al., 1998; Fushman et al., 1997; Hall and Fushman, 2003; Lipari and Szabo, 1982). Isotropic, axially-symmetric and fully anisotropic models for the overall motions were examined and compared. Finally, a fully anisotropic model was selected and the parameters for the overall rotational diffusion of the free EphA5 LBD are shown in Supplementary Table S1. The analysis generated squared generalized order parameters, S^2, which reflect the conformational rigidity on a ps-ns time scale. The regions with secondary structure have higher S^2, indicating their rigidity at ps-ns time scale; the loop regions have lower S^2, indicating their flexibility at ps-ns time scale, ranging from 0 for high internal motion to 1 for completely restricted motion in a molecular reference frame. As shown in Figure 3.4.3A, the regions with secondary structure have higher S^2 values, consistent with the high backbone rigidity, while the loop regions have smaller S^2 values, consistent with high flexibility. In particular, the residues in the D-E, G-H and J-K loops have very low S^2 values, in agreement with the conclusions from hNOE analysis (Figure 3.4.3A and C).

Model-free analysis also yields the conformational exchange contribution values, R_{ex}, which reflects conformational exchanges on μs-ms time scale. Only 10 residues in the EphA5 LBD have Rex values >2 Hz, including residues

Gly87-Val89 in the D strand, Lys103 in the E-F loop, Leu134 in the G-H loop, Asn169-Gln170 in the I-J loop, Glu181 and Met193 in the J-K loop, Lys207 in the K-L loop (Figure 3.4.3B and D).

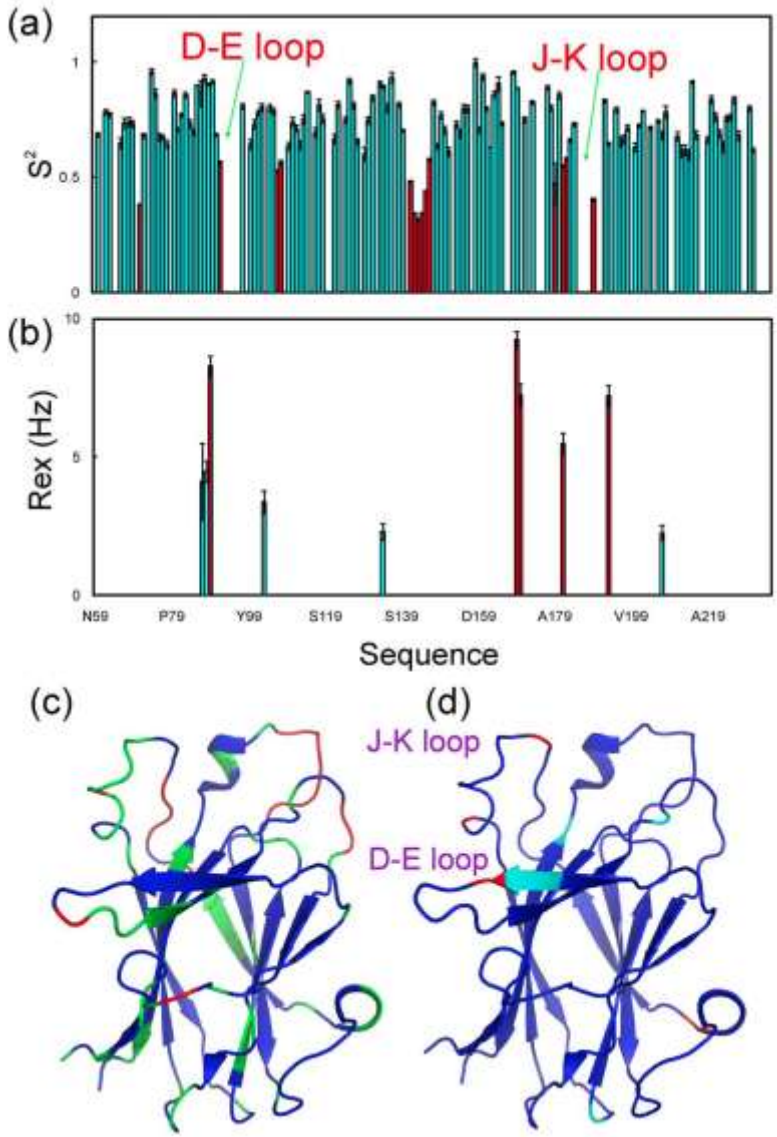

Figure 3.4.3: Model-free analysis of the EphA5 LBD. (A) Generalized squared order parameter (S^2) derived from the Model-free analysis of the relaxation data. (B) Residue-specific Rex values derived from the Model-free analysis of the relaxation data. (C) EphA5 LBD structure with the residues having S^2 < the average (0.7) colored in green and those with S^2 < the average – STD (0.5) in red. (D) EphA5 LBD structure with the residues having Rex > 2 Hz colored in cyan and those > 5 Hz colored in red.

3.4.2.3 Carr-Purcell Meiboom-Gill Relaxation Dispersion (CPMG RD) of Free EphA5 LBD

Carr-Purcell Meiboom-Gill Relaxation Dispersion (CPMG RD) is a powerful approach to obtaining kinetic, thermodynamic and structural information for exchange process of protein including side-chain reorientation, loop motion, secondary structure changes and hinged domain movement (Kleckner and Foster, 2011). Here we used CPMG experiments that are sensitive to μs-ms timescale exchange dynamics between states, to probe motion in the free EphA5 system.

A series of 2D ^{1}H-^{15}N NMR spectra were recorded containing a fixed relaxation time, during which a variable number of spin-echos with different values of τ are applied sequentially. Each value of τ can alternatively be expressed as a CPMG frequency, $\nu_{CPMG} = 1/(4\tau)$ that quantifies the rate of precession of magnetization about the axis of the applied RF pulse (Kleckner and Foster, 2011). A series of fourteen 'spin-echo' pulses with correlated CPMG frequency was applied to transverse magnetization during the relaxation delay (CPMG frequencies are 40, 80, 120, 160, 200, 240, 320, 400, 480, 560, 640, 720, 800, 960 Hz) for EphA5 sample.

In general, the magnetization vectors could be refocused by the spin-echo if each individual vector exhibits the same average chemical shift. While if exchange causes a spin to experience a different chemical shift, then the incomplete refocusing among the ensemble of molecules and would lead to signal broadening which will lead to peak intensity differences of the NMR spectra (Kleckner and

Foster, 2011). The intensity differences between the NMR spectra of CPMG frequency 40 Hz and 960 Hz were plotted against EphA5 ligand binding domain protein sequence. As shown in Figure 3.4.4, only three residues were detected with ΔR2 (τ_{cp}) > 1.5 Hz. Together with the Rex results from the Model-free analysis, this indicates that there is no significant conformational exchange over the EphA5 LBD on μs-ms time scale (Baldwin and Kay, 2009; Boehr et al., 2010; Kleckner and Foster, 2011; Loria et al., 2008; Palmer, 2009). Thus, in the unbound state the EphA5 LBD does not appear to have global conformational exchanges on the μs-ms time scale.

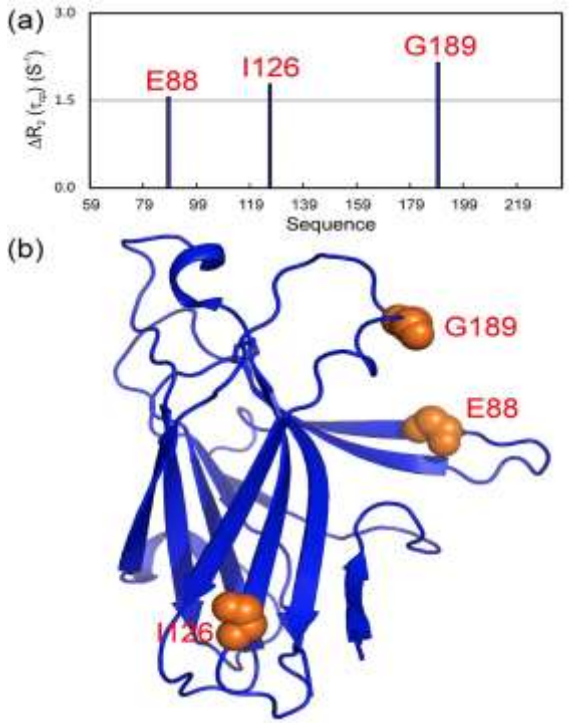

Figure 3.4.4: Dynamics of the free EphA5 LBD in the μs-ms time scale as revealed by CPMG-dispersion measurements. (A) Difference of effective transverse relaxation rate $R_2(\tau_{cp})$ at 80 and 960 Hz. Only three residues have $\Delta R_2(\tau_{cp})$ >1.5 Hz. (B) Crystal structure of the EphA5 LBD with residues having $\Delta R_2(\tau_{cp})$ > 1.5 Hz displayed as spheres.

3.4.2.4 H/D Exchange Experiment for Free EphA5 Ligand Binding Domain

The NMR hydrogen/deuterium (H/D) exchange experiment was conducted to assess the backbone dynamics of the EphA5 ligand-binding domain on min-hr timescale. As well established, in solution labile hydrogen such as amide protons on proteins are continually exchanging with the solvent at different rates, depending on a variety of factors associated with their environment including their exposure to the solvent or their involvement in H-bonds. Consequently, amide H/D exchange experiments offer a sensitive reflection of the exposure degree of amide protons to the solvent (Krishna et al., 2004; Qin et al., 2012). As shown in Figure 3.4.5A and C, upon subjecting to H/D exchange, around 58% of the 172 non-proline residues in the EphA5 LBD have completely exchanged with deuterium with the experimental dead time (15 min). These fast-exchange rate residues located not only on the loop and helical regions, but also on the beta-strands, particularly in the D and E strands (Figure 3.4.5C). After 2 hours, amide protons of additional residues undergo exchanges and only around 27% of the total residues have the HSQC peaks, which mostly located on the beta-stands (Figure 3.4.5C) and defined as slow-exchange-rate residues. After 24 hours, only around 19% of the total residues have persisted HSQC peaks (Figure 3.4.5B and D). These results suggest that the loop region of EphA5 ligand-binding domain is highly dynamic on the min-hr timescale.

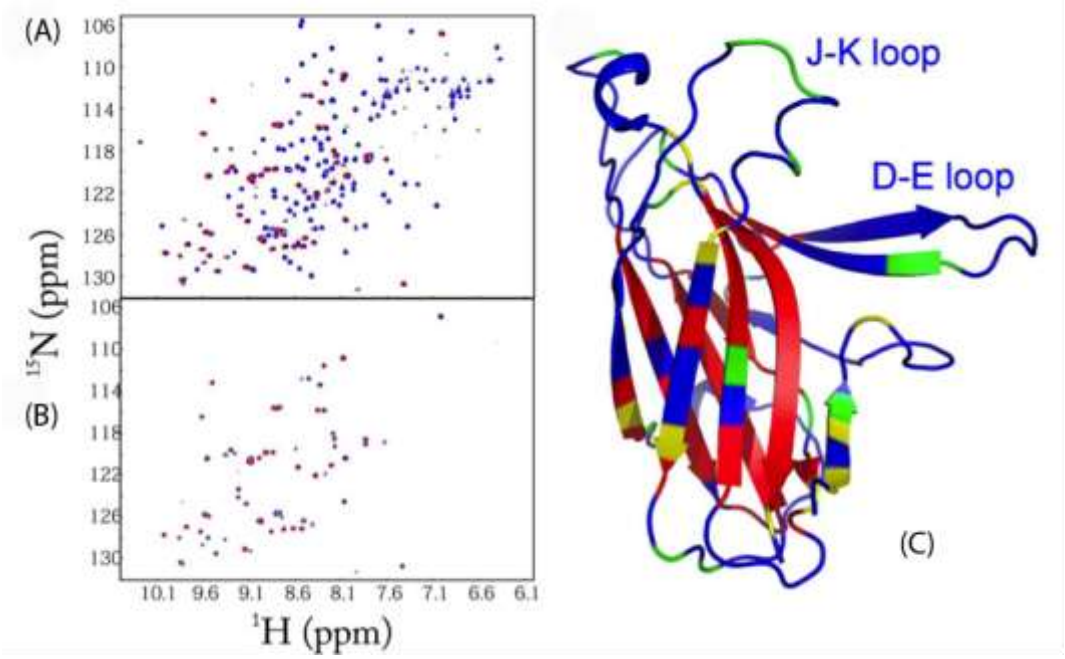

Figure 3.4.5: NMR hydrogen-deuterium (H/D) exchange for free EphA5 ligand binding domain. (A) Superimposition of the ^{1}H-^{15}N NMR HSQC spectra of the ^{15}N-labeled EphA5 LBD (blue) and 15 min after the lyophilized EphA5 LBD powder was re-dissolved in D_2O (red). (B) Superimposition of the ^{1}H-^{15}N NMR HSQC spectra of the ^{15}N-labeled EphA5 LBD, 15 min (blue) and 24 hr (red) after the lyophilized EphA5 LBD powder was re-dissolved in D_2O. (C) The structure of the EphA5 LBD with residues whose HSQC peaks were not detected even in buffer colored in green, residues whose backbone amide protons completely exchanged within 15 min in blue, residues whose backbone amide protons persisted after 15 min but completely exchanged in 2 hours in yellow and residues whose backbone amide protons persisted even after 2 hours in red.

3.4.3 NMR Dynamics Study of EphA5 LBD with WDC Peptide

3.4.3.1 Dynamics Study of EphA5 LBD with WDC Peptide and Analysis of Relaxation Data

As shown in Figure 3.2.5 and Figure 3.2.6, compare the secondary structures calculated for free EphA5 and EphA5 binding with WDC peptide, the binding of WDC to EphA5 did not induce significant conformational changes to the secondary structure of EphA5 ligand binding domain. The relaxation data of EphA5 ligand binding domain with 3-fold WDC was shown in Figure 3.4.6. $\{^{1}H\}$-^{15}N steady-state NOE (hNOE) offers a reliable measure to the backbone flexibility. Similar to the free EphA5 ligand binding domain, as shown in Figure 3.4.6A and B, most residues forming secondary structures have hNOE values higher than 0.75, indicating these residues have significantly limited backbone conformational movement. As shown in the figure, loop regions of EphA5 ligand binding domain have lower hNOE values. Residue G142 to C147 on the G-H loop has an average hNOE value of around 0.54, and residue D180 to L195 on the J-K loop has an average hNOE value of 0.54, compared to the values of free EphA5 ligand binding domain, indicating that these loop regions are more rigid with certain flexibility.

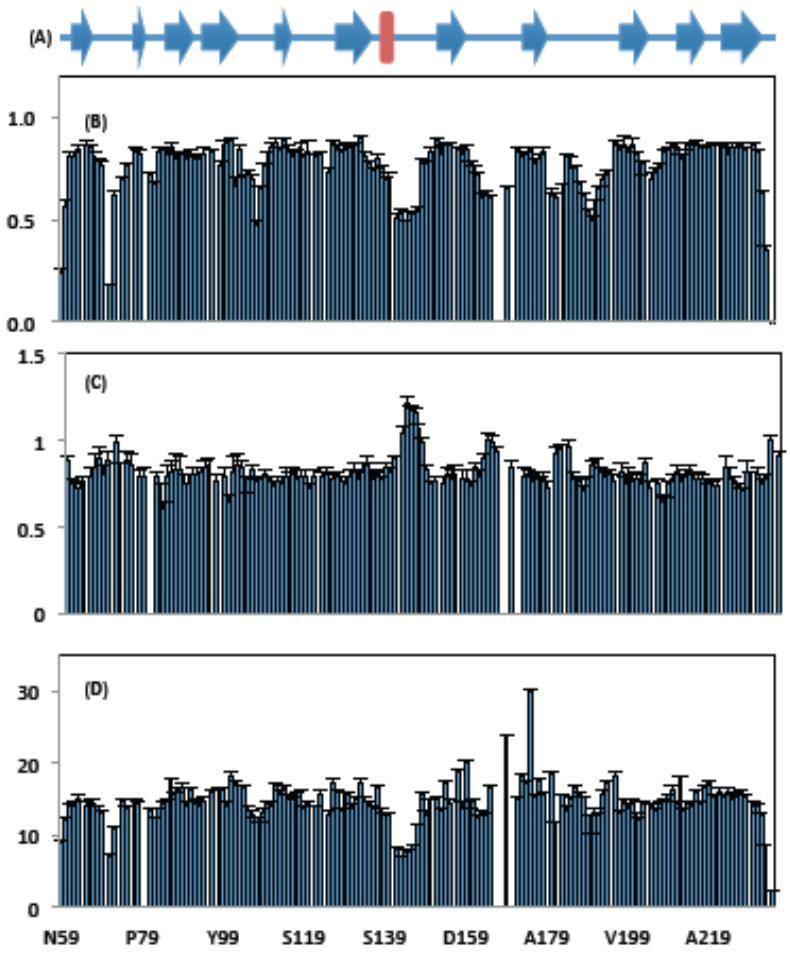

Figure 3.4.6: the ^{15}N NMR backbone relaxation data of the EphA5 ligand-binding domain with 3-fold WDC peptide in the 10 mM phosphate buffer (pH 6.3). (A) The secondary structure segments identified from the crystal structure. (B) {^{1}H}-^{15}N steady-state NOE intensity bars. (C) R1, inverse of ^{15}N T1 (longitudinal) relaxation times. (D) R2, inverse of ^{15}N T2 (transverse) relaxation times.

3.4.3.2 Carr-Purcell Meiboom-Gill Relaxation Dispersion (CPMG RD) of EphA5 LBD with WDC Peptide

Carr-Purcell Meiboom-Gill Relaxation Dispersion (CPMG RD) was also used to probe motion in the EphA5 ligand-binding domain with 3-fold WDC peptide complex system, for its sensitivity to analysis μs-ms timescale exchange dynamics. A series of fourteen 'spin-echo' pulses with correlated CPMG frequency was applied to transverse magnetization during the relaxation delay (CPMG frequencies are 40, 80, 120, 160, 200, 240, 320, 400, 480, 560, 640, 720, 800, 960 Hz) for EphA5 LBD with WDC peptide sample.

As shown in Figure 3.4.7, compared to the CPMG data of free EphA5 ligand binding domain, there are 27 residues with ΔR2 (τ_{cp}) > 1.5 Hz, indicating the complex of EphA5 ligand binding domain with WDC peptide exhibits some exchanges in solution within μs-ms timescale.

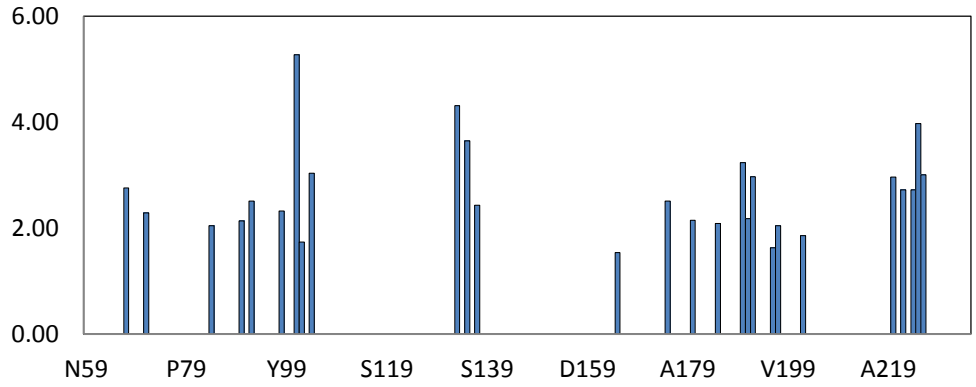

Figure 3.4.7: CPMG data analysis for EphA5 ligand binding domain with 3-fold WDC peptide.

3.4.3.3 H/D Exchange Experiment for EphA5 LBD with 3-fold WDC Peptide

The NMR hydrogen/deuterium (H/D) exchange experiment was conducted to assess the backbone dynamics of the EphA5 ligand-binding domain in present of 3-fold WDC peptide on min-hr timescale. As shown in Figure 3.4.8A, upon subjecting to H/D exchange, around 53% of the total residues have completely exchanged with deuterium with the experimental dead time (15 min) compared to 58% for the free EphA5 ligand binding domain. These fast-exchange rate residues located not only on the loop and helical regions, but also on the beta-strands (Figure 3.4.8C). After 2 hours, around 37% of the total residues have the HSQC peaks (Figure 3.4.8B) compared to 27% for the free EphA5 ligand binding domain, which located on the beta-stands and the loop regions (Figure 3.4.8C) and defined as slow-exchange-rate residues. After 24 hours, around 33% of the total residues have persisted HSQC peaks (data now shown), compared to 19% for the free EphA5 ligand binding domain. In solution labile hydrogen such as amide protons on proteins are continually exchanging with the solvent at different rates, depending on a variety of factors associated with their environment including their exposure to the solvent or their involvement in H-bonds. As shown in Figure 3.4.5C and Figure 3.4.8C, most differences located in or around the ephrin ligand binding channel, especially the D-E and J-K loop regions. For this case, these different results indicate that the interaction between WDC peptide and the EphA5 LBD inside the ligand-binding channel affected the dynamics of EphA5 ligand binding domain on the min-hr timescale, in agreement with the previous analysis.

By adding the WDC peptide, the H/D exchange rate of some residues might be decreased or stopped by involving in H-bonds formation between WDC and EphA5 ligand binding domain, some fast-exchange rate residues became slow-exchange rate residues due to the interaction of WDC and EphA5 LBD.

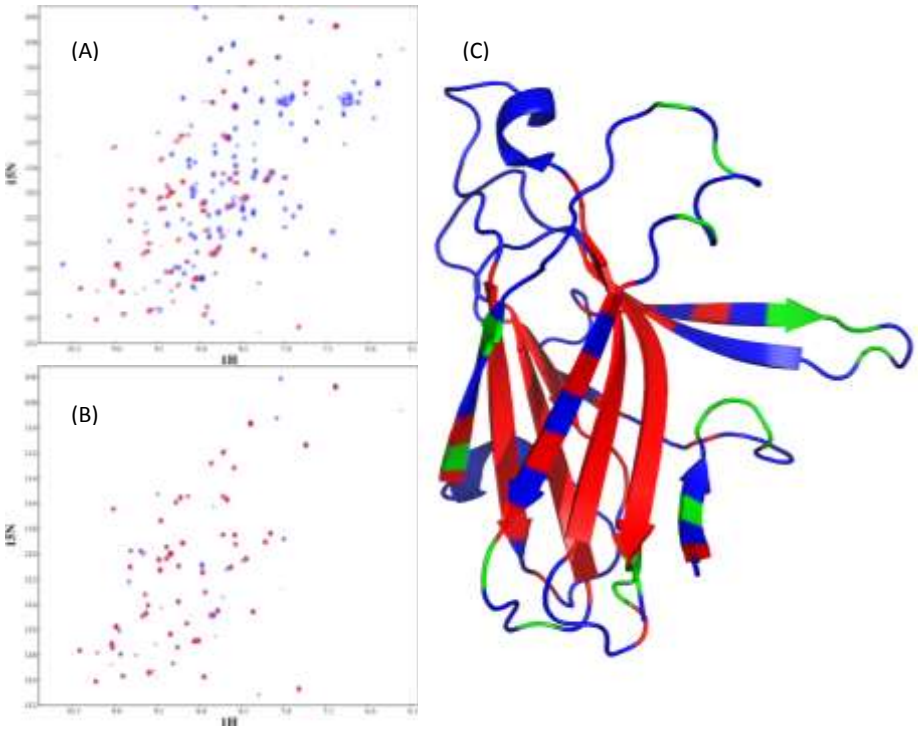

Figure 3.4.8: NMR hydrogen-deuterium (H/D) exchange for EphA5 ligand binding domain with 3-fold WDC peptide. (A) Superimposition of the ^{1}H-^{15}N NMR HSQC spectra of the ^{15}N-labeled EphA5 LBD with WDC (blue) and 15 min (red) after the lyophilized EphA5 LBD with WDC sample powder was re-dissolved in D_2O. (B) Superimposition of the ^{1}H-^{15}N NMR HSQC spectra of the ^{15}N-labeled EphA5 LBD with WDC, 15 min (blue) and 2 hr (red) after the lyophilized EphA5 LBD with WDC sample powder was re-dissolved in D_2O. (C) The structure of the EphA5 LBD with the H/D exchange results mapped onto. Blue: the residues completely exchanged with 15 min; green: residues completely exchanged from 15 min to 2 hr; red: residues un-exchanged after 2 hr.

3.4.4 H/D Exchange Experiment for EphA5 LBD with 5-fold Doxazosin Mesylate

The NMR hydrogen/deuterium (H/D) exchange experiment was also conducted to assess the backbone dynamics of the EphA5 ligand-binding domain in present of 5-fold Doxazosin Mesylate compound on min-hr timescale. As shown in Figure 3.4.9A, upon subjecting to H/D exchange, around 68% of the total residues have completely exchanged with deuterium with the experimental dead time (15 min) compared to 58% for the free EphA5 ligand binding domain (Figure 3.4.9C). After 2 hours, around 24% of the total residues have the HSQC peaks which located on the beta-stands and the loop regions (Figure 3.4.9B and C) and defined as slow-exchange-rate residues. After 24 hours, around 18.6% of the total residues have persisted HSQC peaks (data now shown). As shown in Figure 3.4.5C, Figure 3.4.8C and Figure 3.4.9C, most of the residues showing differences located in or around the ephrin ligand binding channel, including J and K beta-strands, especially the D-E and J-K loop regions. These different results indicate that dislike the interaction between WDC peptide and the EphA5 LBD, the interaction of EphA5 LBD and Doxazosin Mesylate compound did not affect the dynamics of EphA5 ligand binding domain dramatically on the min-hr timescale. Although some of the residues showing increasing the H/D exchange rate rather than decreasing the H/D exchange rate after adding Doxazosin Mesylate, no conclusion could be got until more quantificational experiments could be done.

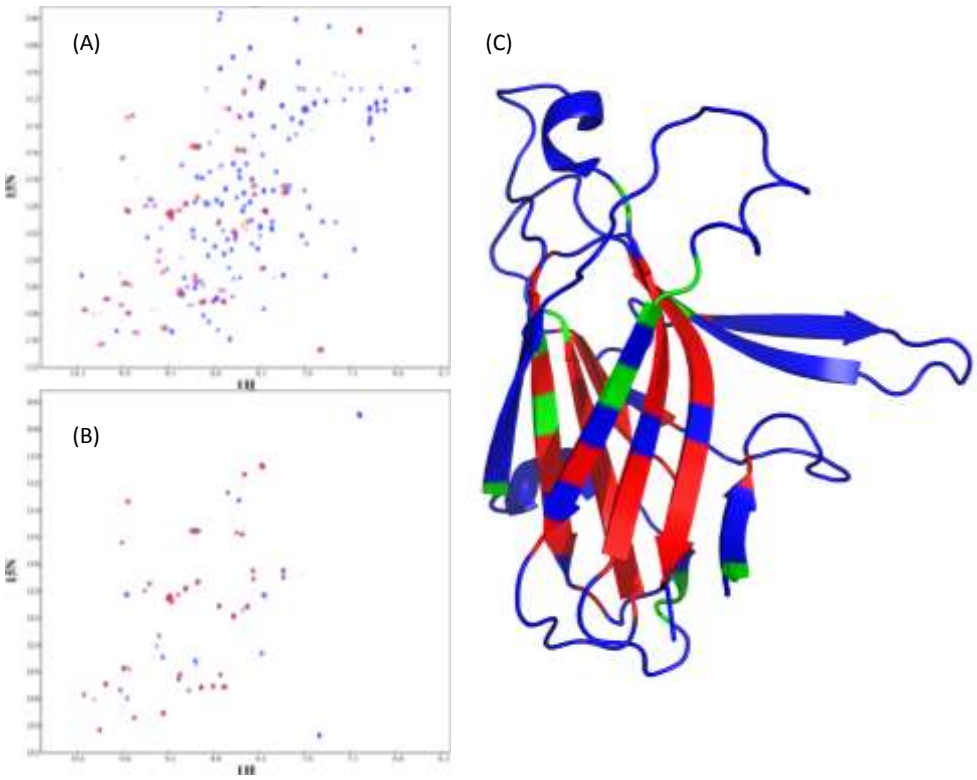

Figure 3.4.9: NMR hydrogen-deuterium (H/D) exchange for EphA5 ligand binding domain with 5-fold Doxazosin Mesylate. (A) Superimposition of the ^{1}H-^{15}N NMR HSQC spectra of the ^{15}N-labeled EphA5 LBD with Doxazosin Mesylate (blue) and 15 min (red) after the lyophilized EphA5 LBD with Doxazosin Mesylate complex sample powder was re-dissolved in D_2O. (B) Superimposition of the ^{1}H-^{15}N NMR HSQC spectra of the ^{15}N-labeled EphA5 LBD with Doxazosin Mesylate, 15 min (blue) and 2 hr (red) after the lyophilized the sample powder was re-dissolved in D_2O. (C) The structure of the EphA5 LBD with the H/D exchange results mapped onto. Blue: the residues completely exchanged with 15 min; green: residues completely exchanged from 15 min to 2 hr; red: residues un-exchanged after 2 hr.

3.4.5 PFG Diffusion Measurements for EphA5 LBD in Free State or with Peptides/compound

Numerous proteins are now recognized to depend on oligomerization for biological activity or receptor binding, so it's important to know the oligomeric state of protein sample before further structural and functional analysis. Self-diffusion is defied as translational motion reflecting the random motions of a molecule in the absence of a concentration gradient. The coefficient of this motion, D_s, is related to the average molecular size. The pulsed field gradient (PFG) NMR self-diffusion measurements can be used to measure the coefficient D_s and demonstrate the aggregation state of protein systems under conditions identical to those used in structure determination and relaxation data analysis (Altieri et al., 1995; Jansma et al., 2010).

As shown in Figure 3.4.10, the free EphA5 ligand binding domain has a D_s value of 1.10×10^{-10} m^2/s. These values are very similar to that of the EphA4 LBD measured at the same protein concentration (1.08×10^{-10} m^2/s). This supports the notion that the EphA5 LBD is a monomer in solution, as previously demonstrated for the EphA4 LBD using a variety of techniques (Bowden et al., 2009; Qin et al., 2008; Singla et al., 2010).

Assuming the interaction as hard-sphere molecular contacts, the dimer to monomer ratio of the diffusion coefficients was estimated to be 0.75 calculated from the Strokes-Einstein equations (Altieri et al., 1995). The D_s value of EphA5 LBD with WDC peptide are 1.05×10^{-10} m^2/s, the D_s value of EphA5 LBD with

WTF peptide are 1.06 × 10^{-10} m^2/s, and the D_s value of EphA5 LBD with Doxazosin Mesylate are 1.05 × 10^{-10} m^2/s. The D_s values measured for the complexes and free EphA5 LBD are quite similar, and the ratio of $D_{s,\ complex}$ to $D_{s,\ free\ EphA5}$ is 95% to 96%. These results of PFG diffusion measurements for EphA5 LBD in free state or complex indicate that adding antagonistic peptides or small compounds would not induce oligomerization or aggregation of EphA5 ligand binding domain. EphA5 ligand binding domain is a monomer in NMR experiments studies.

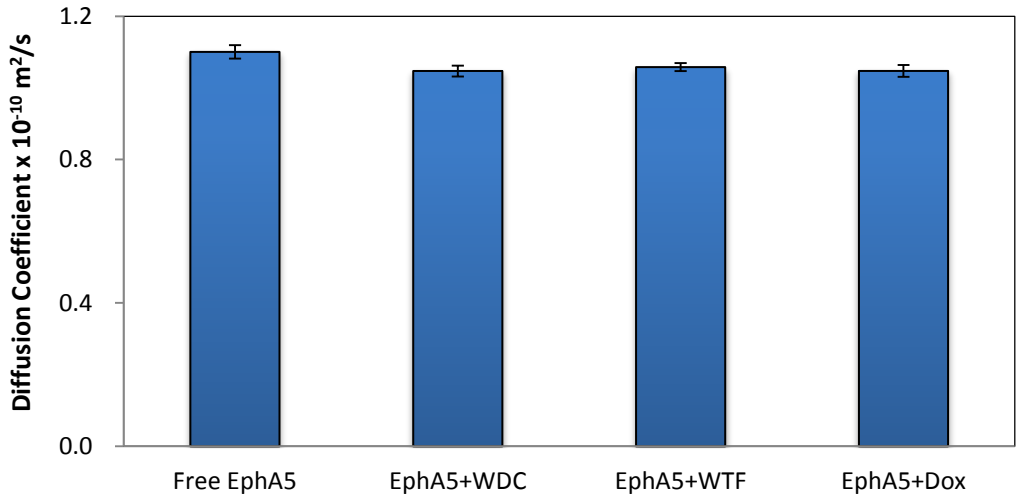

Figure 3.4.10: PFG diffusion analysis of EphA5 ligand binding domain in free state or with peptides/compound.

3.5 Discussion for EphA5 Ligand-Binding Domain

To understand the structural and dynamic mechanisms controlling the ligand binding specificity of Eph receptors, in the present study we determined the crystal structure of the EphA5 LBD without any bound ligand at a resolution of 2.9 Å. Remarkably, except for the C-terminal three residues, all residues of the EphA5 LBD including those in D-E and J-K loops are visible. Overall, the EphA5 LBD has the same jellyroll β-sandwich architecture shared by all Eph LBDs with structures previously determined. Nevertheless, EphA5 residues Ala179-Ser182 and Gly189-Met193 in the J-K loop assume helical-like conformations in the crystal structure, unlike the unbound EphA2, EphA4 and EphB2 LBDs, in which the corresponding residues form a short β-sheet. Further analysis of NMR Cα chemical shifts indicates that these residues also adopt a helical-like conformation in solution. Furthermore, comparison with the other available Eph receptor LBD structures surprisingly reveals that the J-K loop conformation of EphA5 in the unbound state resembles those of other Eph receptor LBDs in complex with ephrins.

This structural feature likely enables the unique binding selectivity of the EphA5 LBD towards different ligands. To test the activity of the EphA5 LBD structure, two antagonistic peptides, WDC and WTF and one agonistic small compound, Doxazosin Mesylate was used. All the three components could bind to EphA5 LBD in the conserved ephrin-binding channels with different binding affinities. For example, the EphA5 LBD is able to bind WDC, a peptide that is

highly selective for EphA5, with a Kd of 6.22 μM. However, it shows no detectable ability to interact with C1, an antagonistic small molecule that preferentially targets the EphA2 and EphA4 LBDs, which have a short β-sheet within their J-K loop.

The role of protein dynamics in modulating protein-ligand interactions is only beginning to be delineated. The differential dynamics on different time scales may explain the variable binding affinities and specificities observed for different Eph receptor LBDs, even though they have the same overall fold. Indeed, we have recently demonstrated that the widely variable loop conformations observed in different EphA4 LBD crystal structures are correlated with the co-existence of multiple conformations in solution, which are interconvertible on the ps-ns time scale. On the other hand, it appears that the binding to ephrins shifts the equilibrium of the conformation assembly of the EphA4 LBD from the closed form characterized by the presence of a short β-sheet in the J-K loop, which is populated in the free state, to an open form where the short β-sheet is transformed into a helical-like conformation. Because of a relatively large energy barrier, the exchange between the closed and open conformations likely occurs on a slower (μs-ms) time scale.

In this study, we have further utilized NMR spectroscopy to assess the dynamic features of the EphA5 LBD on three time scales: ps-ns, μs-ms and min-hr. Analysis of NMR backbone relaxation data show that, similar to what was observed for EphA4, the EphA5 loop regions also have high backbone dynamics

on the ps-ns time scale. This implies that the loops can have multiple conformations that co-exist in solution and that are exchangeable on the ps-ns time scale. Interestingly, these unusually high dynamics of the D-E strands and loop appear to lead to high solvent exposure of the high affinity ephrin-binding pocket of EphA5. This notion is experimentally supported by the H-D exchange experiments, which show that many residues in the EphA5 D-E strands and loop have their backbone amide protons completely exchanged with deuterium within the 15 min dead time of the experiment, while the corresponding residues in the EphA4 LBD remain unexchanged even after 24 hours.

Model-free analysis indicates that very limited conformational exchanges exist in the EphA5 LBD on the μs-ms time scale, which is further confirmed by the CPMG-based relaxation dispersion measurements. These results do not support the existence of multiple conformations of the EphA5 LBD with large structural differences that would require microseconds to milliseconds to interconvert. We therefore propose that unlike the EphA4 LBD, which has very different J-K loop conformations in the free and ephrin-bound states, the EphA5 LBD has very similar conformations in both the free and ephrin-bound states. Supporting this notion, in the free state the populated conformations of the EphA5 LBD are already highly similar to the open form for the EphA2, EphA4 and EphB2 LBDs in complex with ephrins. Therefore, the EphA5 LBD conformations populated in the free state, which are characterized by multiple loop conformations exchangeable on the ps-ns time scale, are likely ready to bind

ephrin-A ligands. On the other hand, the unusual dynamics of the EphA5 D-E loop may depend on the unique conformation of the J-K loop. Because the J-K loop has no large conformational exchanges on the μs-ms time scale, the D-E loop has to be more dynamic on the ps-ns time scale to facilitate the insertion of the ephrin G-H loop. Taken together, our results suggest that the EphA5 receptor may be capable of binding ephrin-A ligands by undergoing only minor rearrangements of the D-E, G-H and J-K loops, which are facilitated by their high intrinsic dynamics on the ps-ns time scale.

3.6 EphA7 Ligand-Binding Domain

3.6.1 Expression and Purification of EphA7 LBD

The recombinant his-tag protein of EphA7 ligand-binding domain was over expressed in *E. coli* Rosetta-gami (DE3) cells (Novagen) to get the correct formation of disulfide bonds. The harvested cells were sonicated in the PBS lysis buffer to release soluble His-tag EphA7 proteins. Then the recombinant proteins were subsequently purified under native condition and cleaved by in-gel cleavage at room temperature with thrombin overnight. The released EphA7 protein was purified on an AKTA FPLC machine using a gel filtration column. The whole expression and purification process and the purity of the purified protein were assessed by SDS-PAGE using 15% gel.

For the crystallization of EphA7 LBD, the harvested cells were sonicated in Tris buffer. To increase the purity of the protein, the eluted fractions from gel filtration step were then purified by ion-exchange chromatography using anion-exchange column (Mono Q 10/100) after purified by gel filtration column. The purity of the protein was verified by the SDS-PAGE, and the identity of EphA7 was verified by MALDI-TOF mass spectrometry (data not shown).

3.6.2 Structural Characterization of EphA7 LBD by CD

The structural properties of EphA7 ligand-binding domain were fist investigated by far-UV CD spectroscopy. As shown in Figure 3.6.1A, the spectrum

of EphA7 protein in 10mM phosphate buffer (pH 6.3) had a maximal negative peak at around 212 nm, which implied that EphA7 ligand-binding domain has a typical β-conformation. The near-UV CD spectra of EphA7 in the absence and presence of 8 M urea were also done to see the overall tertiary packing (Figure 3.6.1B). The near-UV spectra showed that without the 8 M urea, EphA7 adopted tight tertiary packing, while the property was lost under denatured condition with 8 M urea. All the data were from three independent scans and were added and averaged.

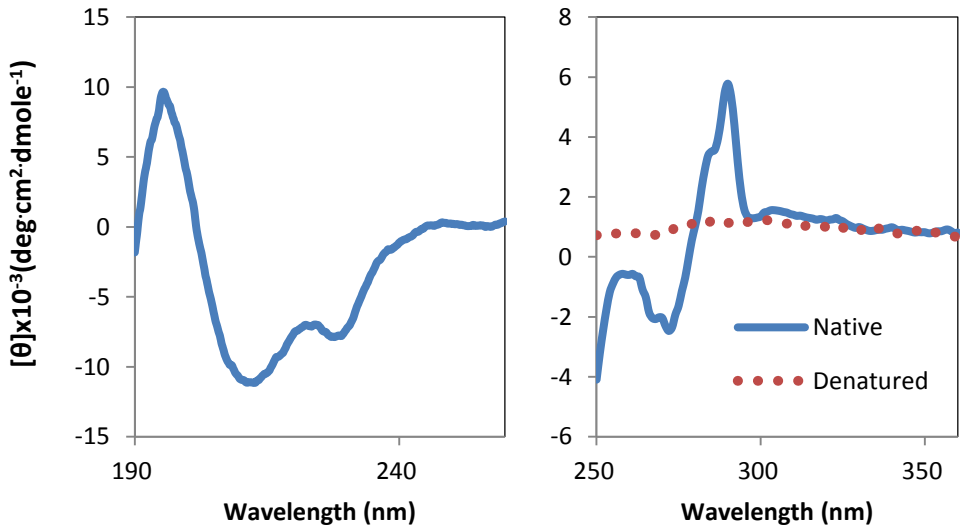

Figure 3.6.1: Preliminary structural characterization of EphA7 ligand binding domain by CD. (A) Far-UV CD spectrum of 20 µM EphA7 in the 10 mM phosphate buffer (pH 6.3). (B) Near-UV CD spectra of EphA7 in 10 mM phosphate buffer (pH 6.3) without (blue) and with 8 M urea (red).

3.6.3 NMR Structural Characterization of EphA7 LBD

NMR HSQC experiment was used to further assess the structural properties of the EphA7 ligand-binding domain, which is a sensitive probe to both secondary structure and tertiary packing. As shown in Figure 3.6.2, ^{1}H-^{15}N NMR HSQC spectra of EphA7 ligand binding domain showed a well-dispersed HSQC spectrum in both dimensions (~4 ppm over ^{1}H and ~25 ppm over ^{15}N dimensions), indicating that this protein had a well-packed tertiary structure as confirm by the CD spectra. Therefore, NMR experiments would be suitable for studying the structure of EphA7, binding affinity of EphA7 interacting with its ligands.

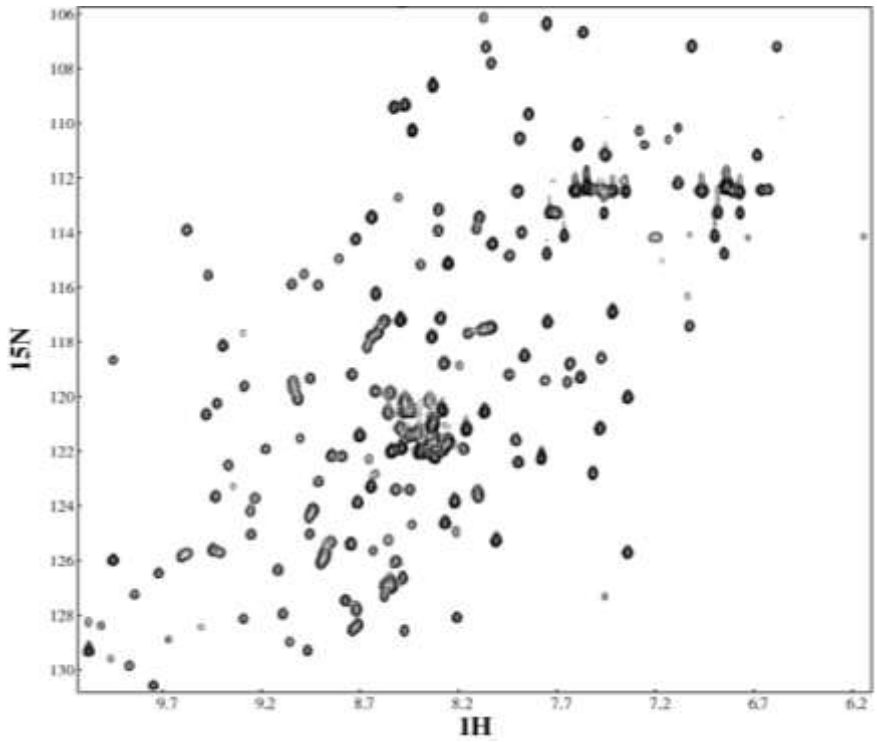

Figure 3.6.2: ^{1}H-^{15}N HSQC spectrum of the EphA7 ligand-binding domain collected in a phosphate buffer at pH 6.3.

3.6.4 Crystal Structure of EphA7 LBD

The EphA7 ligand binding domain was prepared in a buffer containing 25 mM Tris-HCl (pH 7.8), 150 mM NaCl and 5 mM $CaCl_2$ at a concentration of 10 mg/ml. Crystal screen was set up by preparing 1 µl of the protein solution mixed with 1µl of the reservoir solution as hanging drops at room temperature in a well containing the reservoir solution. Rock-like crystals formed in the well containing 1.4 M sodium chloride, 0.1 M sodium acetate trihydrate, and pH 4.6 after 3 days.

3.6.4.1 Structure of EphA7 LBD Determined from Crystal

X-ray diffraction images for a single crystal were collected using an in-house Bruker X8 PROTEUM x-ray generator with a CCD detector. The crystal was protected by cryoprotectant (1.4 M sodium chloride, 0.1 M sodium acetate trihydrate, 25% glycol, pH 4.6). The data were indexed and scaled in the space group $C222_1$ (a=128.89, b=138.32, c=143.31), with six molecules per asymmetric unit (AU), using the program HKL2000. The Matthews coefficient was 2.6 with 52.75% solvent constant.

The crystal structure of EphA7 ligand binding domain was determined by the Molecular Replacement method using EphA4 ligand binding domain (Protein Data Bank code 3CKH) as a search module using Phaser and MolRep in the Suite CCP4. The crystal structure was subsequently completed by manual fitting with the program COOT and further refined with program suite Crystallography & NMR System (CNS) (Brunger et al., 1998) at 3.0 Å resolution with a final

R-factor of 0.2468 (R_{free}=0.3220). The final structure was analyzed by PROCHECK, and details of the data collection and refinement statistics are shown in Table 3.6.1.

As shown in Figure 3.6.3, there are six molecules in one asymmetric unit (AU). The EphA7 ligand-binding domain adopts the jellyroll folding architecture, identical to other previous revealed Eph receptors (Figure 3.6.4). The jellyroll consists of 11 anti-parallel beta-sheets arranged as a compact beta-sandwich, which connected by loops of different length and two disulfide bonds. Most of the electron density map is complete for EphA7 LBD structure. While dislike the crystal structure of EphA5 LBD, the J-K loops are partially invisible, like some previous determined unbound Eph receptor LBD structures. This might due to the high intrinsic dynamics of the loop regions.

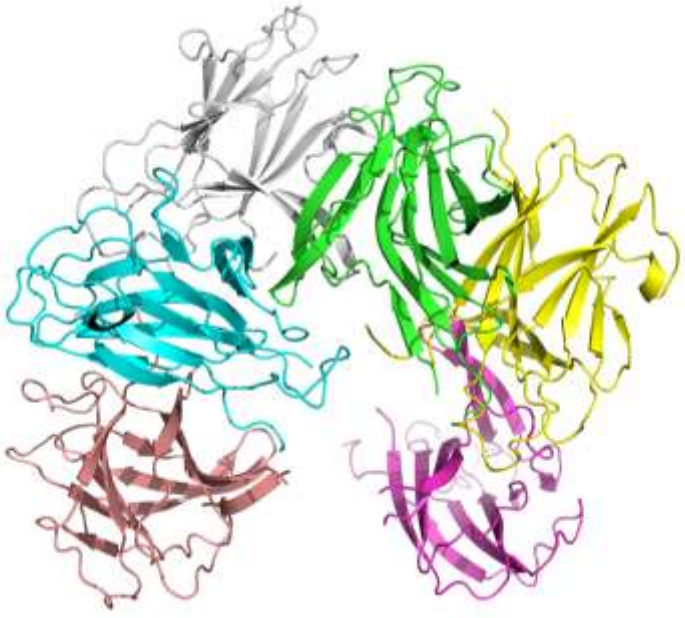

Figure 3.6.3: Pattern of the EphA7 LBD clusters.

Table 3.6.1: Crystallographic data and refinement statistics for the EphA7 ligand-binding domain structure.

Data collection	
Wavelength (Å)	1.5418
Resolution range (Å)	50.0 to 3.0
Space group	C222(1)
Cell parameters	
a, b, c (Å)	128.89, 138.32, 143.31,
α, β, γ (°)	90, 90, 90
Observed Reflections	305369
Unique Reflections	26019
Redundancy	11.9
Completeness (%)	94.92
Overall (*I/σI)*	13.809
Rsym	0.133
Refinement	
Resolution range (Å)	50.0 to 3.0
R_{work}*	0.2468
No. of reflections	25996
R_{free}**	0.3220
No. of reflections	1418
RMSD bond lengths (Å)	0.0104
RMSD bond angles (°)	1.655
Ramachandran Plot	
Most favored region (%)	66.1
Additional allowed regions (%)	28.4
Generously allowed regions (%)	4.4
Disallowed regions (%)	1.1
B-factors	
Protein	24.261
Water	23.907

*$R_{work}= \Sigma |F_{obs} - F_{calc}|/ \Sigma F_{obs}$ where F_{calc} and F_{obs} are the calculated and observed structure factor amplitudes, respectively.
**R_{free}=as for R_{work}, but for 10.3% of the total reflections chosen at random and omitted from refinement.

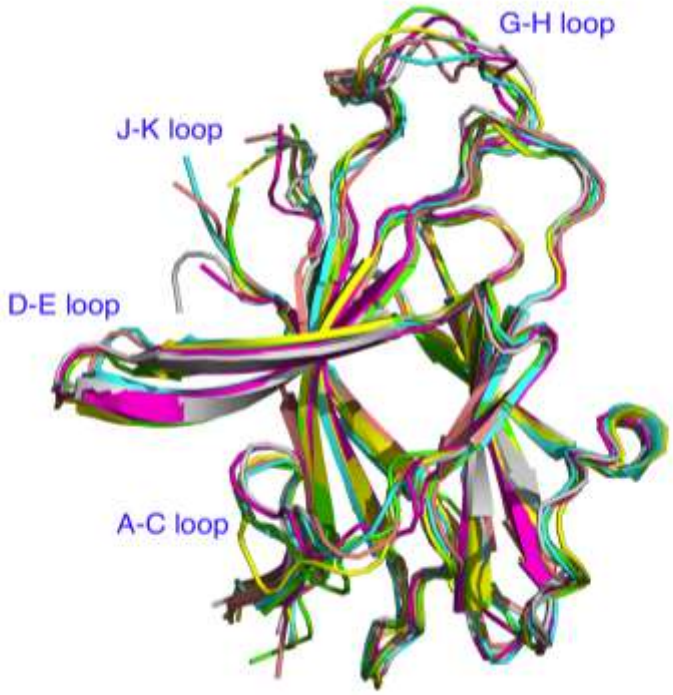

Figure 3.6.4: Comparison between 6 EphA7 LBD structures.

3.6.4.2 Comparison between 6 EphA7 LBD Structures and Previous EphA7 Structures

Comparison of the six EphA7 LBD structures shows that except for the loop regions, the regions with secondary structure are highly superimposed (Figure 3.6.4). For the loop regions, especially A-C, D-E, G-H and J-K loop region, the adoption of various conformations shows their high flexibility.

The previous released EphA7 LBD crystal structure (3NRU) was expressed in an insect system. Although our EphA7 LBD protein was expressed in *E.coli*, the protein has correctly formed two disulfide bridges, one within the G-H loop (Cys^{109}-Cys^{119}) and the other between the E-F and L-M loops (Cys^{74}-Cys^{192}) (Figure 3.6.5). This pattern of disulfide bonds is identical to that observed

previously in other EphA and EphB receptor ligand binding domains. The previous released EphA7 LBD crystal structure (3NRU) adopts 12 molecules in one asymmetric unit (AU), and they are almost the same except for some small differences in the loop regions. As shown in Figure 3.6.5, compare our EphA7 LBD structure with the previous one, only the loop regions show some differences.

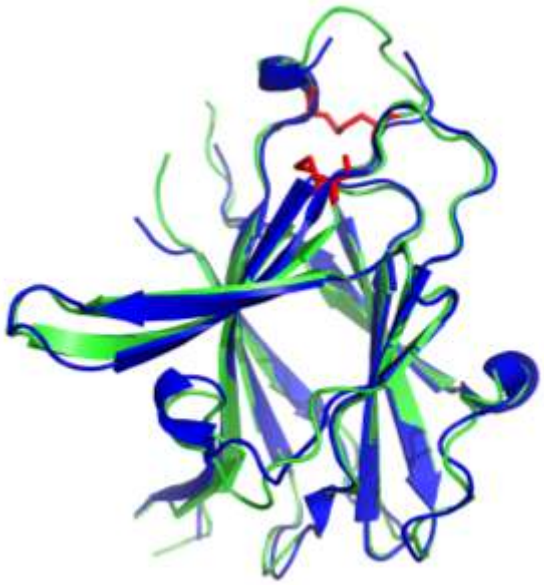

Figure 3.6.5: Comparison of our solved EphA7 LBD structure with the previous released EphA7 structure (3NRU). The disulfide bonds of our EphA7 LBD structure are colored in red. Our solved EphA7 LBD structure is green and the previous released EphA7 structure (3NRU) is blue.

The structure of EphA7 ligand binding domain bears a highly similar jellyroll folding architecture composed of 11 antiparallel beta-stands to the previously determined ligand binding domains of the EphA2, EphA4, EphB2 and EphB4 receptors (Figure 3.6.6). The backbone r.m.s.d. of the EphA7 ligand binding domain over 11 beta-strands are quite small compared with the previous solved Eph receptor structures. On the other hand, although failed to compare the J-K

loop region of the structures due to the invisibility of J-K loop of EphA7, very large variations could be observed for the D-E loop regions, which are critical for ligand binding, not only between EphA7 and the EphB receptors but also between Eph receptors from the same A- or B-subclasses.

Figure 3.6.6: Structure comparison. Stereo view of the superimposition of EphA7 LBD structure (blue) with previously determined EphA2 (3C8X), EphA4 (3CKH) and EphB2 (3ETP) structures.

3.6.5 Structure Properties of EphA7 LBD Studied by NMR

As shown in Figure 3.6.2, ^{1}H-^{15}N NMR HSQC spectra of EphA7 ligand binding domain showed a well-dispersed HSQC spectrum in both dimensions (~4

ppm over ^{1}H and ~25 ppm over ^{15}N dimensions), indicating that NMR experiments would be suitable for further study of EphA7.

A pair of triple-resonance NMR spectra, HNCACB and (H)CC(CO)NH were collected from a $^{15}N/^{13}C$ double-labeled EphA7 protein sample to obtain the preliminary backbone sequential assignment for EphA7. Almost all 177 residues were assigned except Lys1, Glu2, Val3, Lys9, Pro21, Pro22, Pro37, Pro49, Asn64, Pro83, Asp101, Arg106, Arg109, Pro146 and Ala161, whose HSQC peaks could not be observed under the experimental conditions (Figure 3.6.7).

After finishing all the chemical shift assignment, secondary structure of free EphA7 ligand-binding domain was also calculated by both Cα and Cβ chemical shifts. Figure 3.6.8 A and B showed that the secondary structures calculated by Cα and Cβ. The deviation of Cα is negative in most regions and the deviation of Cβ is positive in most regions, indicating that these regions are β-strands. To enhance the chemical shift differences, as shown in Figure 3.6.8C, ΔCα-ΔCβ (differences of Cα-$Cα_0$ and Cβ-$Cβ_0$) was plotted to show the secondary structure characterization of EphA7 ligand binding domain. Similar to other Eph receptors, EphA7 is also composed of β-strands together with some loops.

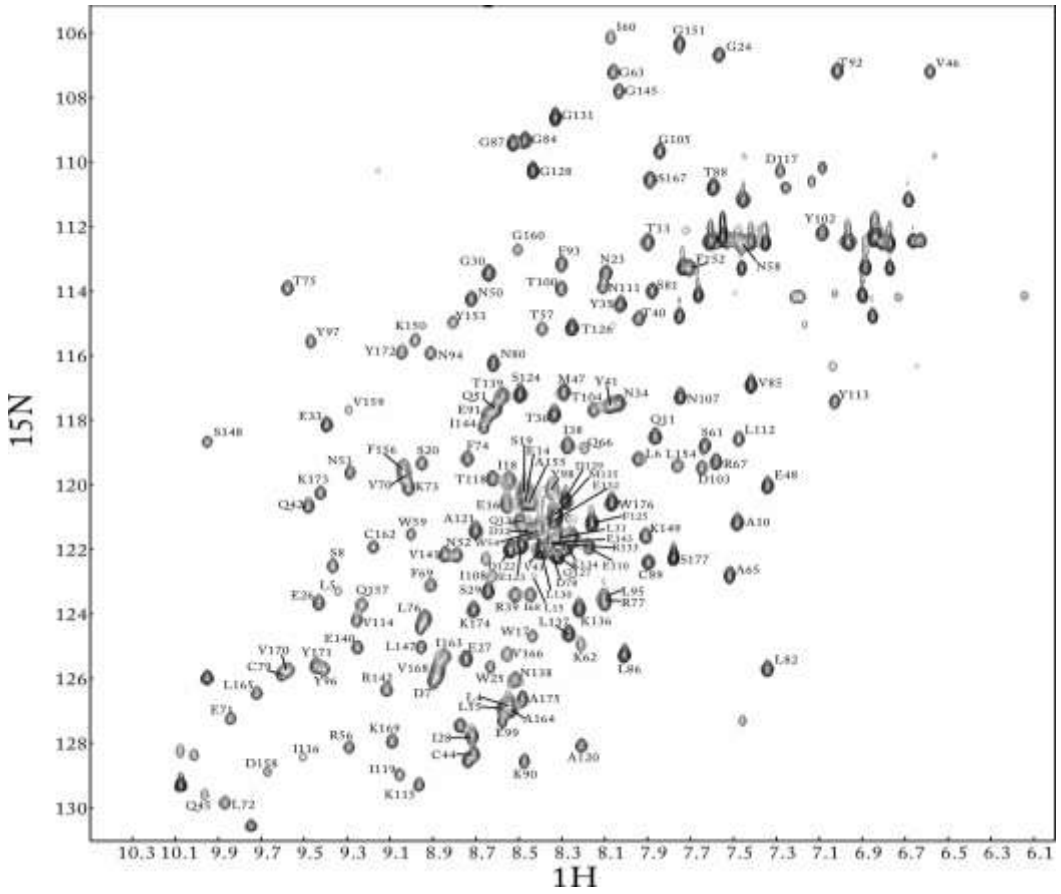

Figure 3.6.7: Assigned ^{1}H-^{15}N HSQC spectrum of the EphA7 ligand-binding domain.

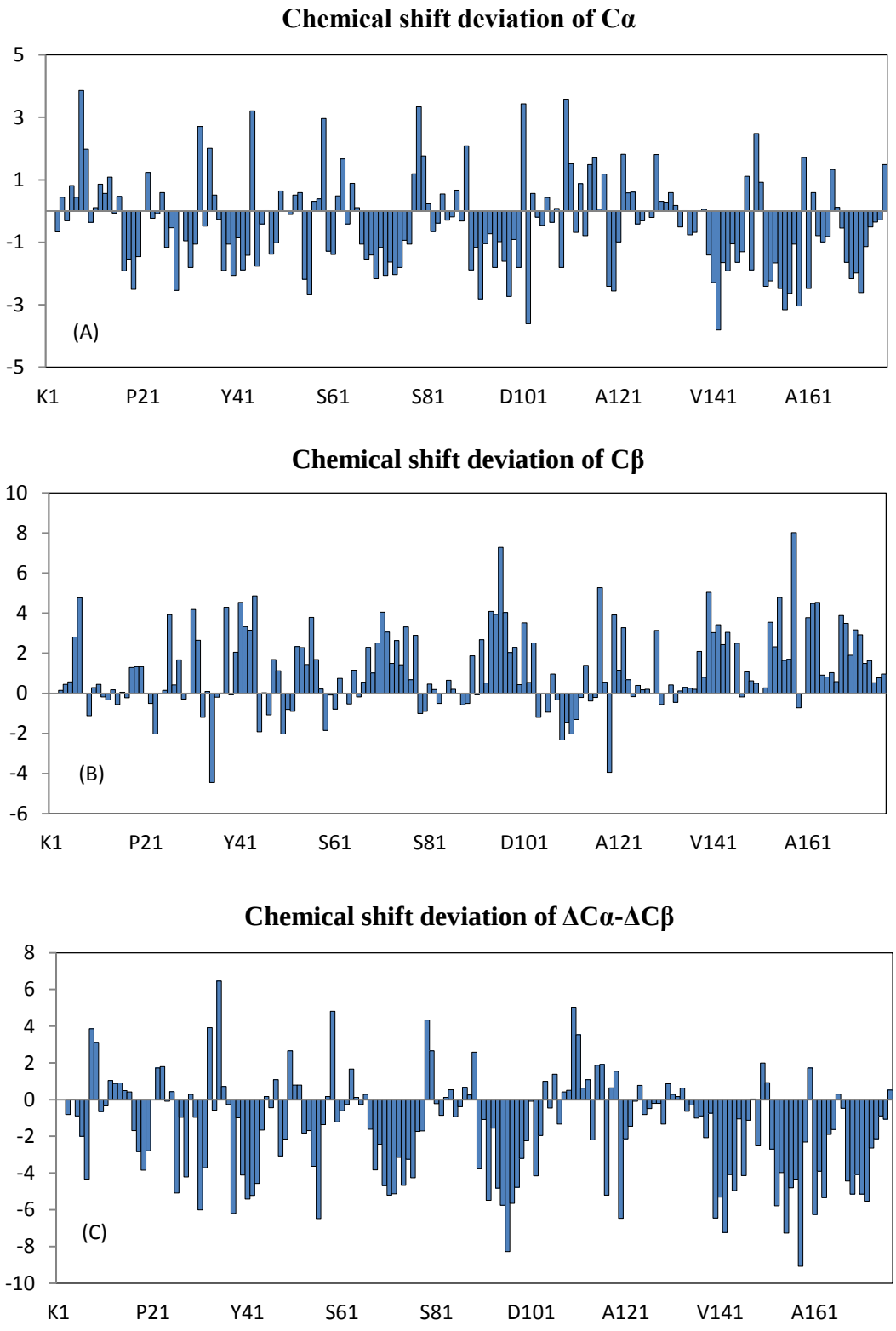

Figure 3.6.8: EphA7 LBD chemical shift deviations provide insights in its secondary structure. (A) Chemical shift deviation of Cα. (B) Chemical shift deviation of Cβ. (C) Chemical shift deviation ofΔCα-ΔCβ.

3.6.6 Interactions of EphA7 LBD with small molecules

Binding Interactions between EphA7 Ligand-binding Domain and Doxazosin Mesylate was also investigated by NMR titration experiments. For visible precipitations would form with adding the Doxazosin Mesylate solutions into the EphA7 ligand binding domain samples, ITC experiment failed and need to be further optimized. While the NMR experiments clearly showed that Doxazosin Mesylate have interaction with the ligand-binding domain of EphA7.

As shown in Figure 3.6.9, the NMR spectra showed that some of the HSQC peaks of the complex of EphA7 ligand binding domain and Doxazosin Mesylate shifted obviously compared to the free ^{15}N-labeled EphA7 when the molar ratio of EphA7 to Doxazosin Mesylate reached 1:14. From the NMR titration experiments, several peaks of the EphA7 HSQC spectra shifted gradually, correlating with the increase concentration of Doxazosin Mesylate molecules, which suggested that the free and bond EphA7 molecules undergo a fast exchange on the chemical shift timescale. To further identify the exact binding interface of EphA7 LBD with Doxazosin Mesylate complex, chemical shift perturbation analysis was done upon titration of the small compounds.

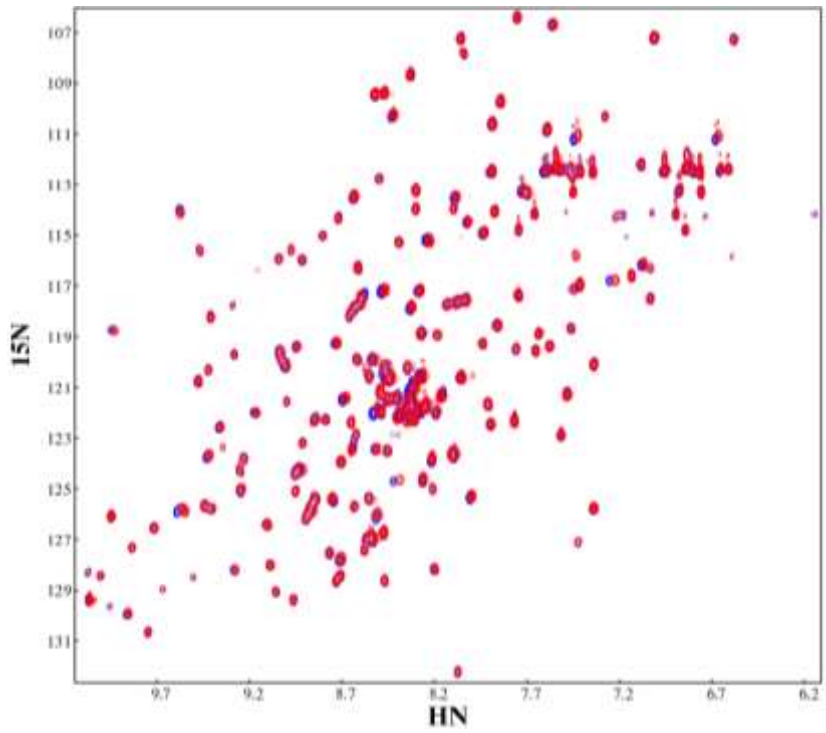

Figure 3.6.9: Characterization of the binding between EphA7 and Doxazosin Mesylate studied by NMR. Superimposition of the HSQC spectra of the ^{15}N-labeled EphA7 in the absence (blue) and presence (red) of Doxazosin Mesylate at a molar ratio of 1:14.

Compared to the binding between EphA5 and Doxazosin Mesylate which most of the EphA5 HSQC peaks shifted more or less after adding Doxazosin Mesylate, most of the EphA7 HSQC peaks remain the same after adding Doxazosin Mesylate and only several of them showed shifts (Figure 3.3.2 and Figure 3.6.9). The chemical shift differences (CSD) between the free EphA7 state and the complex state was calculated according to the formula $((\Delta^{1}H)^{2} + (\Delta^{15}N)^{2}/5)^{1/2}$, and the results were plotted against EphA7 sequence as shown in Figure 3.6.10.

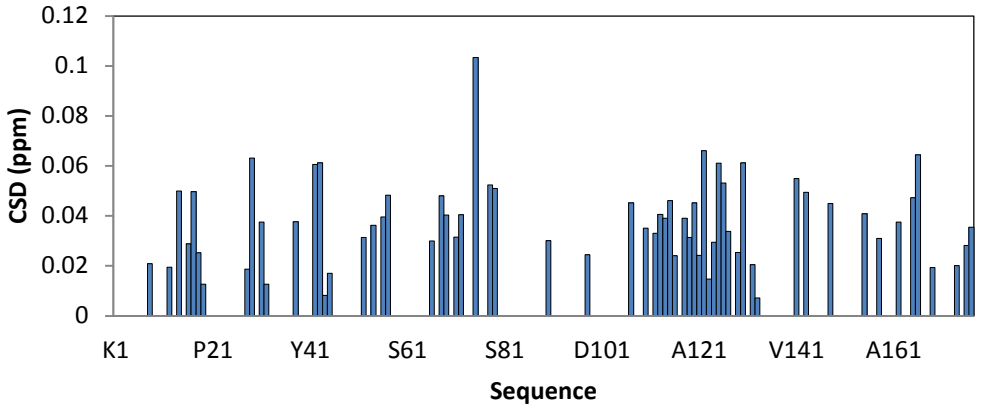

Figure 3.6.10: Residue-specific chemical shift differences (CSD) of the EphA7 ligand-binding domain in the presence of Doxazosin Mesylate.

From the results, eleven residues of EphA7 that gave shifted resonance peaks with significant CSD (peaks of EphA7 with CSD value larger than 0.05 ppm, more than 3.0 standard deviations from the mean CSD). Residues S29 was located on the D β-strand, D32, Q42 and V43 were located on the E β-strand, T75 on the G β-strand and gave the largest CSD value, D78 and C79 were located on the G-H loop, D122, F125, T126 and L130 was on the J-K loop and V166 was located on the M β-strand. All the identified residues of EphA7 ligand binding domain were labeled on the crystal structure of EphA7 as shown in Figure 3.6.11. Similar to the binding between EphA5 and Doxazosin Mesylate, all these residues given high CSD values are located inside the traditional binding pocket of EphA7 ligand binding domain surrounded by D-E and J-K loops or on the D-E and J-K loops. While compared to EphA5, fewer residues are involved in the interaction and the CSD values are lower.

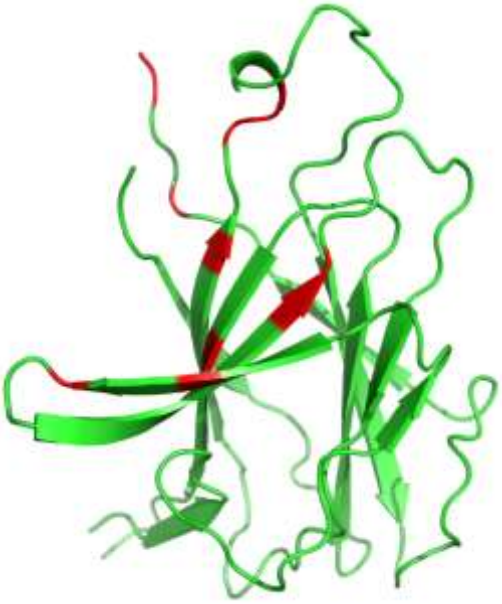

Figure 3.6.11: Crystal structure of EphA7 ligand binding domain with red color indicating residues of EphA7 with CSD larger than 0.05 ppm after binding with Doxazosin Mesylate.

3.6.7 H/D Exchange Experiment for Free EphA7 LBD

The NMR hydrogen/deuterium (H/D) exchange experiment was conducted to assess the backbone dynamics of the EphA7 ligand-binding domain on min-hr timescale. As shown in Figure 3.6.12A and C, upon subjecting to H/D exchange, around 58% of the total residues have completely exchanged with deuterium with the experimental dead time (15 min). These fast-exchange rate residues located not only on the loop and helical regions, but also on the beta-strands (Figure 3.6.12C). After 2 hr, only around 29% of the total residues have the HSQC peaks (Figure 3.6.12B) which mostly located on the beta-stands (Figure 3.6.12C) and defined as slow-exchange-rate residues. After 24 hr, around 26% of the total residues have persisted HSQC peaks. These results suggest that the EphA7

ligand-binding domain is also highly dynamic on the min-hr timescale.

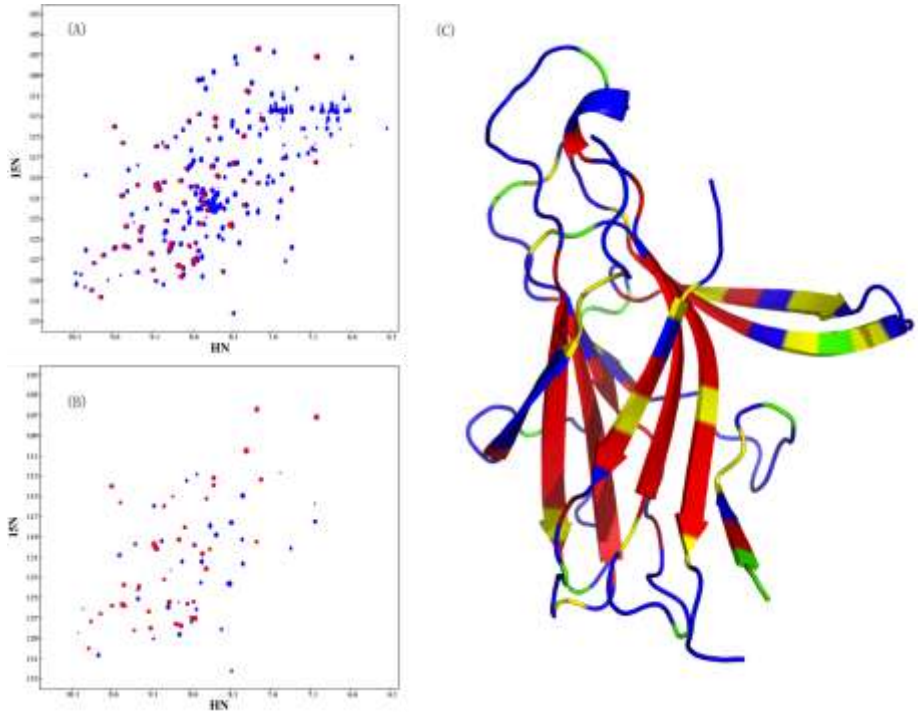

Figure 3.6.12: NMR hydrogen-deuterium (H/D) exchange for free EphA7 ligand binding domain. (A) Superimposition of the ^{1}H-^{15}N NMR HSQC spectra of the ^{15}N-labeled EphA7 LBD (blue) and 15 min after the lyophilized EphA7 LBD powder was re-dissolved in D_2O (red). (B) Superimposition of the ^{1}H-^{15}N NMR HSQC spectra of the ^{15}N-labeled EphA7 LBD, 15 min (blue) and 24 hr (red) after the lyophilized EphA7 LBD powder was re-dissolved in D_2O. (C) The structure of the EphA7 LBD with residues whose HSQC peaks were not detected even in buffer colored in green, residues whose backbone amide protons completely exchanged within 15 min in blue, residues whose backbone amide protons persisted after 15 min but completely exchanged in 2 hours in yellow and residues whose backbone amide protons persisted even after 2 hours in red.

3.6.8 Discussion

The crystal structure of EphA7 ligand-binding domain was solved. Unlike EphA5, this crystal structure of EphA7 has six molecules in one asymmetric unit (AU). It bears a highly similar jellyroll folding architecture composed of 11 antiparallel beta-stands to the previous determined ligand binding domains structures. While by conducting the H-D exchange experiments and mapping the binding site of Doxazosin Mesylate, we can tell that the protein dynamic property and binding affinity of EphA7 is different from EphA5. When binding to Doxazosin Mesylate, although Dox could bind to both ephrin-binding channel of EphA7 and EphA5, it clearly binds to EphA5 with a much higher affinity and with more residues involved. The results of H-D exchange experiments also showed that although EphA7 and EphA5 have the same jellyroll folding architecture, dynamic properties of their loop regions are quite different. After 24 hours, around 26% of the total residues of EphA7 have persisted HSQC peaks, while for EphA5, it only have 19% left. This result suggests the ligand-binding domain of EphA7 is more rigid than EphA5 in a min-hr time scale, although its loop regions are also very flexible. Compared to the "open" form that EphA5 adopts most of the time, EphA7 may adopts a "close" form when it is in the unbound state.

A previous study showed that co-expression of a truncated form of EphA7 suppresses tyrosine phosphorylation of the full-length EphA7 receptor and shifts the cellular response from repulsion to adhesion *in vitro* (Holmberg et al., 2000). And a soluble splice variant of EphA7 ($EphA7^{TR}$) can interfere with full-length

EphA2 and blocks oncogenic signals in lymphoma cells (Oricchio et al., 2011). This study proved that EphA7 receptor could act as a tumor suppressor in follicular lymphoma with immediate therapeutic potential. With the availability of EphA7 LBD crystal structure, the interaction characterizations of above studies could be invested deeper in a different aspect. Furthermore, the design of antagonistic/agonistic molecules with high affinity and specificity might be achieved by targeting a special dynamic state of the Eph LBDs, although they have the same jellyroll β-sandwich fold.

3.7 Nogo-54 in Medaka Fish

3.7.1 Expression and Purification of Nogo-54

The recombinant his-tag Nogo-54 protein was expressed in the bacterial strain BL21. The harvested cells were sonicated in the PBS lysis buffer to release soluble His-tag Nogo-54 proteins. Then the Nogo-54 protein was purified by Ni^{2+}-affinity chromatography under native conditions and subsequently purified by HPLC on a reverse-phase C8 column (Vydac). The whole expression and purification process and the purity of the purified protein were assessed by SDS-PAGE using 15% gel.

^{15}N isotope-labeled Nogo-54 protein sample was prepared for heteronuclear NMR experiments followed the similar expression and purification procedures.

3.7.2 Structural Characterization of Nogo-54 by CD

The structural properties of Nogo-54 were fist investigated by CD spectroscopy. As shown in Figure 3.7.1, the spectrum of Nogo-54 in 5mM phosphate buffer (pH 5.2) had a maximal negative peak at around 202 nm, which implied that Nogo-54 has a typical α-helix conformation. All the data were from three independent scans and were added and averaged.

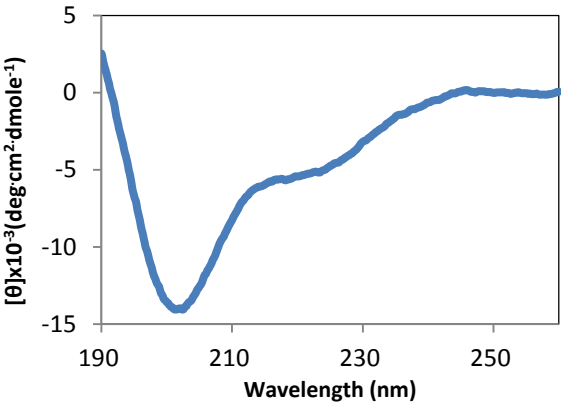

Figure 3.7.1: Preliminary structural characterization of Nogo-54 by far-UV CD. Far-UV CD spectrum of Nogo-54 in 5 mM phosphate buffer (pH 5.2).

3.7.3 NMR Structural Characterization of Nogo-54

NMR HSQC experiment was used to further assess the structural properties of Nogo-54. As shown in Figure 3.7.2, ^{1}H-^{15}N NMR HSQC spectra of Nogo-54 showed a well-separated HSQC spectrum (~1.8 ppm dispersed over ^{1}H and ~20 ppm dispersed over ^{15}N dimensions), recommending their suitability for further NMR structure determination.

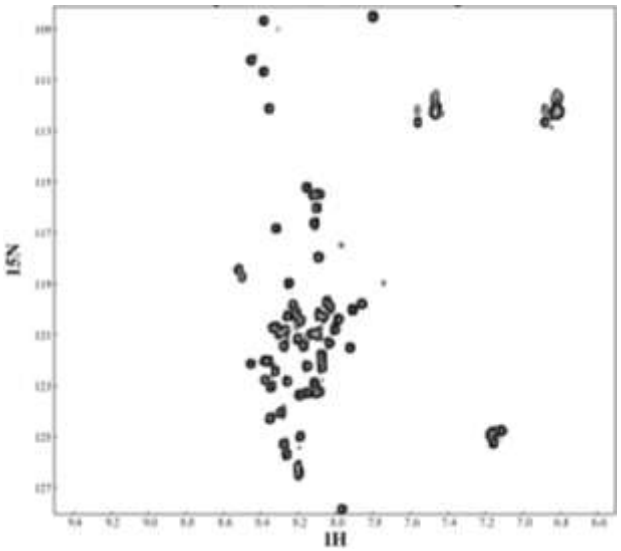

Figure 3.7.2: ^{1}H-^{15}N HSQC spectrum of Nogo-54 collected in 5 mM phosphate buffer at pH 5.2.

A pair of NMR spectra, ^{15}N-edited HSQC-TOCSY and HSQC-NOESY was collected from a ^{15}N -labeled Nogo-54 protein sample to obtain the preliminary backbone sequential assignment and 3D structural determination for Nogo-54. All the 54 residues were assigned except Pro18 whose HSQC peak could not be observed under the experimental conditions (Figure 3.7.3).

After finishing all the chemical shift assignment, secondary structure of Nogo-54 protein was calculated by Hα chemical shifts. Figure 3.7.4 showed that the secondary structure calculated by Hα. The deviation of Hα is negative in most regions, indicating that these regions are α-Helix.

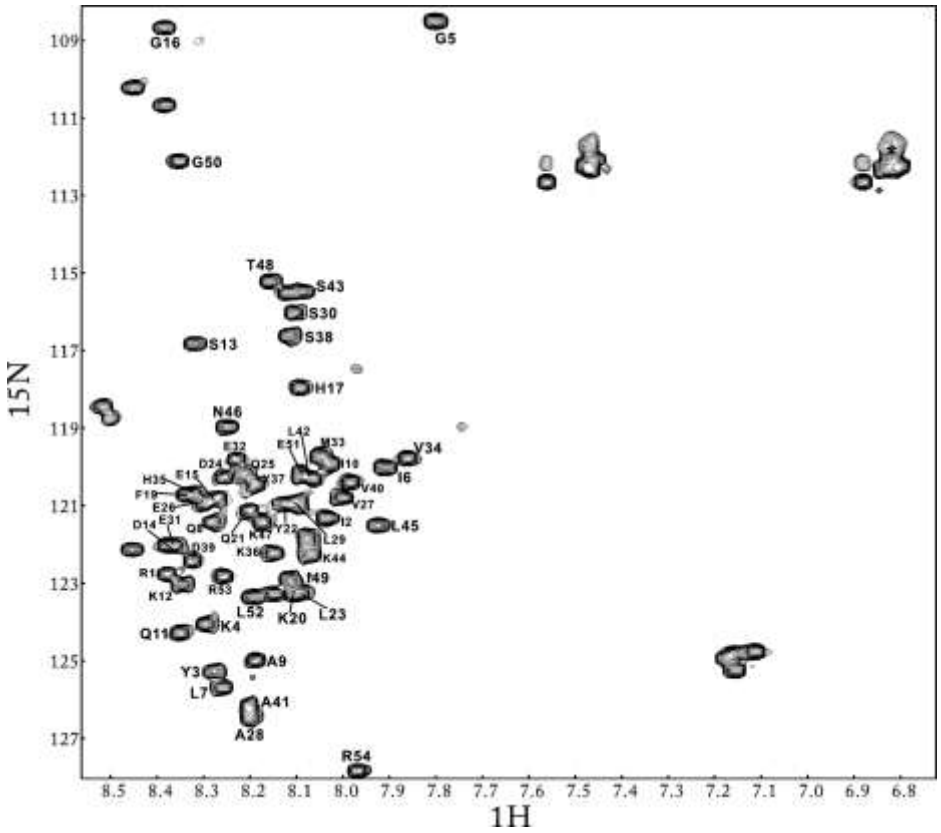

Figure 3.7.3: Assigned ^{1}H-^{15}N HSQC spectrum of the Nogo-54 protein.

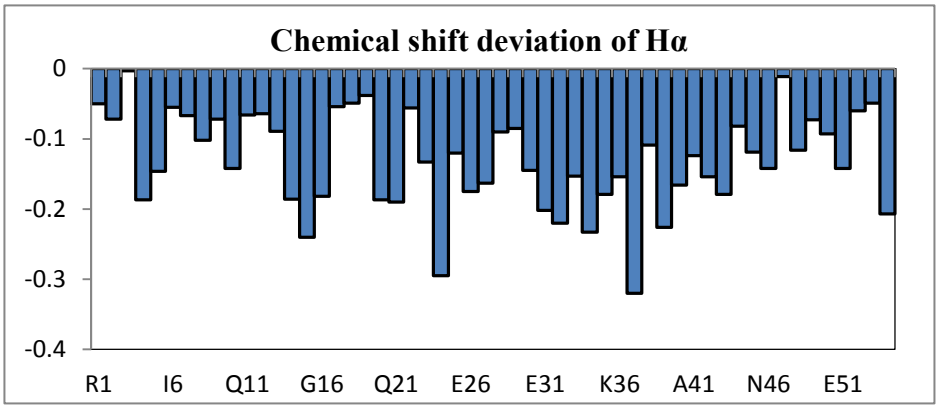

Figure 3.7.4: Nogo-54 chemical shift deviation of Hα provides insights in its secondary structure.

3.7.4 NMR Structure Determination of Nogo-54

After backbone chemical shifts assignment of Nogo-54, the NOE assignment was done according to ^{15}N-edited HSQC-TOCSY and HSQC-NOESY spectra and the NMR structure of Nogo-54 was calculated from the experimental NMR constraints by CYANA program (Guntert, 2004). Table 3.7.1 summaries the constraints used and structural statistics for the ten accepted CYANA structures of Nogo-54. As shown in Figure 3.7.5, Nogo-54 adopted a helical structure composed of two well-formed α-Helix spanning over residues 8-15 and 25-50, linked by a loop. If superimposed separately, both helixes were well refined. Furthermore, the first helix had long-range packing with the second one, showed by the long-range NOEs. Figure 3.7.6 summarizes NOE patterns critical for defining secondary structures. According to Figure 1.2.3, based on the dNN(i, i+2), dαN(i, i+3) and dαN(i, i+4) NOE patterns, it was very obvious that Nogo-54 had a well-formed helical structure constituted by two helical segments.

Table 3.7.1: NMR constraints used and structural statistics for the ten accepted CYANA structures of Nogo-54.

NOE upper distance limits	
Intra-residue	167
Sequential	212
Medium range	136
Long range	12
Total	527
Dihedral angle restrains	85
Final CYANA structures	
CYANA target function	1.57±0.09Å
Distance restraint violations (>0.20Å)	0
Angle restraint violations (>5º)	0
Ramachandran analysis	
Residues in favored regions	96.3%
Residues in allowed regions	3.7%
Residues in outlier regions	0%
Root mean square deviation (Å)	
Residues 8-15 (the first helix)	0.075(backbone atoms)
Residues 25-50 (the secondary helix)	1.465 (backbone atoms)

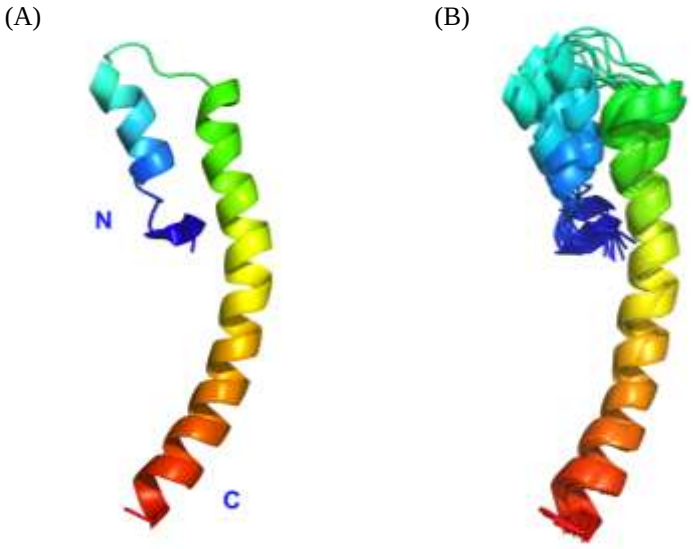

Figure 3.7.5: NMR structure of Nogo-54. (A) The NMR structure of Nogo-54 of Medaka fish in the ribbon mode. (B) All ten accepted Nogo-54 structures superimposed over residue 25-50.

Figure 3.7.6: The NOE patterns critical for defining the secondary structure of Nogo-54.

Previous studies proposed that the charged pockets on the NgR surface might play an important role in interacting with Nogo-66 (Barton et al., 2003; He et al., 2003; Lauren et al., 2007; Schimmele and Pluckthun, 2005). Therefore, the electrostatic potential surface of the fish Nogo-54 model was examined to identify the candidate residues for binding to NgR. Interestingly, as shown in Figure 3.7.7, the fish Nogo-54 contains unique charged patches. Putting the N-terminal short helix facing to the front, both the N-terminal helix and the C-terminal residues formed negative patches, while residues in the middle of the model has a positive patch. While a 180° rotation of the model showed a positive N-terminal patch and a negative patch in the middle of fish Nogo-54.

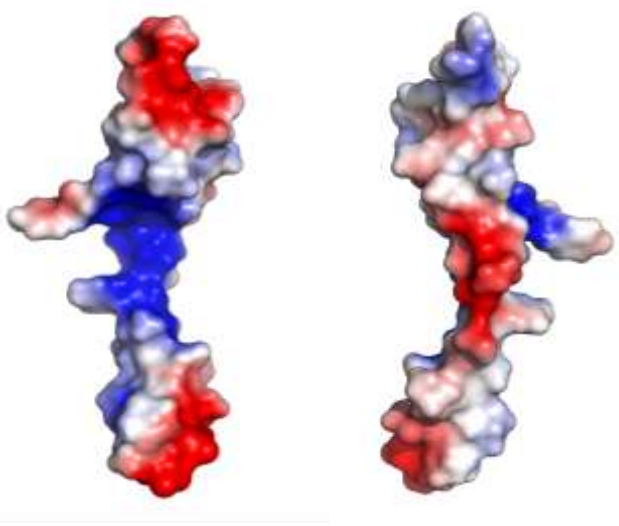

Figure 3.7.7: The electrostatic potential surface of Nogo-54 in Medaka fish.

3.7.5 Discussion

Nogo (RTN4) belongs to the reticulon family of membrane proteins, which is a eukaryotic gene family with ubiquitous expression and distinctive topological features (Oertle et al., 2003). Three different isoforms of Nogo, Nogo-A, -B and -C, are involved in a variety of functional processes including apoptosis, CNS neurite regeneration, neuron pathologies, vascular remodeling and so on. Two inhibitory domains of Nogo-A are responsible for the neurite growth inhibiting: The first one is a unique N-terminal region, which do not exist in Nogo-B and –C (Oertle et al., 2003). The second one is an extracellular 66 amino acid loop (Nogo-66) shared by all the three isoforms which can bind to the Nogo-66 receptor family (NgR) consisting in three glycophosphatidylinositol (GPI)-anchored receptors (NgR1, NgR2 and NgR3) (Fournier et al., 2001; Li et al., 2006; Li et al., 2004). Nogo-66 is an important region with multiple functions, especially in inhibiting of human CNS axonal regeneration, by interacting with NgR. Unfortunately, Nogo-66 itself was insoluble and unstructured. Previously, Nogo-54, a soluble form of Nogo-66 of human, was rationally designed and the NMR structure was solved (Li et al., 2008). It is not only buffer soluble, well structured but also able to mimic Nogo-66 in inhibiting neurite outgrowth.

In contrary to human CNS, CNS in fish is able to regenerate axons. Previous study showed that the first inhibitory domain, Nogo-A-specific domain is lost in fish, and the second domain, Nogo-66 was modified so that Nogo does not impair axon regeneration (Abdesselem et al., 2009; Diekmann et al., 2005; Schweigreiter,

2008). Experiments showed that via binding to the same receptors, Nogo-66 in Zebrafish is growth permissive for both Zebrafish and mouse neurons in the Zebrafish optic nerve, while the Nogo-66 homolog in rat inhibits growth in both species, even the two homologs have 70% sequence similarity (Abdesselem et al., 2009).

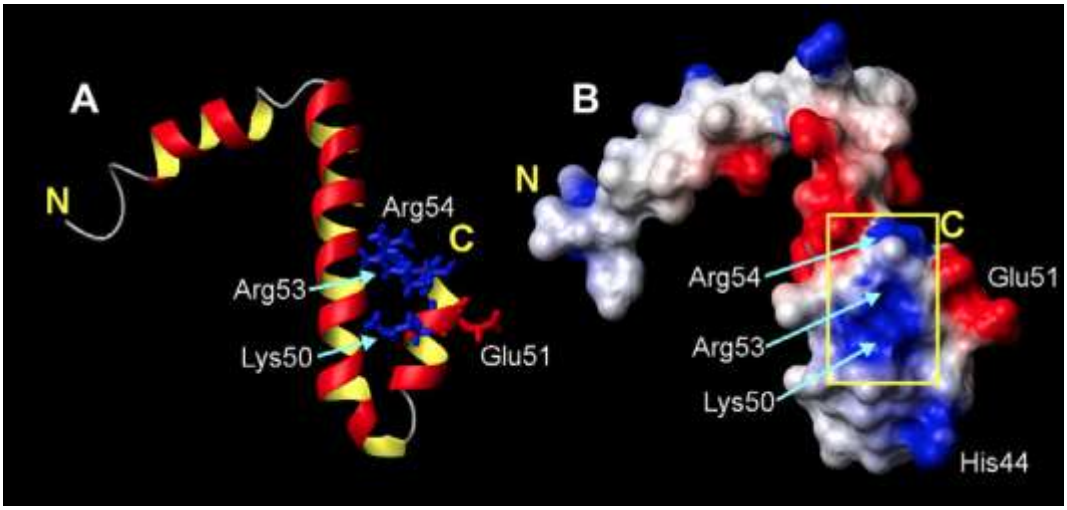

Figure 3.7.8: Structural model of human Nogo-54. (A) Structural model of human Nogo-54 in the ribbon mode, with Lys50, Arg53 and Arg54 side chains displayed in blue sticks; and Glu51 side chain in red sticks. (B) The electrostatic potential surface of human Nogo-54 with the charged patches not presented in Nogo-40 labeled (Li et al., 2008).

As shown in Figure 3.7.8A, Nogo-54 in human adopted a helical structure composed of three helices and with the long-range packing between the C-half of the middle helix and the last helix (Li et al., 2008). Compared with the human Nogo-54 NMR structure, the fish Nogo-54 NMR structure is quite different. As shown in Figure 3.7.5, Nogo-54 in Medaka fish also has a helical structure, while it only contains two helices and the long-range packing is between the first helix

and the N-half of the second helix.

The crystal structure of the NgR ectodomain showed one potential Nogo-66 binding site on NgR, which has characteristics of a negative cavity (Barton et al., 2003; He et al., 2003; Lauren et al., 2007; Schimmele and Pluckthun, 2005). Previous studies also demonstrated that Lys50, Glu51, Arg53 and Arg54 of human Nogo-54 could form a large positive surface and it was responsible for the NgR-binding (Figure 3.7.8B). The NMR and mutation results showed that the four charged residues are crucial in binding with NgR to initiate the inhibitory action (Li et al., 2008). Compared to the human Nogo-54, fish Nogo-54 does not have this positive patch, while it still has the ability to bind with both fish and rat NgR (Abdesselem et al., 2009). Taken together with above results, it is possible that fish Nogo-54 bind to its NgR with a different region (e.g. the positive patch in the middle of Nogo-54) without inhibitory activity, which need to be further investigated.

The molecular interaction between Nogo-66 and NgR poses permissive or inhibitory effects on the CNS neuronal regeneration in different species; therefore the Nogo-66-NgR interface is an extremely promising target for design of molecules to treat CNS injuries. The availability of the Nogo-54 structure offered us rationales for deeply analyzing the different effects in different species. Furthermore, the Nogo-54 structure in fish may serve as a promising starting point for further design of therapeutics to enhance human CNS neuronal regeneration.

CHAPTER IV. Conclusion and Future Work

CHAPTER IV. Conclusion and Future Work

Although all the solved Eph ligand-binding domain structures adopt the same jellyroll β-sandwich fold, their high-affinity ephrin-binding channels have their own unique features. By using crystallography and NMR spectroscopy, we determined the crystal structure of the EphA5 ligand-binding domain. Unlike the previously determined unbound Eph receptor ligand-binding domain structures, over residues Ala^{179}-Ser^{182} and Gly^{189}-Met^{193} in the J-K loop, the EphA5 ligand-binding domain assumes helical conformations while the corresponding residues adopt a short β-sheet in EphA2, EphA4 and EphB2 in the free state. The EphA5 helical conformation in the J-K loop resembles the open form of the high-affinity ephrin-binding channel previously observed in Eph receptor LBDs in complex with ephrins. The existence of this helical conformation is also confirmed by NMR chemical shifts in solution. The uniqueness associated with the high-affinity ephrin-binding channel of EphA5 may be exploited for the identification of small molecules selectively targeting EphA5 with high affinity.

To test the activity of the EphA5 LBD structure, two antagonistic peptides, WDC and WTF and one agonistic small compound, Doxazosin Mesylate was used. Their bindings with EphA5 LBD were studied by NMR spectroscopy, ITC and computer dockings. All the three components could bind to EphA5 LBD in the conserved ephrin-binding channels with different binding affinities.

NMR studies and MD simulations reveal that like the EphA4 LBD, the

β-strands constituting the jellyroll β-sandwich fold are highly rigid but the loops can adopt multiple conformations exchangeable on the ps-ns time scale. Unlike the EphA4 LBD, the EphA5 LBD is characterized by unusually high dynamics over the D-E loop, which appears to result in an extensive exposure of the residues in the D and E strands over the min-hr time scale, as experimentally confirmed by the NMR H-D exchange results. On the other hand, Mode-free analysis of the relaxation data and CPMG-based relaxation dispersion measurements reveal that the EphA5 LBD lacks significant conformational exchanges on the μs-ms time scale.

Based on the structural and dynamic results obtained, it appears that even in the unbound state the open form of the high-affinity ephrin-binding channel of EphA5 is highly populated. As a consequence, EphA5 is ready for binding ephrin-As and other ligands, such as antagonistic peptides or small molecules, without needing significant conformational exchanges on the μs-ms time scale. By contrast, the highly populated conformation of EphA4 in the unbound state is the closed form while the open form only represents a minor population. Therefore, ephrin binding to EphA4 is needed to shift the equilibrium from the closed to the open form, which occurs on the μs-ms time scale. The current results with EphA5 thus strengthen the proposal derived from our studies on EphA4 that the binding of Eph LBDs to different ligands follows a conformational selection scenario [17,39], consequently highlighting the central role of protein dynamics in the bidirectional Eph-ephrin signaling.

The crystal structure of EphA7 ligand-binding domain was also solved. Unlike EphA5, this crystal structure of EphA7 has six molecules in one asymmetric unit (AU). It bears a highly similar jellyroll folding architecture composed of 11 antiparallel beta-stands to the previous determined ligand binding domains structures. While by conducting the H-D exchange experiments and mapping the binding site of Doxazosin Mesylate, we can tell that the protein dynamic property and binding affinity of EphA7 is different from EphA5. When binding to Doxazosin Mesylate, although Dox could bind to both ephrin-binding channel of EphA7 and EphA5, it clearly binds to EphA5 with a much higher affinity and with more residues involved. The results of H-D exchange experiments also showed that although EphA7 and EphA5 have the same jellyroll folding architecture, dynamic properties of their loop regions are quite different. It suggests the ligand-binding domain of EphA7 is more rigid than EphA5 in a min-hr time scale, although its loop regions are also very flexible. Compared to the "open" form that EphA5 adopts most of the time, EphA7 may adopts a "close" form when it is in the unbound state. A previous study showed that co-expression of a truncated form of EphA7 suppresses tyrosine phosphorylation of the full-length EphA7 receptor and shifts the cellular response from repulsion to adhesion *in vitro* (Holmberg et al., 2000). And a soluble splice variant of EphA7 ($EphA7^{TR}$) can interfere with full-length EphA2 and blocks oncogenic signals in lymphoma cells (Oricchio et al., 2011). This study proved that EphA7 receptor could act as a tumor suppressor in follicular lymphoma with immediate

therapeutic potential. With the availability of EphA7 LBD crystal structure, the interaction characterizations of above studies could be invested deeper in a different aspect. Furthermore, the design of antagonistic/agonistic molecules with high affinity and specificity might be achieved by targeting a special dynamic state of the Eph LBDs, although they have the same jellyroll β-sandwich fold.

The structure of the buffer-soluble form of Nogo-66, Nogo-54 was solved by NMR spectroscopy. Nogo-54 adopted a helical structure composed of two well-formed α-Helix, linked by a loop. If superimposed separately, both helixes were well refined. Furthermore, the first helix had long-range packing with the N-term half of the second one, showed by the long-range NOEs. Unlike Nogo-54 in fish, the protein in human adopted a helical structure composed of three helices and with the long-range packing between the C-half of the middle helix and the last helix (Li et al., 2008). The crystal structure of the NgR ectodomain showed one potential Nogo-66 binding site on NgR, which has characteristics of a negative cavity. The C-terminal residue, Lys50, Glu51, Arg53 and Arg54 of human Nogo-54 could form a large positive surface, which could bind to the negative cavity of NgR. Compared to the human Nogo-54, fish Nogo-54 does not have this positive patch in its N-terminal, while it still can bind to both fish and rat NgR. These results suggest that fish Nogo-54 bind to its NgR with a different region and without inhibitory activity. To further understand this phenomenon, the characteristics of the binding between NgR with both human and fish Nogo-54 could be studied by NMR titration and ITC experiments. After mapping their

binding sites on the structure of the proteins, site mutation of each protein could be designed to specify the detailed interacting site. By analyzing the specific binding site, protein interactions could be mimic by docking. The protein dynamic properties of the unbound proteins and complexes can be achieved by NMR spectroscopy, MD simulation and H/D exchange at the same time. Based on above investigation, we might be able to explain why human CNS has the neuronal regeneration inhibition while fish CNS does not. And it may serve as a promising starting point for further design of therapeutics to enhance human CNS neuronal regeneration.

REFERENCE:

Abdesselem, H., Shypitsyna, A., Solis, G.P., Bodrikov, V., and Stuermer, C.A.O. (2009). No Nogo66-and NgR-Mediated Inhibition of Regenerating Axons in the Zebrafish Optic Nerve. Journal of Neuroscience *29*, 15489-15498.

Altieri, A.S., Hinton, D.P., and Byrd, R.A. (1995). Association of Biomolecular Systems Via Pulsed-Field Gradient Nmr Self-Diffusion Measurements. J Am Chem Soc *117*, 7566-7567.

Alzheimer's-Association (2011). 2011 Alzheimer's Disease Facts and Figures. Alzheimer's & Dementia: The Journal of the Alzheimer's Association *7*, 208-244.

Baldwin, A.J., and Kay, L.E. (2009). NMR spectroscopy brings invisible protein states into focus. Nature Chemical Biology *5*, 808-814.

Barton, W.A., Liu, B.P., Tzvetkova, D., Jeffrey, P.D., Fournier, A.E., Sah, D., Cate, R., Strittmatter, S.M., and Nikolov, D.B. (2003). Structure and axon outgrowth inhibitor binding of the Nogo-66 receptor and related proteins. The EMBO journal *22*, 3291-3302.

Battaglia, A.A., Sehayek, K., Grist, J., McMahon, S.B., and Gavazzi, I. (2003). EphB receptors and ephrin-B ligands regulate spinal sensory connectivity and modulate pain processing. Nature neuroscience *6*, 339-340.

Berman, H.M., Westbrook, J., Feng, Z., Gilliland, G., Bhat, T.N., Weissig, H., Shindyalov, I.N., and Bourne, P.E. (2000). The Protein Data Bank. Nucleic Acids Research *28*, 235-242.

Boehr, D.D., McElheny, D., Dyson, H.J., and Wright, P.E. (2010). Millisecond timescale fluctuations in dihydrofolate reductase are exquisitely sensitive to the bound ligands. P Natl Acad Sci USA *107*, 1373-1378.

Bowden, T.A., Aricescu, A.R., Nettleship, J.E., Siebold, C., Rahman-Huq, N., Owens, R.J., Stuart, D.I., and Jones, E.Y. (2009). Structural plasticity of eph receptor A4 facilitates cross-class ephrin signaling. Structure *17*, 1386-1397.

Brantley-Sieders, D.M., and Chen, J. (2004). Eph receptor tyrosine kinases in angiogenesis: from development to disease. Angiogenesis *7*, 17-28.

Brittis, P.A., and Flanagan, J.G. (2001). Nogo domains and a Nogo receptor: implications for axon regeneration. Neuron *30*, 11-14.

Brownlee, H., Gao, P.P., Frisen, J., Dreyfus, C., Zhou, R., and Black, I.B. (2000). Multiple ephrins regulate hippocampal neurite outgrowth. J Comp Neurol *425*, 315-322.

Brunger, A.T., Adams, P.D., Clore, G.M., DeLano, W.L., Gros, P., Grosse-Kunstleve, R.W., Jiang, J.S., Kuszewski, J., Nilges, M., Pannu, N.S., *et al.* (1998). Crystallography & NMR system: A new software suite for macromolecular structure determination. Acta Crystallogr D *54*, 905-921.

Caligiuri, M., Molz, L., Liu, Q., Kaplan, F., Xu, J.P., Majeti, J.Z., Ramos-Kelsey, R., Murthi, K., Lievens, S., Tavernier, J., *et al.* (2006). MASPIT: three-hybrid trap for quantitative proteome fingerprinting of small molecule-protein interactions in mammalian cells. Chemistry & biology *13*, 711-722.

Caroni, P., Savio, T., and Schwab, M.E. (1988). Central nervous system

regeneration: oligodendrocytes and myelin as non-permissive substrates for neurite growth. Prog Brain Res *78*, 363-370.

Caroni, P., and Schwab, M.E. (1988). Two membrane protein fractions from rat central myelin with inhibitory properties for neurite growth and fibroblast spreading. J Cell Biol *106*, 1281-1288.

Castellani, V., Yue, Y., Gao, P.P., Zhou, R., and Bolz, J. (1998). Dual action of a ligand for Eph receptor tyrosine kinases on specific populations of axons during the development of cortical circuits. J Neurosci *18*, 4663-4672.

Chen, Y., Tang, X., Cao, X., Chen, H., and Zhang, X. (2006). Human Nogo-C overexpression induces HEK293 cell apoptosis via a mechanism that involves JNK-c-Jun pathway. Biochem Biophys Res Commun *348*, 923-928.

Chrencik, J.E., Brooun, A., Kraus, M.L., Recht, M.I., Kolatkar, A.R., Han, G.W., Seifert, J.M., Widmer, H., Auer, M., and Kuhn, P. (2006a). Structural and biophysical characterization of the EphB4*ephrinB2 protein-protein interaction and receptor specificity. J Biol Chem *281*, 28185-28192.

Chrencik, J.E., Brooun, A., Recht, M.I., Kraus, M.L., Koolpe, M., Kolatkar, A.R., Bruce, R.H., Martiny-Baron, G., Widmer, H., Pasquale, E.B., *et al.* (2006b). Structure and thermodynamic characterization of the EphB4/Ephrin-B2 antagonist peptide complex reveals the determinants for receptor specificity. Structure *14*, 321-330.

Chrencik, J.E., Brooun, A., Recht, M.I., Nicola, G., Davis, L.K., Abagyan, R., Widmer, H., Pasquale, E.B., and Kuhn, P. (2007). Three-dimensional structure of the EphB2 receptor in complex with an antagonistic peptide reveals a novel mode

of inhibition. The Journal of biological chemistry *282*, 36505-36513.

Clore, G.M., Driscoll, P.C., Wingfield, P.T., and Gronenborn, A.M. (1990). Analysis of the backbone dynamics of interleukin-1 beta using two-dimensional inverse detected heteronuclear 15N-1H NMR spectroscopy. Biochemistry *29*, 7387-7401.

David, S., and Aguayo, A.J. (1981). Axonal elongation into peripheral nervous system "bridges" after central nervous system injury in adult rats. Science *214*, 931-933.

Dawson, D.W., Hong, J.S., Shen, R.R., French, S.W., Troke, J.J., Wu, Y.Z., Chen, S.S., Gui, D., Regelson, M., Marahrens, Y., *et al.* (2007). Global DNA methylation profiling reveals silencing of a secreted form of Epha7 in mouse and human germinal center B-cell lymphomas. Oncogene *26*, 4243-4252.

de Vries, S.J., van Dijk, A.D., Krzeminski, M., van Dijk, M., Thureau, A., Hsu, V., Wassenaar, T., and Bonvin, A.M. (2007). HADDOCK versus HADDOCK: new features and performance of HADDOCK2.0 on the CAPRI targets. Proteins-Structure Function and Bioinformatics *69*, 726-733.

Diekmann, H., Klinger, M., Oertle, T., Heinz, D., Pogoda, H.M., Schwab, M.E., and Stuermer, C.A. (2005). Analysis of the reticulon gene family demonstrates the absence of the neurite growth inhibitor Nogo-A in fish. Mol Biol Evol *22*, 1635-1648.

Ding, L., Getz, G., Wheeler, D.A., Mardis, E.R., McLellan, M.D., Cibulskis, K., Sougnez, C., Greulich, H., Muzny, D.M., Morgan, M.B., *et al.* (2008). Somatic mutations affect key pathways in lung adenocarcinoma. Nature *455*, 1069-1075.

Dominguez, C., Boelens, R., and Bonvin, A.M.J.J. (2003). HADDOCK: A protein-protein docking approach based on biochemical or biophysical information. J Am Chem Soc *125*, 1731-1737.

Dyson, H.J., and Wright, P.E. (2004). Unfolded proteins and protein folding studied by NMR. Chem Rev *104*, 3607-3622.

Edwards, C.M., and Mundy, G.R. (2008). Eph receptors and ephrin signaling pathways: a role in bone homeostasis. Int J Med Sci *5*, 263-272.

Emsley, P., and Cowtan, K. (2004). Coot: model-building tools for molecular graphics. Acta Crystallogr D *60*, 2126-2132.

Eph-Nomenclature-Committee (1997). Unified nomenclature for Eph family receptors and their ligands, the ephrins. Cell *90*, 403-404.

Fabes, J., Anderson, P., Brennan, C., and Bolsover, S. (2007). Regeneration-enhancing effects of EphA4 blocking peptide following corticospinal tract injury in adult rat spinal cord. Eur J Neurosci *26*, 2496-2505.

Fabes, J., Anderson, P., Yanez-Munoz, R.J., Thrasher, A., Brennan, C., and Bolsover, S. (2006). Accumulation of the inhibitory receptor EphA4 may prevent regeneration of corticospinal tract axons following lesion. Eur J Neurosci *23*, 1721-1730.

Fairbrother, W.J., Liu, J., Pisacane, P.I., Sliwkowski, M.X., and Palmer, A.G., 3rd (1998). Backbone dynamics of the EGF-like domain of heregulin-alpha. J Mol Biol *279*, 1149-1161.

Farrow, N.A., Muhandiram, R., Singer, A.U., Pascal, S.M., Kay, C.M., Gish, G., Shoelson, S.E., Pawson, T., Forman-Kay, J.D., and Kay, L.E. (1994). Backbone dynamics of a free and phosphopeptide-complexed Src homology 2 domain studied by 15N NMR relaxation. Biochemistry *33*, 5984-6003.

Flanagan, J.G., and Vanderhaeghen, P. (1998). The ephrins and Eph receptors in neural development. Annual review of neuroscience *21*, 309-345.

Fournier, A.E., GrandPre, T., and Strittmatter, S.M. (2001). Identification of a receptor mediating Nogo-66 inhibition of axonal regeneration. Nature *409*, 341-346.

Fry, D.C., and Vassilev, L.T. (2005). Targeting protein-protein interactions for cancer therapy. J Mol Med (Berl) *83*, 955-963.

Fushman, D., Cahill, S., and Cowburn, D. (1997). The main-chain dynamics of the dynamin pleckstrin homology (PH) domain in solution: analysis of 15N relaxation with monomer/dimer equilibration. J Mol Biol *266*, 173-194.

Gale, N.W., Holland, S.J., Valenzuela, D.M., Flenniken, A., Pan, L., Ryan, T.E., Henkemeyer, M., Strebhardt, K., Hirai, H., Wilkinson, D.G., *et al.* (1996). Eph receptors and ligands comprise two major specificity subclasses and are reciprocally compartmentalized during embryogenesis. Neuron *17*, 9-19.

Gerlai, R., Shinsky, N., Shih, A., Williams, P., Winer, J., Armanini, M., Cairns, B., Winslow, J., Gao, W., and Phillips, H.S. (1999). Regulation of learning by EphA receptors: a protein targeting study. J Neurosci *19*, 9538-9549.

Goldshmit, Y., Galea, M.P., Wise, G., Bartlett, P.F., and Turnley, A.M. (2004).

Axonal regeneration and lack of astrocytic gliosis in EphA4-deficient mice. J Neurosci *24*, 10064-10073.

Guntert, P. (2004). Automated NMR structure calculation with CYANA. Methods Mol Biol *278*, 353-378.

Hall, J.B., and Fushman, D. (2003). Characterization of the overall and local dynamics of a protein with intermediate rotational anisotropy: Differentiating between conformational exchange and anisotropic diffusion in the B3 domain of protein G. J Biomol NMR *27*, 261-275.

He, X.L., Bazan, J.F., McDermott, G., Park, J.B., Wang, K., Tessier-Lavigne, M., He, Z., and Garcia, K.C. (2003). Structure of the Nogo receptor ectodomain: a recognition module implicated in myelin inhibition. Neuron *38*, 177-185.

Himanen, J.P., Chumley, M.J., Lackmann, M., Li, C., Barton, W.A., Jeffrey, P.D., Vearing, C., Geleick, D., Feldheim, D.A., Boyd, A.W., *et al.* (2004). Repelling class discrimination: ephrin-A5 binds to and activates EphB2 receptor signaling. Nat Neurosci *7*, 501-509.

Himanen, J.P., Goldgur, Y., Miao, H., Myshkin, E., Guo, H., Buck, M., Nguyen, M., Rajashankar, K.R., Wang, B., and Nikolov, D.B. (2009). Ligand recognition by A-class Eph receptors: crystal structures of the EphA2 ligand-binding domain and the EphA2/ephrin-A1 complex. EMBO Rep *10*, 722-728.

Himanen, J.P., Henkemeyer, M., and Nikolov, D.B. (1998). Crystal structure of the ligand-binding domain of the receptor tyrosine kinase EphB2. Nature *396*, 486-491.

Himanen, J.P., and Nikolov, D.B. (2003). Eph signaling: a structural view. Trends Neurosci *26*, 46-51.

Himanen, J.P., Rajashankar, K.R., Lackmann, M., Cowan, C.A., Henkemeyer, M., and Nikolov, D.B. (2001). Crystal structure of an Eph receptor-ephrin complex. Nature *414*, 933-938.

Himanen, J.P., Saha, N., and Nikolov, D.B. (2007). Cell-cell signaling via Eph receptors and ephrins. Curr Opin Cell Biol *19*, 534-542.

Holland, S.J., Gale, N.W., Mbamalu, G., Yancopoulos, G.D., Henkemeyer, M., and Pawson, T. (1996). Bidirectional signalling through the EPH-family receptor Nuk and its transmembrane ligands. Nature *383*, 722-725.

Holmberg, J., Clarke, D.L., and Frisen, J. (2000). Regulation of repulsion versus adhesion by different splice forms of an Eph receptor. Nature *408*, 203-206.

Horner, P.J., and Gage, F.H. (2000). Regenerating the damaged central nervous system. Nature *407*, 963-970.

Hu, Z., Yue, X., Shi, G., Yue, Y., Crockett, D.P., Blair-Flynn, J., Reuhl, K., Tessarollo, L., and Zhou, R. (2003). Corpus callosum deficiency in transgenic mice expressing a truncated ephrin-A receptor. J Neurosci *23*, 10963-10970.

Ireton, R.C., and Chen, J. (2005). EphA2 receptor tyrosine kinase as a promising target for cancer therapeutics. Current cancer drug targets *5*, 149-157.

Jansma, A.L., Kirkpatrick, J.P., Hsu, A.R., Handel, T.M., and Nietlispach, D. (2010). NMR analysis of the structure, dynamics, and unique oligomerization

properties of the chemokine CCL27. The Journal of biological chemistry *285*, 14424-14437.

Karaman, M.W., Herrgard, S., Treiber, D.K., Gallant, P., Atteridge, C.E., Campbell, B.T., Chan, K.W., Ciceri, P., Davis, M.I., Edeen, P.T., *et al.* (2008). A quantitative analysis of kinase inhibitor selectivity. Nature biotechnology *26*, 127-132.

Kay, L.E., Torchia, D.A., and Bax, A. (1989). Backbone dynamics of proteins as studied by 15N inverse detected heteronuclear NMR spectroscopy: application to staphylococcal nuclease. Biochemistry *28*, 8972-8979.

Kendrew, J.C., Bodo, G., Dintzis, H.M., Parrish, R.G., Wyckoff, H., and Phillips, D.C. (1958). A three-dimensional model of the myoglobin molecule obtained by x-ray analysis. Nature *181*, 662-666.

Kleckner, I.R., and Foster, M.P. (2011). An introduction to NMR-based approaches for measuring protein dynamics. Biochim Biophys Acta *1814*, 942-968.

Klein, R. (2004). Eph/ephrin signaling in morphogenesis, neural development and plasticity. Curr Opin Cell Biol *16*, 580-589.

Koolpe, M., Burgess, R., Dail, M., and Pasquale, E.B. (2005). EphB receptor-binding peptides identified by phage display enable design of an antagonist with ephrin-like affinity. The Journal of biological chemistry *280*, 17301-17311.

Koolpe, M., Dail, M., and Pasquale, E.B. (2002). An ephrin mimetic peptide that selectively targets the EphA2 receptor. J Biol Chem *277*, 46974-46979.

Koradi, R., Billeter, M., and Wuthrich, K. (1996). MOLMOL: a program for display and analysis of macromolecular structures. J Mol Graph *14*, 51-55, 29-32.

Krishna, M.M., Hoang, L., Lin, Y., and Englander, S.W. (2004). Hydrogen exchange methods to study protein folding. Methods *34*, 51-64.

Kullander, K., and Klein, R. (2002). Mechanisms and functions of Eph and ephrin signalling. Nature reviews Molecular cell biology *3*, 475-486.

Kumar, S.R., Masood, R., Spannuth, W.A., Singh, J., Scehnet, J., Kleiber, G., Jennings, N., Deavers, M., Krasnoperov, V., Dubeau, L., *et al.* (2007). The receptor tyrosine kinase EphB4 is overexpressed in ovarian cancer, provides survival signals and predicts poor outcome. Br J Cancer *96*, 1083-1091.

Kumar, S.R., Scehnet, J.S., Ley, E.J., Singh, J., Krasnoperov, V., Liu, R., Manchanda, P.K., Ladner, R.D., Hawes, D., Weaver, F.A., *et al.* (2009). Preferential induction of EphB4 over EphB2 and its implication in colorectal cancer progression. Cancer research *69*, 3736-3745.

Lamberto, I., Qin, H., Noberini, R., Premkumar, L., Bourgin, C., Riedl, S., Song, J., and Pasquale, E.B. (2012). Distinctive Binding of Three Antagonistic Peptides to the Ephrin-Binding Pocket of the EphA4 Receptor. The Biochemical journal.

Laskowski, R.A., Macarthur, M.W., Moss, D.S., and Thornton, J.M. (1993). Procheck - a Program to Check the Stereochemical Quality of Protein Structures. J Appl Crystallogr *26*, 283-291.

Lauren, J., Hu, F., Chin, J., Liao, J., Airaksinen, M.S., and Strittmatter, S.M. (2007). Characterization of myelin ligand complexes with neuronal Nogo-66

receptor family members. J Biol Chem *282*, 5715-5725.

Li, M., Li, Y., Liao, X., Liu, J., Qin, H., Xiao, Z.C., and Song, J. (2008). Rational design, solution conformation and identification of functional residues of the soluble and structured Nogo-54, which mimics Nogo-66 in inhibiting the CNS neurite outgrowth. Biochem Biophys Res Commun *373*, 498-503.

Li, M.F., Liu, J.X., and Song, J.X. (2006). Nogo goes in the pure water: Solution structure of Nogo-60 and design of the structured and buffer-soluble Nogo-54 for enhancing CNS regeneration. Protein Sci *15*, 1835-1841.

Li, M.F., Shi, J.H., Wei, Z., Teng, F.Y.H., Tang, B.L., and Song, J.X. (2004). Structural characterization of the human Nogo-A functional domains - Solution structure of Nogo-40, a Nogo-66 receptor antagonist enhancing injured spinal cord regeneration. Eur J Biochem *271*, 3512-3522.

Li, M.F., and Song, J.X. (2007). The N- and C-termini of the human Nogo molecules are intrinsically unstructured: Bioinformatics, CD, NMR characterization, and functional implications. Proteins-Structure Function and Bioinformatics *68*, 100-108.

Li, Q., Qi, B., Oka, K., Shimakage, M., Yoshioka, N., Inoue, H., Hakura, A., Kodama, K., Stanbridge, E.J., and Yutsudo, M. (2001). Link of a new type of apoptosis-inducing gene ASY/Nogo-B to human cancer. Oncogene *20*, 3929-3936.

Lipari, G., and Szabo, A. (1982). Model-Free Approach to the Interpretation of Nuclear Magnetic-Resonance Relaxation in Macromolecules .1. Theory and Range of Validity. J Am Chem Soc *104*, 4546-4559.

Liu, J., Li, M., Ran, X., Fan, J.S., and Song, J. (2006). Structural insight into the binding diversity between the human Nck2 SH3 domains and proline-rich proteins. Biochemistry *45*, 7171-7184.

Loria, J.P., Berlow, R.B., and Watt, E.D. (2008). Characterization of enzyme motions by solution NMR relaxation dispersion. Accounts of chemical research *41*, 214-221.

Matsuo, K. (2010). Eph and ephrin interactions in bone. Adv Exp Med Biol *658*, 95-103.

Miao, R.Q., Gao, Y., Harrison, K.D., Prendergast, J., Acevedo, L.M., Yu, J., Hu, F., Strittmatter, S.M., and Sessa, W.C. (2006). Identification of a receptor necessary for Nogo-B stimulated chemotaxis and morphogenesis of endothelial cells. P Natl Acad Sci USA *103*, 10997-11002.

Murai, K.K., Nguyen, L.N., Koolpe, M., McLennan, R., Krull, C.E., and Pasquale, E.B. (2003). Targeting the EphA4 receptor in the nervous system with biologically active peptides. Mol Cell Neurosci *24*, 1000-1011.

Noberini, R., De, S.K., Zhang, Z., Wu, B., Raveendra-Panickar, D., Chen, V., Vazquez, J., Qin, H., Song, J., Cosford, N.D., *et al.* (2011). A disalicylic acid-furanyl derivative inhibits ephrin binding to a subset of Eph receptors. Chemical biology & drug design *78*, 667-678.

Noberini, R., Koolpe, M., Peddibhotla, S., Dahl, R., Su, Y., Cosford, N.D., Roth, G.P., and Pasquale, E.B. (2008). Small molecules can selectively inhibit ephrin binding to the EphA4 and EphA2 receptors. J Biol Chem *283*, 29461-29472.

Noren, N.K., and Pasquale, E.B. (2007). Paradoxes of the EphB4 receptor in cancer. Cancer Res *67*, 3994-3997.

Nussinov, R., and Ma, B. (2012). Protein dynamics and conformational selection in bidirectional signal transduction. BMC Biology *10*, 2.

Oertle, T., van der Haar, M.E., Bandtlow, C.E., Robeva, A., Burfeind, P., Buss, A., Huber, A.B., Simonen, M., Schnell, L., Brosamle, C., *et al.* (2003). Nogo-A inhibits neurite outgrowth and cell spreading with three discrete regions. J Neurosci *23*, 5393-5406.

Oricchio, E., Nanjangud, G., Wolfe, A.L., Schatz, J.H., Mavrakis, K.J., Jiang, M., Liu, X.P., Bruno, J., Heguy, A., Olshen, A.B., *et al.* (2011). The Eph-Receptor A7 Is a Soluble Tumor Suppressor for Follicular Lymphoma. Cell *147*, 554-564.

Otwinowski, Z., and Minor, W. (1997). Processing of X-ray diffraction data collected in oscillation mode. Method Enzymol *276*, 307-326.

Pace, C.N., Vajdos, F., Fee, L., Grimsley, G., and Gray, T. (1995). How to measure and predict the molar absorption coefficient of a protein. Protein Sci *4*, 2411-2423.

Palmer, A., and Klein, R. (2003). Multiple roles of ephrins in morphogenesis, neuronal networking, and brain function. Genes Dev *17*, 1429-1450.

Palmer, A.G. (2009). A topical issue: NMR investigations of molecular dynamics. Journal of Biomolecular Nmr *45*, 1-4.

Palmer, A.G., Rance, M., and Wright, P.E. (1991). Intramolecular Motions of a Zinc Finger DNA-Binding Domain from Xfin Characterized by Proton-Detected

Natural Abundance C-12 Heteronuclear Nmr-Spectroscopy. J Am Chem Soc *113*, 4371-4380.

Pardi, A., Billeter, M., and Wuthrich, K. (1984). Calibration of the angular dependence of the amide proton-C alpha proton coupling constants, 3JHN alpha, in a globular protein. Use of 3JHN alpha for identification of helical secondary structure. J Mol Biol *180*, 741-751.

Pasquale, E.B. (2005). Eph receptor signalling casts a wide net on cell behaviour. Nat Rev Mol Cell Biol *6*, 462-475.

Pasquale, E.B. (2008). Eph-ephrin bidirectional signaling in physiology and disease. Cell *133*, 38-52.

Pasquale, E.B. (2010). Eph receptors and ephrins in cancer: bidirectional signalling and beyond. Nat Rev Cancer *10*, 165-180.

Prevost, N., Woulfe, D., Tanaka, T., and Brass, L.F. (2002). Interactions between Eph kinases and ephrins provide a mechanism to support platelet aggregation once cell-to-cell contact has occurred. P Natl Acad Sci USA *99*, 9219-9224.

Prevost, N., Woulfe, D.S., Tognolini, M., Tanaka, T., Jian, W., Fortna, R.R., Jiang, H., and Brass, L.F. (2004). Signaling by ephrinB1 and Eph kinases in platelets promotes Rap1 activation, platelet adhesion, and aggregation via effector pathways that do not require phosphorylation of ephrinB1. Blood *103*, 1348-1355.

Prinjha, R., Moore, S.E., Vinson, M., Blake, S., Morrow, R., Christie, G., Michalovich, D., Simmons, D.L., and Walsh, F.S. (2000). Inhibitor of neurite outgrowth in humans. Nature *403*, 383-384.

Qin, H., Lim, L., and Song, J. (2012). Protein dynamics at Eph receptor-ligand interfaces as revealed by crystallography, NMR and MD simulations. BMC Biophysics *5*, 2.

Qin, H.N., Shi, J.H., Noberini, R., Pasquale, E.B., and Song, J.X. (2008). Crystal Structure and NMR Binding Reveal That Two Small Molecule Antagonists Target the High Affinity Ephrin-binding Channel of the EphA4 Receptor. Journal of Biological Chemistry *283*, 29473-29484.

Ramon y Cajal, S. (1928). Degeneration and Regeneration of he Nervous System. Hafner, New York, .

Ran, X., and Song, J. (2005). Structural insight into the binding diversity between the Tyr-phosphorylated human ephrinBs and Nck2 SH2 domain. The Journal of biological chemistry *280*, 19205-19212.

Ran, X.Y., Qin, H.N., Liu, J.X., Fan, J.S., Shi, J.H., and Song, J.X. (2008). NMR structure and dynamics of human ephrin-B2 ectodomain: The functionally critical C-D and G-H loops are highly dynamic in solution. Proteins-Structure Function and Bioinformatics *72*, 1019-1029.

Sandvig, A., Berry, M., Barrett, L.B., Butt, A., and Logan, A. (2004). Myelin-, reactive glia-, and scar-derived CNS axon growth inhibitors: expression, receptor signaling, and correlation with axon regeneration. Glia *46*, 225-251.

Schimmele, B., and Pluckthun, A. (2005). Identification of a functional epitope of the Nogo receptor by a combinatorial approach using ribosome display. J Mol Biol *352*, 229-241.

Schuttelkopf, A.W., and van Aalten, D.M.F. (2004). PRODRG: a tool for high-throughput crystallography of protein-ligand complexes. Acta Crystallogr D *60*, 1355-1363.

Schweigreiter, R. (2008). The natural history of the myelin-derived nerve growth inhibitor Nogo-A. Neuron Glia Biol *4*, 83-89.

Simon, B., and Sattler, M. (2004). Speeding up biomolecular NMR spectroscopy. Angew Chem Int Ed Engl *43*, 782-786.

Singla, N., Goldgur, Y., Xu, K., Paavilainen, S., Nikolov, D.B., and Himanen, J.P. (2010). Crystal structure of the ligand-binding domain of the promiscuous EphA4 receptor reveals two distinct conformations. Biochem Biophys Res Commun *399*, 555-559.

Smith, F.M., Vearing, C., Lackmann, M., Treutlein, H., Himanen, J., Chen, K., Saul, A., Nikolov, D., and Boyd, A.W. (2004). Dissecting the EphA3/Ephrin-A5 interactions using a novel functional mutagenesis screen. The Journal of biological chemistry *279*, 9522-9531.

Spera, S., and Bax, A. (1991). Empirical Correlation between Protein Backbone Conformation and C-Alpha and C-Beta C-13 Nuclear-Magnetic-Resonance Chemical-Shifts. J Am Chem Soc *113*, 5490-5492.

Tang, F.Y., Chiang, E.P., and Shih, C.J. (2007). Green tea catechin inhibits ephrin-A1-mediated cell migration and angiogenesis of human umbilical vein endothelial cells. J Nutr Biochem *18*, 391-399.

Tello, F. (1911). The influence of neurotropism in the regeneration of nerve

centers. Trab Lab Invest Biol *9*, 123-159.

Toth, J., Cutforth, T., Gelinas, A.D., Bethoney, K.A., Bard, J., and Harrison, C.J. (2001). Crystal structure of an ephrin ectodomain. Dev Cell *1*, 83-92.

Wei, Z., and Song, J. (2005). Molecular mechanism underlying the thermal stability and pH-induced unfolding of CHABII. J Mol Biol *348*, 205-218.

Wilkinson, D.G. (2001). Multiple roles of EPH receptors and ephrins in neural development. Nat Rev Neurosci *2*, 155-164.

Wimmer-Kleikamp, S.H., and Lackmann, M. (2005). Eph-modulated cell morphology, adhesion and motility in carcinogenesis. IUBMB Life *57*, 421-431.

Wishart, D.S., and Sykes, B.D. (1994). Chemical shifts as a tool for structure determination. Methods Enzymol *239*, 363-392.

Wishart, D.S., Sykes, B.D., and Richards, F.M. (1991). Relationship between nuclear magnetic resonance chemical shift and protein secondary structure. J Mol Biol *222*, 311-333.

Wuthrich, K. (1986). NMR of proteins and nucleic acid.

Yamaguchi, Y., and Pasquale, E.B. (2004). Eph receptors in the adult brain. Curr Opin Neurobiol *14*, 288-296.

Yu, G., Luo, H.Y., Wu, Y.L., and Wu, J.P. (2004). EphrinB1 is essential in T-cell-T-cell co-operation during T-cell activation. Journal of Biological Chemistry *279*, 55531-55539.

Yue, Y., Chen, Z.Y., Gale, N.W., Blair-Flynn, J., Hu, T.J., Yue, X., Cooper, M., Crockett, D.P., Yancopoulos, G.D., Tessarollo, L., *et al.* (2002). Mistargeting hippocampal axons by expression of a truncated Eph receptor. P Natl Acad Sci USA *99*, 10777-10782.

PUBLICATION:

1. **Xuelu Huan**, Jiahai Shi, et al. (2012). Protein Dynamics in Eph-ephrin Bidirectional Signaling: Distinctive Structure and Dynamics of the EphA5 Ligand-Binding Domain as Revealed by Crystallography, NMR and Molecular Dynamics Simulations. (Submitted)

2. Qin, H., R. Noberini, **Huan, X.**(co-first author), et al. (2010). Structural characterization of the EphA4-Ephrin-B2 complex reveals new features enabling Eph-ephrin binding promiscuity. Journal of Biological Chemistry 285(1): 644-654;

3. Qin, H. N., F. D. Chen, **Huan, X. L.**(co-first author), et al. (2010). Structure of the Arabidopsis thaliana DCL4 DUF283 domain reveals a noncanonical double-stranded RNA-binding fold for protein-protein interaction. Rna-a Publication of the Rna Society 16(3): 474-481;